The Development of a ZnO Nanoforce Biosensor for Mortalin - A Novel Biomarker for Parkinson's Disease

by

Semai Naicker

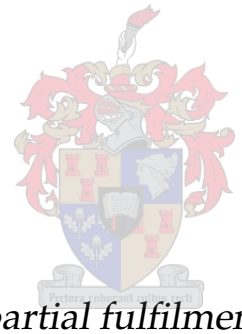

Thesis presented in partial fulfilment of the requirements for the degree of Master of Electronic Engineering in the Faculty of Engineering at Stellenbosch University

Supervisor: Prof. W.J. Perold

Co-supervisor: Prof. R Pretorius

April 2022

Declaration

By submitting this thesis electronically, I declare that the entirety of the work contained therein is my own, original work, I am the sole author thereof (save to the extent explicitly otherwise stated), that reproduction and publication thereof by Stellenbosch University will not infringe any third party rights and that I have not previously in its entirety or in part submitted it for obtaining any qualification.

April 2022

Acknowledgements

I would like to express my heartfelt gratitude to the following people and organisations. Without whom, this study would never have been possible.

- Prof Willem J. Perold, thank you for believing in my every idea, and for giving me the confidence that I needed to put my thesis together. Thank you for always being available and willing to tackle every issue (big and small) with me, without any hesitation. Your constant support has been the backbone of my success over the past 2 years.
- Prof Resia Pretorius, thank you for your advice and for sharing your passion for physiology. Thank you for making it possible for me to develop my interdisciplinary skills.
- Daniel Retief, thank you for taking the role as my third supervisor and my voice of courage and reason. Thank you for always helping me to make sense of everything in your methodological way and for putting things into perspective for me, when I was too stressed to do so myself.
- Dr Alicia Botes and Mr Herschel Achilles (CAF), thank you for always accommodating my every request and for making me feel at home in your laboratory spaces. Alicia, thank you for helping me to develop a new skill in conjunction with getting my work done. Your pep talks were often the highlight of my days.
- Dr Andre du Toit and Dr Chantelle Venter, thank you for never hesitating to help me with my physiology needs, and for helping me to develop my understanding and skills. Thank you for sharing your knowledge and expertise and for always finding time in your schedule to help me with my every request.
- Mr Wessel Croukamp, Mr Wynand van Eeden and Mrs Jenny Martin, thank you for always being ready to lend me a hand or a piece of advice whenever I needed. Thank you for always going out of your way to make every one of my hundreds of requests possible. You are invaluable.

- Mr Mbuso Dludlu (Polymer Science department) thank you for your advice at the early stages of my study. Your input truly helped me to get the ball rolling.
- Dr Remy Bucher (iThemba Labs) thank you for taking the time to explain the XRD analysis to me. Without you, my understanding of my results would never have developed as far as it has.
- Whelan Mohali and Taskeen Ebrahim, thank you both for the time and interest that you dedicated towards me being able to achieve a successful study. Your support never goes unnoticed.
- To all the members of the SAND research group, thank you for the fun, laughter and lighthearted atmosphere. Without the motivation in the office, I would still be busy writing my thesis today.
- To my friends, my chosen family, thank you for every word and thought of encouragement. It makes me feel like the luckiest girl in the world to know that I have all of you on my team, cheering for me every step of the way. Thank you for being on this journey with me.
- And last, but absolutely not least, thank you to Managa Pillay, Jonathan Naicker and Senthan Naicker, my precious mother, father and brother. Your strength, motivation and unconditional love (from near and far) has been the reason for my every success. You are the wind beneath my wings. Thank you for making it possible for me to fly.

Dedications

To my parents, Managa and Jonathan - for your never-ending support and motivation throughout this journey. Not a drop of what I have achieved would have been possible without you.

And to my brother, Senthan - you inspire me to do better and to be a better person everyday.

Abstract

The Development of a ZnO Nanoforce Biosensor for Mortalin - A Novel Biomarker for Parkinson's Disease

S. Naicker

Department of Electrical and Electronic Engineering,
University of Stellenbosch,
Private Bag X1, Stellenbosch 7602, South Africa.

Thesis: MEng (Electronic Engineering)

April 2022

Parkinson's disease, affecting 0.5 to 1% of persons aged 65 to 69 and up to 3% of persons aged 80 and older [1], is currently incurable. The typical diagnosis of Parkinson's disease is performed clinically, after the onset of symptoms, which means that progressive symptoms must be controlled, as opposed to the possibility of prevention of symptoms. Mortalin protein, a participant in various essential physiological functions, has been found to be down-regulated in the blood serum of Parkinson's disease patients and can be identified as an indicative biomarker for Parkinson's. With a biosensor for Mortalin, the antigen's concentration levels can be detected from early life stages. This introduces the prospect of preventative measures being put into place, to reduce the severity of Parkinson's disease symptoms that may develop at a later stage.

Therefore, the aim of this thesis was to develop a biosensor with the ability to detect the concentration levels of Mortalin in a biological sample. This was achieved through the development of a ZnO nanowire-based nanoforce biosensor. An electrochemical deposition process, for the deposition of well-aligned, *c*-axis orientated nanowires on Silicon substrates, was optimised. The nanowire array was further developed into a ZnO nanowire-based nanogenerator, and anti-Mortalin antibodies were immobilised onto the surface, using a Cysteamine self-assembled monolayer and a Glutaraldehyde cross-linker. The final biosensor was realised by addition

of an electronic measurement system, in the form of signal amplification and appropriate conditioning, to reduce noise and amplify the small signals generated by the nanowires. The nanoforce biosensor was tested with biological samples (solutions of Mortalin antigen in PBS) of different concentrations, and the response of the biosensor, due to the addition of each sample, was recorded. The changes in voltage, observed in the different responses, were compared and it was found that the magnitude of the response correlates with the Mortalin concentration level in the biological sample, although no clear proportionality was observed. Therefore, it was concluded that the Mortalin nanoforce biosensor was successfully able to detect the Mortalin antigen concentration. However, further testing needs to be performed to determine the relationship between the voltage response and the Mortalin concentration.

Uittreksel

Ontwikkeling van ’n Sinkoksied Nanodruk Biosensor vir Mortalien - ’n Nuwe Biomerker vir Parkinson-siekte

S. Naicker

Departement Elektries en Elektroniese Ingenieurswese,
Universiteit van Stellenbosch, Suid Afrika.

Tesis: MEng (Elektroniese Ingenieurswese)

April 2022

Geen behandeling bestaan tans vir Parkinson-siekte nie, wat 0.5 tot 1% van alle mense tussen die ouderdom van 65 en 69, en 3% van dié ouer as 80, affekteer. Die siekte word huidiglik slegs klinies gediagnoseer na die aanvang van simptome. Dit was onlangs bevind dat mortalien, ’n proteïen wat in menigde noodsaaklike fisiologiese prosesse deelneem, afgereguleer word in die bloed serum van diegene met Parkinson-siekte, asook dat dit as ’n voorspellende biomerker gebruik kan word vir die diagnose van Parkinson-siekte.

Die doel van hierdie tesis was om ’n biosensor te ontwikkel om die konsentrasie van mortalien in ’n biologiese monster te meet. Hierdie doel was bewerkstellig deur die gebruik van ’n sinkoksied nanodraad-gebaseerde biosensor. Om so sensor te ontwikkel, was ’n elektrochemiese proses aanvanklik geoptimeer vir die groei van belynde, *c*-as geörienteerde, nanodrade op ’n intrinsieke silikon substraat. Om die vervaardigde nanodrade as biosensor te gebruik, was dit in ’n nanogenerator omgeskakel deur teenliggaampies op die nanodrade te immobiliseer deur middel van ’n sisteamien self-georganiseerde monolaag en glutaaraldehied kruiskoppeling. Verder, was die finale biosensor gerealiseer deur die gebruik van elektroniese meet komponente, in die vorm van seinversterking en gepaste kondisionering om ontslae te raak van ruis en die bruikbare sein na vore te bring uit die lae potensiaalverskille geïnduseer deur hierdie soort nanogenerator. Die bogenoemde biosensor het daarin geslaag om die konsentrasie van mortalien in biologiese monsters in beplande toetse te meet.

Contents

List of Figures

List of Tables

Nomenclature & Abbreviations

Variables

m	Mass	[Gram]
v	Volume	[Liter]
I	Current	[Ampere]
L	Length	[Meter]
M	Molar mass	[Grams/mol]
V	Voltage	[Volt]
ΔV	Voltage change	[ ]

Abbreviations

3-MPA	3-Mercaptopropionic Acid
AD	Alzheimer's Disease
AFM	Atomic Force Microscope
BSA	Bovine Serum Albumin
CAS	Chemical Abstracts Service
CVD	Chemical Vapour Deposition
EDX	Energy-dispersive X-ray spectroscopy
EDC	(N-(3-Dimethylaminopropyl)-N'-ethylcarbodiimide hydrochloride
GRP	Glucose Regulated Protein
HSP	Heat Shock Protein
IgG	Immunoglobulin
ITO	Indium doped Tin Oxide

MEA Monoethanolamine

NHS N-Hydroxysuccinimide

NMO Nanostructured Metal Oxides

NW Nanowires

PD Parkinson's Disease

PEG Poly-ethylene Glycol

PMMA Polymethyl Methacrylate

POC Point of Care

POCT Point of Care Testing

SAM Self-Assembled Monolayer

SEM Scanning Electron Microscope

SPR Surface Plasmon Resonance

SPW Surface Plasmon Waves

VLS Vapour Liquid Solid

XRD X-Ray Diffraction analysis

ZnO Zinc Oxide

Chapter 1

Introduction

A ZnO nanowire-based nanoforce biosensor is designed and developed for the detection of the Mortalin protein - a novel biomarker for Parkinson's disease. The aim of this study was to produce an optimised ZnO nanowire deposition system, find the means of successfully immobilising anti-Mortalin antibodies onto the biosensor's surface, and develop a fully functional biosensor with the ability of detecting the Mortalin concentration levels in biological samples.

The binding of the Mortalin protein (antigen) to the anti-Mortalin antibody, immobilised onto a ZnO nanogenerator (to develop the nanoforce biosensor), causes bending of the ZnO nanowires and therefore the displacement of Zn cations and O anions in the ZnO crystal structure. This results in the production of piezoelectricity (an inherent characteristic of ZnO nanowires) which enables the measurement of a resulting output voltage from the nanoforce biosensor. This voltage is proportional to the concentration of the Mortalin antigen detected by the biosensor.

1.1 Motivation

Until now, Parkinson's Disease (due to the nature of its characteristics) is conventionally clinically diagnosed after the onset of symptoms. These symptoms may include slowed movement, small tremors, balancing difficulties and the reduction of handwriting size. Unfortunately, there is currently no cure for Parkinson's disease. However, there are treatments (in the form of medication and, in extreme cases, surgical procedures) that can be put in place to ease the symptoms of the disease. Often, once a patient is diagnosed with Parkinson's disease, the progression of their symptoms happens quickly and without medical treatment, there is no way to eliminate the vast effects that a Parkinson's disease diagnosis can have on a person's life.

The concentration level of Mortalin in the blood is speculated (with further research

being completed) to have a correlation with the diagnosis of Parkinson's disease. Mortalin is a protein that exists in the circulating blood of all people. However, studies have shown that patients with Parkinson's disease have lower Mortalin concentration levels than healthy people. Therefore, with a Mortalin biosensor, the levels of Mortalin in a patients blood can be detected, from early life stages, to determine the probability of developing Parkinson's disease. If the concentration level of Mortalin indicates a high chance of a patient developing Parkinson's disease, certain measures can be put into place, from early on, to reduce the symptoms that may arise during the onset of the disease. These measures include regular aerobic exercises, a healthy diet including an increased consumption of Omega-3 fatty acids, fresh fruits and vegetables and vitamin D, and any other practices that minimise the long-term progressive damage done by stress.

1.2 Research Objectives

The main objective of this study was the development of a biosensor with the ability to detect the Mortalin protein concentration in a biological sample. This overarching objective includes the following:

- The optimisation of ZnO nanowire growth using an electrochemical deposition process.
- The development of a ZnO nanowire-based nanogenerator.
- The integration of the ZnO nanogenerator into a nanoforce biosensor for Mortalin.
- The detection of different levels of Mortalin in biological samples.

1.3 Thesis Outline

Chapter One serves as an introduction, stating the motivation for the study, defining the research aims and objectives and outlining the contents of the chapters in this thesis.

Chapter Two is as a literature study and gives an overview of Mortalin and its correlation with Parkinson's disease, the different types of biosensors, deeper insight into the working of piezoelectric based biosensors and discusses the different methods that can be employed for the growth of homogeneous and well-orientated ZnO nanowire arrays. Furthermore, Chapter Two discusses

antibodies as a biosensor bio-recognition element and the strategies associated with the immobilisation of anti-Mortalin antibodies onto the surface of the biosensor.

Chapter Three gives insight into the production process of homogeneous, well-orientated ZnO nanowire arrays. The selection of the growth substrate is discussed along with the optimised substrate preparation and electrochemical deposition process developed for increased repeatability of ZnO nanowire array production. A temperature control system, aiding in the successful electrochemical deposition is also discussed. This is followed by an in-depth analysis of the ZnO nanowire arrays produced, including SEM image analysis, EDX composition analysis and XRD orientation analysis.

Chapter Four describes the methods used in transforming the ZnO nanowire arrays into working nanogenerators. The optimised PMMA spin coating procedure is discussed along with the disturbance testing performed on the nanogenerators (including tapping tests and gas pressure tests) to determine the success of the nanogenerator development. Chapter Four also discusses the design and testing of the electronic system developed for integration into the biosensor setup. This system was also simulated and the comparison between the results of the simulation and the real system are discussed.

Chapter Five lays out the antibody immobilisation strategies tested for the immobilisation of anti-Mortalin antibodies onto the surface of the nanoforce biosensor. The success of each strategy is discussed for immobilisation onto both Au-coated Si substrate samples and Au-coated ZnO nanowire array samples. Furthermore, the procedure performed for the confirmation of anti-Mortalin antibody and Mortalin antigen binding is discussed.

Chapter Six discusses the integration of the ZnO nanowire arrays with the anti-Mortalin antibody immobilisation and the electronic system to develop the final nanoforce biosensor system. The biosensor testing setup is briefly discussed, followed by a discussion of the testing procedures followed for the confirmation of the working of the Mortalin biosensor.

Chapter Seven summarises all results obtained and provides a discussion of all processes developed and followed. Chapter Seven also discusses various shortcomings experienced during this study.

Chapter Eight discusses the success of this project and makes suggestions for future improvements and testing.

Chapter 2

Literature Study

This chapter documents the literature study done on the Mortalin protein and its association with Parkinson's disease. It goes on to discuss biosensors, their purpose and the various implementations for successful biosensing. ZnO nanostructures (particularly ZnO nanowires) and their growth methods are outlined along with the piezoelectric effects that allow for the production of a ZnO nanowire-based nanoforce biosensor. Furthermore, this chapter discusses research done on biosensor bio-recognition elements, focusing on antibodies and their immobilisation methods.

2.1 Parkinson's and Neuro-degenerative Diseases

Parkinson's disease, a cumulative nervous system disorder that affects the movement of the body, is a disease for which there is currently no cure. Parkinson's disease is the second most common neuro-degenerative disorder (after Alzheimer's disease) and is most prevalent in 0.5 to 1% of persons aged 65 to 69 and up to 3% of persons aged 80 and older [1].

Due to the nature of the characteristics and symptoms of Parkinson's disease (including rest tremor, bradykinesia, rigidity and postural instability), it is typically diagnosed in a clinical manner and it is vital to recognise the early symptoms and signs suggesting parkinsonism so that treatment can begin as early as possible. Recent years have presented a vast expansion in treatments for Parkinson's disease in early and late stages, with a greater awareness of the non-motor aspects [2]. However, there is still no way of completely eliminating all symptoms experienced by patients so it is vital to tackle the complications as soon as possible.

Early testing for possible physiological indications of the development of Parkinson's disease will be beneficial for the purpose of medical clinicians recommending lifestyle changes for people that show this indication. These lifestyle changes may

include activities such as increased aerobic exercise, frequent walking and the increased consumption of green tea. There is also a speculation that people who intake more caffeinated beverages are less likely to develop Parkinson's disease [3].

Often, the initial indications of Parkinson's disease may go unrecognised because the early symptoms are subtle and transpire moderately. This means that for a patient that does not have genetic predisposition to Parkinson's disease, their diagnosis may occur far beyond the time when any preventative actions can take place. As yet, Parkinson's disease is primarily diagnosed in a clinical manner, and physiological testing is done only to confirm that there is no other underlying illness that may be causing the clinical symptoms.

2.2 Biomarker: Mortalin

2.2.1 What is a Biomarker?

According to the United States National Institute of Health Definitions Working Group, a biomarker is a "characteristic that is objectively measured and evaluated as an indicator of normal biological processes, pathogenic processes, or pharmacologic responses to therapeutic intervention" [4].

The analysis of biomarker concentrations can be used to detect measurable biological changes linked to specific diseases, or health conditions, in the body. A serological biomarker concentration level may deviate from a specified baseline level in the presence of a disease or physiological condition and tend back towards the baseline level once the condition returns to normal [5]. Biomarkers can, therefore, be used to determine the presence of a disease (diagnostic biomarkers), the likely course of the condition and response to treatments (prognostic biomarkers), the success of treatments and identify people at high risk of developing disease (antecedent biomarkers) [6].

2.2.2 Mortalin

Mortalin (mtHsp70 or GRP75), a member of the heat shock protein 70 (Hsp70) family, is a 74 kDa stress chaperone that plays a role in diseases such as cancer, neurodegeneration and generalised aging [7][8]. It is a protein that plays a part in various essential functions such as apoptosis, cellular proliferation, functional maintenance and the stress response of cells [7][9]. Mortalin, in association with numerous physiological constituents, is responsible for mitochondrial homeostasis [10], including energy metabolism, maintenance of mitochondrial protein integrity and the correct folding and refolding of proteins [7].

Through a study conducted by Wadhwa *etal*., it was found that the level of Mortalin is upregulated in many human tumor tissues and cells and that the upregulation of Mortalin is related to various malignant properties in human cells [9]. It is possible that present inflammation and other stress responses cause a secretion of Mortalin into circulation from metastatic cells and non-cancerous tissues as Mortalin plays a role in the stress response of cells [11]. According to Rozenburg *etal*., in a study done on elevated levels of Mortalin in the blood of colorectal cancer patients, higher serum Mortalin levels correlated with faster disease progression and patients with higher levels of Mortalin had a higher hazard or mortality and a shorter median survival time [11]. It is, therefore, suggested that the elevated levels of Mortalin expression contribute to tumorigenesis [9].

Mortalin also plays a crucial role in reducing the toxicity of Lewy bodies [10]. Lewy bodies, intracellular elements found in various neuro-degenerative diseases, are closely related to the pathology of Parkinson's disease, dementia with Lewy bodies and Alzheimer's disease [12]. Lewy bodies are closely correlated with progressive cognitive dysfunction and are part of the neuro-pathological spectrum found in an Alzheimer's disease brain [13]. This forms a link between Lewy bodies, Parkinson's disease and Alzheimer's disease. Lewy bodies are composed predominantly of the protein α-synuclein [13][14], which was found to have a negative correlation with Mortalin in Parkinson's disease [10]. Some of the major known risk factors associated with Parkinson's disease are protein misfolding, aggregation and abnormal accumulation of the protein α-synuclein [10]. It can, therefore, be concluded that serum Mortalin levels are down-regulated in neuro-degenerative diseases and that Mortalin can be a target for Parkinson's disease diagnostics.

Table 2.1 shows the expected down-regulated circulating Mortalin levels that were found to be indicators of Parkinson's disease. As it can be seen, compared to the levels in a healthy person's blood, the Mortalin concentration level in Parkinson's disease serum has been found to be down-regulated.

Table 2.1: Mortalin concentration levels.

Disease	**Mortalin Concentration Range**	**References**
No disease	$3.13 \pm 0.48\,\mu g/ml$	[10]
Parkinson's disease	$1.98 \pm 0.53\,\mu g/ml$	[10]

The level of circulating Mortalin expression can, due to the information in Table 2.1, be used as a diagnostic, prognostic and antecedent serological biomarker for Parkinson's disease.

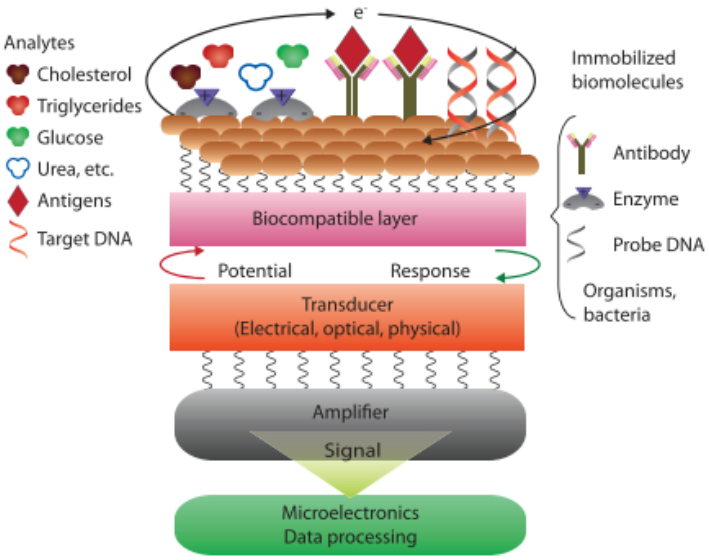

Figure 2.1: Operating principles of a biosensor [16]

2.3 Biosensors

2.3.1 What is a Biosensor?

According to the International Union of Pure and Applied Chemistry, a biosensor is "a device that uses specific biochemical reactions mediated by isolated enzymes, immunosystems, tissues, organelles or whole cells to detect chemical compounds usually by electrical, thermal or optical signals". From this definition, it can be deduced that there are three vital components that make up a biosensor[15]:

1. A biological element that can sensitively and specifically detect a bio-recognition element. This phase typically involves the binding of a biological recognition element to the biological target on the biosensor.

2. A transducer element with the ability to transform the biological interaction process into some sort of quantifiable signal. This may include various aspects such as the detection of a change in mass, a change in voltage or a change in impedance during the biological interaction.

3. An electronic element that can read the signal from the transducer element and convert or transform it into user-friendly data. This phase is vital in transforming raw data into readable information, possibly by amplifying the signal, filtering out noise or by performing data processing procedures.

Figure 2.1 shows a schematic of a typical biosensor. In this schematic, it can be seen that there will be a biological interaction between the bio-recognition elements (such

as antibodies, enzymes or probe DNA) and the corresponding target analytes (such as antigens, glucose or target DNA) which will cause a signal to be sent through a transducer towards some sort of electronic process. The bio-recognition elements are typically designed, manufactured or reproduced with a particular specificity to the target analyte.

The bio-recognition elements are immobilised, using a tested immobilisation strategy, onto a biocompatible layer (such as gold or carbon films) that is coated onto the transducer element. This biocompatible layer is important in order to ensure that the transducer elements do not interfere with the functionalisation and biological properties of the bio-recognition elements.

There are various transducer elements that are designed to perform different functions, such as detecting the levels of light intensity through a sample (optical), changes in electrical charge, temperature, voltage, current or mass. Depending on the type of analyte that needs to be sensed, different transducer methods would be suitable for the various applications.

In the next section, different transducer mechanisms will be considered and the most suitable method will be selected for the application with the required bio-marker (target analyte), Mortalin, that is relevant to this study.

2.4 Transducer Mechanisms

2.4.1 Optical-based Biosensors

Optical-based biosensors provide an effective method of analysis due to their high sensitivity, small size and cost-effectiveness. The most common optical biosensor applications are based on Surface Plasmon Resonance (SPR) or fluorescence integrated with optical fibres [17]. Optical biosensors are attractive because they are able to provide real-time and label-free detection of biological substances. However, the integration of optical biosensing with nanodevices and the cost of mass-production of optical biosensors are two major drawbacks that are still to be overcome [18].

2.4.1.1 Surface Plasmon Resonance (SPR)

Surface Plasmon Resonance (SPR) biosensors, an application of label-free optical biosensing, depend on an electromagnetic phenomenon in which surface plasmon waves (SPW) are utilised to determine the interactions between biological molecules [19]. SPR biosensors are useful for providing information on non-covalent interactions of biological molecules, including antibody-antigen interactions [20]. The interaction between the target antigen and the immobilised antibody on the surface

of the sensor causes a change in the refractive index at the sensor surface. Energy is resonantly transferred into the SPW, due to the excitation of a SPW by an optical wave, and SPR acts upon the resonant absorption of the energy of the optical wave. By analysing the interaction between the SPW and the optical wave, the change in the optical parameters of the transduction medium can be measured [21][18].

Table 2.2 shows the advantages and disadvantages of SPR biosensors.

Table 2.2: Advantages and disadvantages of SPR biosensors [5].

Advantages	**Disadvantages**
Non-invasive detection	Non-specific binding of target to other surfaces
Real-time assay and continuous measurement	Quality of immobalisation affects sensor performance
Suitable for label-free detection	Complex data analysis
High sensitivity	Steric hindrance related to binding
Small sample quantity needed	Limitations in nano-applications [18]

2.4.2 Electrochemical Biosensors

According to the International Union of Pure and Applied Chemistry (IUPAC), "an electrochemical biosensor is a self-contained integrated device, which is capable of providing specific quantitative or semi-quantitative analytical information using a biological recognition element (biochemical receptor) which is retained in direct spatial contact with an electrochemical transduction element" [22].

The application of electrochemical biosensors is attractive due to the low cost of production, short analysis/response time and high sensitivity and specificity [18][5]. Electrochemical biosensors also have the capability of being used for point-of-care testing (POCT) by untrained personnel [5].

Electrochemical biosensors can be separated into four categories (according to their analyte detection technique used): impedance, potentiometric, amperometric and conductometric, and voltammetric.

Electrochemical impedance spectroscopy (EIS) uses the principle of impedance, the ability of a circuit to resist electrical current flow, to measure the current of a cell by an applied AC potential to an electrochemical cell [18]. The impedance, a measure of the hindered flow of ions in a solution, can be used to indicate the concentration of a specific biomarker in a sample.

Potentiometric biosensor measurements rely on the potential difference between two electrodes (either an indicator and a reference node or two reference nodes) separated by a permselective membrane, when no current is flowing between them.

This potential difference is proportional to the accumulation of ions at the surface of the membrane [22][5].

Amperometric sensors measure the change in current, when a constant voltage is applied, resulting from oxidation and reduction of an electroactive sample species. The analytical value detected by the biosensor is deduced from the proportional relationship between this measured current and the concentration of the species in the sample [23]. If the voltage applied is varied, the biosensor is known as voltammetric [5].

Conductometric biosensors measure the change in electrical conductivity of a solution using two electrodes, separated by a distance. This change in conductivity is due to the change in the ionic species concentration produced by the reaction of the bio-recognition process on the sensor's surface [18].

2.4.3 Piezoelectric Biosensors

Piezoelectric biosensors, based on the principle of piezoelectricity, have been greatly researched and improved over the last decade. Many piezoelectric biosensors, with the ability to produce highly sensitive and stable results, have been made commercially available and are being successfully implemented in many research facilities [5]. Piezoelectricity, derived from the Greek work *piezo* meaning to squeeze or press, is the combination of a material's mechanical and electrical behaviour. When a stress is applied, an electric charge is induced in a material, which can be seen as a sensing signal [24]. Piezoelectricity is a reverse process during which a crystal elongates or compresses once it is put in an electric field [25]. The piezoelectric effect can convert mechanical motion into an electric signal and vice versa.

Piezoelectric sensors, which are sensitive to changes in mass, density and viscosity of samples on their active surface, have various advantages, which include the rapid sensitive detection of biological molecules. Piezoelectric sensors are also known to be one of the best implementations for point-of-care testing (POCT) and applications [5]. The advantages and disadvantages of piezoelectric biosensors and shown in Table 2.3 below.

Table 2.3: Advantages and disadvantages of Piezoelectric biosensors.

Advantages	**Disadvantages**
Rapid and sensitive disease detection for diagnosis [5]	Sensitivity depends on a large range of factors [24]
Provides stable results [5]	Technical difficulties [24]
Good temperature stability [5]	Immobalisation of antibodies affects sensor performance [5]
Small sample quantity needed [5]	Mechanical character, enclosure and sample handling systems can all affect sensor performance [18]
Wide and dynamic range of applications [24]	
High selectivity for target molecules (antibodies) [24]	

2.4.4 Piezoelectric Nanogenerators

Nanotechnology-based devices have been of great interest in recent years due to the low-power consumption and specificity in bio-sensing devices. One of the only drawbacks in the use of nano-material devices is that, because the power consumption is very low, it is often difficult to supply power to these devices while keeping them at the nano-scale [26]. Piezoelectric nanogenerators eliminate this issue entirely due to the principle of piezoelectricity - the phenomenon which allows for nanoscale mechanical energy to be converted into electrical energy.

The principle of a piezoelectric nanogenerator relies on the fact that upon an external disturbance, such as a vibrational disturbance, a sonic wave of an external mass being applied to a nanowire array, bending will occur in the nanowire arrays. When this lateral bending takes place, a voltage drop occurs over the nanowires in the array [26] - referred to a Piezoelectricity. In short, this means that if a mass is added onto a ZnO nanowire array, it will cause the nanowires in the array to bend, and this will result in an electronic voltage signal that can be measured over the terminals of the nanowire array. When the nanowires are caused to bend laterally, the resulting voltage drop that occurs over the nanowire's cross section has a positive voltage on the tensile side and a negative voltage on the compressive side, if the electrode at the nanowires' base is grounded [26]. This potential difference is induced by the displacement of the O^{2-} anions relative to the Zn^{2+} cations in the nanowires (due to the piezoelectric effect of the wurzite crystal structure). It is important to note that the potential difference in the nano-wires is only present for the time that the mechanical deformation is actually taking place.

Figure 2.2 shows a representation of how the charge builds up in the different ar-

eas of a ZnO nanowire upon mechanical deflection (bending). The straight ZnO nanowire (Figure 2.2 (a)) is bent, which causes a strain field to be created in the nanowire. When a nanowire is deflected in a specific direction, the outer surface is stretched and positive strain is present, and the inner surface is compressed which induces negative strain (Figure 2.2 (b)). An electric field is created along the length of the nanowire (in the z-direction). This electric field can be represented by Equation 2.1 where ε_{NW} is the strain in the nanowire and d is the piezoelectric constant:

$$E_{NW} = \frac{\varepsilon_{NW}}{d} \tag{2.1}$$

Through simplification, this electric field is converted to a electric potential difference that ranges from $+V^T$ at the stretched side to $-V^C$ at the compressed side (Figure 2.2 (c)), provided that the base of the nanowire is grounded, as mentioned before.

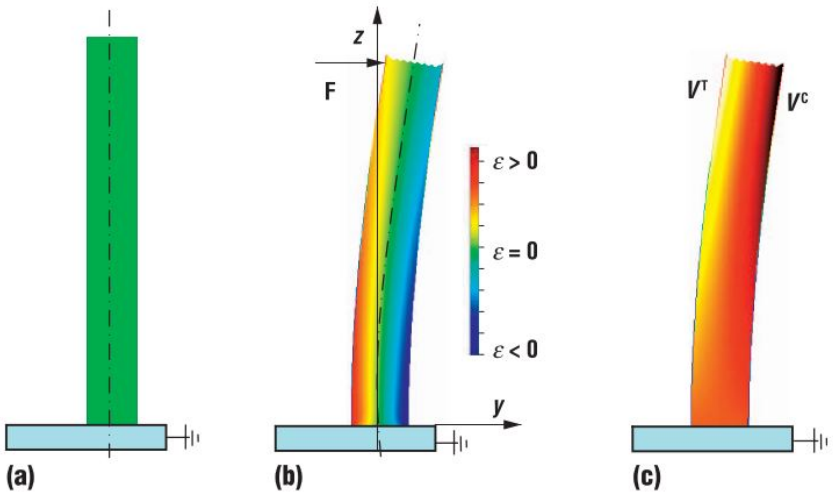

Figure 2.2: Charge building in a ZnO nanowire upon bending [26]. (a) A vertical, straight nanowire without deflection, (b) A bent nanowire with a strain field being created in the nanowire, (c) Due to the piezoelectric effect, the strain field causes an electric field in the nanowire which is converted to a potential difference across the nanowire.

In order to successfully measure the induced potential difference in the nanowires, a Schottky barrier, formed as a result of the semiconductor-metal interface between the ZnO nanowires and Au-coating, is required. With the presence of the Schottky barrier, rectifying the piezoelectric signal, a potential difference can be measured due to the accumulation of charge in the nanowire (upon deformation) and the release of charge (upon relaxation). A Schottky barrrier enables the measurement of a resulting output voltage across a resistor [25].

Due to the presence of a Schottky barrier, it is possible to measure the voltage drop

(potential difference) across the two ends of a nanowire and in turn, over the two terminals of a nanowire array - where the one terminal is a metal layer below the nanowire array and the other is the metal-semiconductor interface on top of the nanowire array.

For this study, a ZnO piezoelectric nanogenerator will be developed as the transducer for the Mortalin biosensing application. This is based on the fact that, if the ZnO nanowire-based nanogenerator is developed successfully, the instrumentation and electronics needed for the biosensor application and the confirmation of the working of the biosensor are readily available and are not expensive to acquire (as opposed to that of electrochemical biosensor applications). To achieve this, the ZnO nanowire production and the processes followed for the development of the nanogenerator will have to be iteratively optimised.

For the application of a ZnO nanowire-based nanogenerator in a ZnO nanoforce biosensor, it is possible to obtain the relationship between the nanoforce and the voltage generated in the piezoelectric nanowires.

2.5 Zinc Oxide Nanostructures

Nanostructures can be organised into different classes, namely [27]:

- Zero-dimensional (0D) - including quantum dots and nanoparticles;
- One-dimensional (1D) - including nanowires, nanorods, nanofibres, nanobelts, and nanotubes;
- Two-dimensional (2D) - including thin films and sheets.

ZnO structures are simply described as multiple alternating planes of tetrahedrally organized O^{2-} and Zn^{2+} stacked along the c-axis (the typically vertically aligned, unique symmetry axis in tetragonal crystal structures [28]). ZnO has different polar surfaces, the most common being the basal plane [0001]. This basal plane has one end which stops with partly positive zinc lattice sites and another end which stops with partly negative oxygen lattice cites. These oppositely charged produce positively chared Zn surfaces and negatively charged O surfaces and result in spontaneous polarization along the c-axis. This $\pm$[0001] surface is inherently atomically flat and stable. The other two most common surfaces are $[2\tilde{1}\tilde{1}0]$ and $[01\tilde{1}0]$ which are non-polar [29]. Due to the lower energy, the area of these two surfaces are typically maximised. Figure 2.3 shows the surfaces and their directions of growth translated onto x, y and z axes.

Figure 2.3: Axial orientations of ZnO surfaces [30]

A wide range of unique ZnO nanostructures can be grown by adjusting the rate of growth along these three primary directions: [2$\tilde{1}\tilde{1}$0] ($\pm$ [$\tilde{1}$2$\tilde{1}$0], $\pm$ [2$\tilde{1}\tilde{1}$0], $\pm$ [$\tilde{1}\tilde{1}$20]); [01$\tilde{1}$0] ($\pm$ [01$\tilde{1}$0], $\pm$ [10$\tilde{1}$0], $\pm$ [1$\tilde{1}$00]) and $\pm$ [0001] [29].

Figure 2.4 shows various ZnO nanostructures that have been successfully fabricated using a variety of fabrication methods.

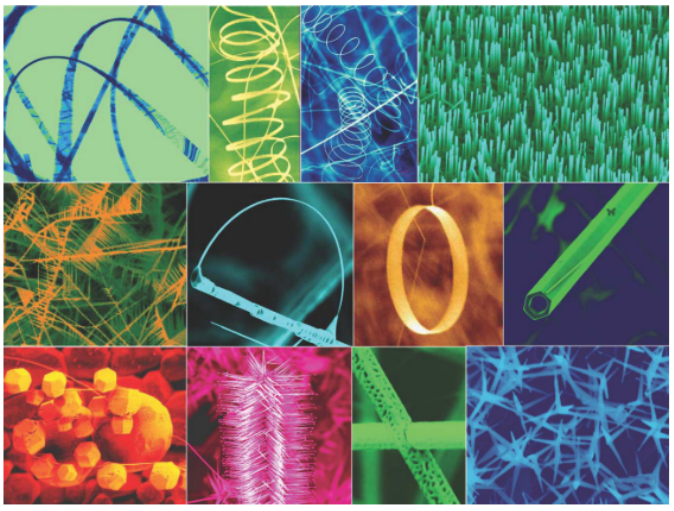

Figure 2.4: Different ZnO nanostructures that have been successfully fabricated [31]

Recently, 1D nanostructures have been under the spotlight in the nanoscience and nanotechnology realms [29].

2.5.1 Zinc Oxide Nanowires

Zinc Oxide (ZnO), widely used to produce piezoelectricity in various electro-mechanical devices and biosensors [32], is one of the most abundant groups of nanostructures among the entire one-dimensional (1D) nanostructure family [33]. ZnO has three major advantages that has resulted in its widespread popularity. Firstly, ZnO is a semiconductor with a large excitation binding energy of 60 meV and a direct wide bandgap or 3.37 eV [33][34]. Secondly, ZnO is bio-safe and biocompatible and can, therefore, be used in many biomedical applications without any insulation or concern of contamination and toxicity. Lastly, due to its non-centrosymmetric crystal structure (the absence of a centre of symmetry in its wurzite structure [29]), ZnO is piezoelectric and hence, is popularly used in electro-mechanical biosensing [33][35][36]. Figure 2.5 shows the wurzite structure of ZnO. As opposed to bulk

ZnO, ZnO nanostructures have mechanical properties (especially Young's modulus) that allow ZnO nanowires to produce more mechanical strain energy. This strain energy can be converted, by the piezoelectric effect, into detectable electrical energy [30]. Lending to these advantages, as well as the fact that ZnO has a high resistivity to severe environments [34] and an improved compatability with biological activities, it is one of the best prospects for the production of biosensor devices [36].

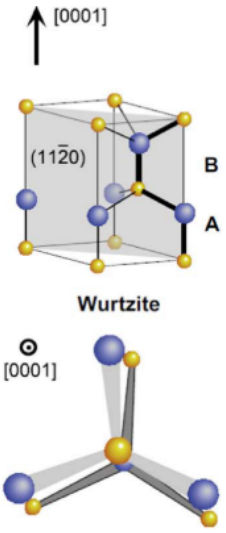

Figure 2.5: Stick and ball representation of the wurzite structure of ZnO [37]

ZnO nanowires (ZnO NW) and other nanostructured metal oxides (NMO) have been surrounded by great amounts of attention for the production of biosensors with high levels of sensitivity and efficiency [16]. NMO enable enhanced electron-transfer movement and a high level of adsorption, which allows for efficient immobilisation of biomolecules [18]. The successful immobilisation of biomolecules onto a ZnO NW array depends largely on the size, shape and characteristics of the NW [36]. It is imperative to produce well-aligned ZnO NW of a high quality to successfully produce nanoscale biosensing devices [38].

2.6 ZnO Nanowire Fabrication Methods

In this section, various ZnO NW synthesis methods will be discussed. A variety of ZnO nanostructures (nanowires, nanorods, nanorings and nanotubes etc.) have been successfully grown using methods including chemical vapour deposition, thermal evapouration, electrodeposition, sol-gel, polymer assisted growth, hydrothermal growth and vapour transport synthesis methods [39][40].

2.6.1 Vapour-Liquid-Solid Growth

The widely used vapour transport synthesis method can be grouped into the vapour-solid (VS) process, which is catalyst free and the vapour-liquid-solid (VLS) process, which is a catalyst assisted process. The VLS process forms the control over the geometry, alignment and location of the ZnO nanostructures during their growth [40][39], is easier to perform and is more cost effective than other vapour deposition methods [38]. In the VS process, nanostructures are produced by the process of deposition when a solid is formed directly from the vapour phase. In the VLS process, different nanoparticles or nanoclusters (e.g. Au, Cu, Sn etc.) are used as catalysts. The VLS process involves vapour (composed of the resultant solid components), liquid (eutectic alloy catalyst) and solid (the resultant precipitated nanostructures) phases [41]. Figure 2.6 shows a schematic diagram of the process of the VLS growth method.

The metal catalyst forms eutectic alloy droplets at each catalyst site at a high temperature by adsorbing the vapour components (Figure 2.6(b)). Supersaturation of the liquid droplets, which may be due to the variation in vapour pressure or the temperature at which this process takes place, occurs (Figure 2.6(c)). The nucleation and growth of solid ZnO nanowires take place as a result of this supersaturation (Figure 2.6(d)).

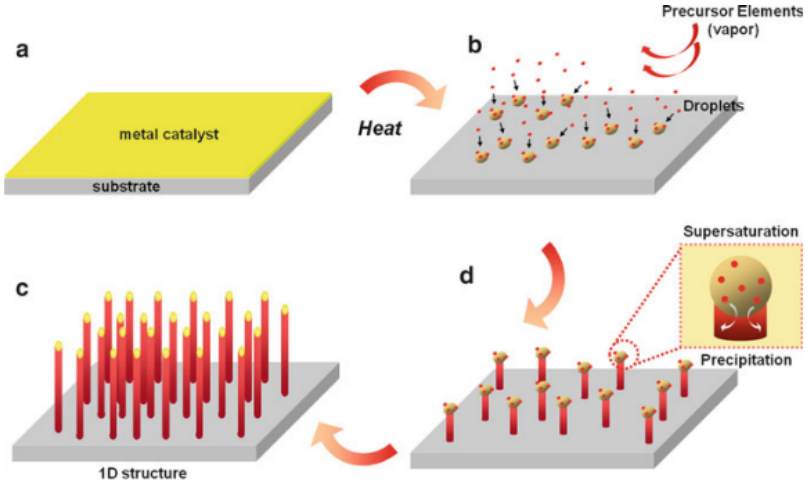

Figure 2.6: VLS growth process [41]

2.6.2 Hydrothermal Growth

The hydrothermal growth method is a type of solution phase synthesis that takes place in an aqueous solution. Although the hydrothermal growth method is cheaper, can be achieved at lower temperatures and is simpler than vapour phase synthesis methods [42], hydrothermally grown wires have more crystalline flaws than others

- mainly due to oxygen vacancies [27]. According to Zhang *etal*., the hydrothermal process of the growth of vertically aligned ZnO NW on a substrate is as follows [27]:

1. A fine seeding layer of ZnO nanoparticles, which progresses nucleation for the growth of nanowires, is planted onto a chosen substrate.
2. An alkaline reagent (such as hexamethylenetetramine) and Zn^{2+} mixture aqueous solution is used as a growth solution.
3. The ZnO seeding layer is retained in this growth solution at a specific temperature for a specific amount of time.
4. The resulting substrate and growth layer is rinsed and left to dry off.

A common growth solution (precursor) is the combination of hexamethylenetetramine ($(CH_2)_6N_4$ or HMT) and $Zn(NO_3)_2$. The chemical reactions that take place with this precursor can be expressed by the following equations:

Decomposition reaction:

$$(CH_2)_6N_4 + 6H_2O \longrightarrow 6HCHO + 4NH_3, \tag{2.2}$$

Hydroxyl supply reaction:

$$NH_3 + H_2O \longleftrightarrow NH_4^+ + OH^- \tag{2.3}$$

Supersaturation reaction:

$$2OH^- + Zn^{2+} \longrightarrow Zn(OH)_2 \tag{2.4}$$

ZnO nanowire growth reaction:

$$Zn(OH)_2 \longrightarrow ZnO + H_2O \tag{2.5}$$

Chen *etal*. successfully fabricated ZnO nanowires on an inidium tin oxide (ITO) glass substrate using a hydrothermal growth method. Figure 2.7 shows the process followed.

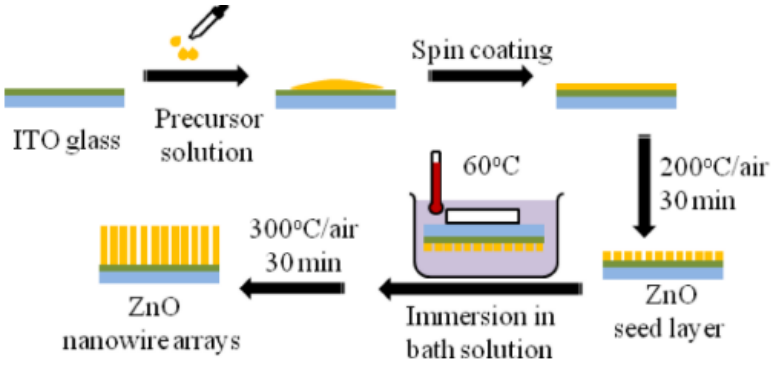

Figure 2.7: Hydrothermal growth process [43]

2.6.3 Electrochemical deposition

Similarly to the hydrothermal growth method, the electrochemical deposition growth method of ZnO nanowires takes place in an aqueous solution, in this case referred to as an electrolyte. The difference between hydrothermal growth and electrochemical deposition of ZnO nanowires is that this process does not only require heat as a catalyst of the nanowire growth, but a supply voltage too and the growth process takes place inside an electrochemical (electrolytic) cell.

An electrolytic cell is a system in which work is done on a chemical process by providing an electric current through the system. It consists of two half-cells, one reduction half-cell (the cathode) and one oxidation half-cell (the anode). Figure 2.8 shows the typical construct of an electrolytic cell. It can be seen that electrons are deposited from the anode onto the cathode. This means that in an electrochemical deposition process of ZnO nanowires, the substrate onto which the ZnO nanowires are to be deposited should be attached to the cathode (the negative terminal).

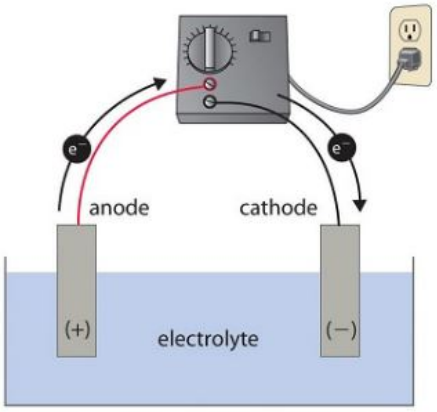

Figure 2.8: The basic construct of an electrolytic cell [44]

It is important to note that, in an electrolytic cell, the parameters and conditions under which the reduction-oxidation reaction takes place are vital in performing

successful electrochemical deposition of ZnO nanowires [44]. ZnO nanowire orientation, dimensions (length and diameter) and density are affected by [45]:

1. The composition, consistency and thickness of the seed layer deposited onto the growth substrate.
2. The concentration of the electrolyte/growth solution present in the electrolytic cell.
3. The density of the charge supplied to the electrolytic cell (the supply voltage and the current running through the system).

The main advantages of the electrochemical deposition of ZnO nanowires include the fact that, due to the addition of the voltage catalyst, both the the time and the temperature required for a complete, consistent array of nanowires to be "grown" is greatly reduced, compared to the hydrothermal growth method. Another aspect to consider is that, with the electrochemical deposition method, depending on the size of the equipment and cells, the amount of chemicals used during the growth of the ZnO nanowires can be greatly reduced. This means that if the growth parameters for the electrochemical deposition of ZnO nanowires can be optimised, the efficiency of development of ZnO nanowire arrays for, but not limited to, biosensor applications can be improved.

Due to the above-mentioned points, one of the main focus points of this study will be the optimisation of the electrochemical deposition growth method of ZnO nanowires, specifically for point-of-care biosensor applications.

2.7 Bio-recognition Elements

As discussed previously in Section 2.3.1, biosensors are designed to sensitively and specifically detect a certain bio-recognition element that is identified as an indicator or biomarker for a particular disease. Various biological elements (such as DNA, aptamers, enzymes and antibodies) are used for different biosensor applications. This study will be specifically focusing on antibody-antigen interaction as the bio-recognition component due to Mortalin being the biomarker of interest.

2.7.1 Antibodies

Antibody-based biosensors are the most common type of biosensors. Antibodies are produced by living systems as a mechanism to fight off unwanted bacteria and viruses intruding the body. With a combination of hydrogen bonds and non-covalent

interactions, antibodies bind to proteins (antigens) with a high specificity. This binding takes place at a binding site on the antibody that is specific to its complementary antigen. Figure 2.9 shows a typical antibody-antigen interaction.

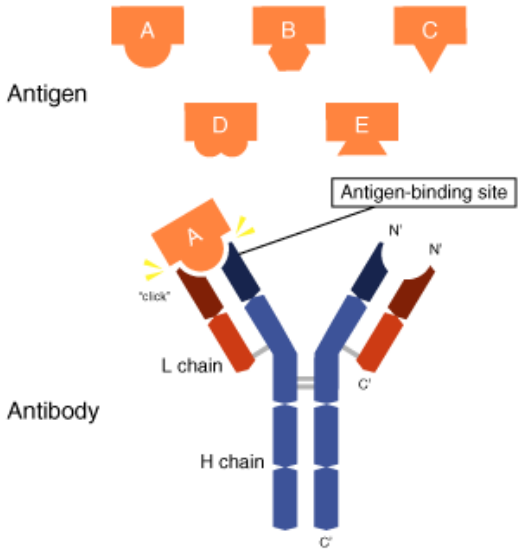

Figure 2.9: Antibody-Antigen interaction [46]. A-D represent the different antigens that are available for binding. The antibody is specific to antigen A.

Antibodies consist of two heavy chains (referred to as H-chains) and two light chains (L-chains) that are arranged in a Y-shape with the antigen binding site found at the tip of the 'Y'. Because each binding site has a high specificity for the complementary antigen, antibodies are the ideal biological element for use in biosensor applications.

There are 5 different isotypes (namely IgG, IgM, IgA, IgD and IgE) of antibodies and different antibodies are classified according to the arrangement of their H-chains. Each isotype performs a different function or role and these are summarised in Figure 2.10.

For biosensor applications, IgG antibodies are ideal because they are found in the circulatory system (and are therefore easily accessible) and, if correctly orientated on the surface of a biosensor, the antigen binding sites can be readily available for the detection of antigens in a biological sample.

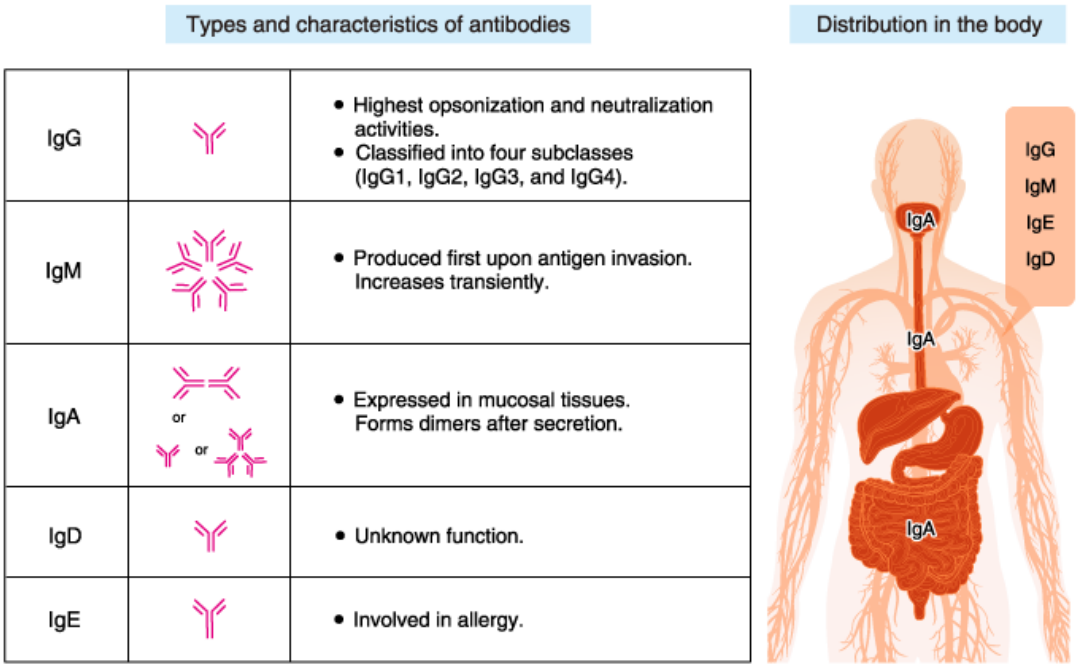

Figure 2.10: Antibody isotypes and their functions [47]

2.8 Antibody Immobilisation Strategies

Immobilisation is commonly defined as the attachment of molecules to a surface resulting in reduction or loss of mobility [48]. The immobilisation of proteins onto gold/gold-coated substrates has become widely used in many applications, including that of biosensors. In this study, anti-Mortalin antibodies are to be immobilised onto gold-coated ZnO nanowires as the biological element on a ZnO NW-based nanoforce biosensor. This makes the detection and quantification of the bioregocnition element (Mortalin antigen), in blood serum, possible.

The various protein immobilisation strategies, developed over the years, can be seen in Figure 2.11. The choice of which strategy to employ is typically based on the physiochemical properties of both the protein and the surface onto which it is to be immobilised. In this study, binding immobilisation strategies are going to be the primary focus. There are three main principles upon which these developed strategies are based, namely physical adsorption, covalent immobilization and streptavidin-biotin immobilization [49][48].

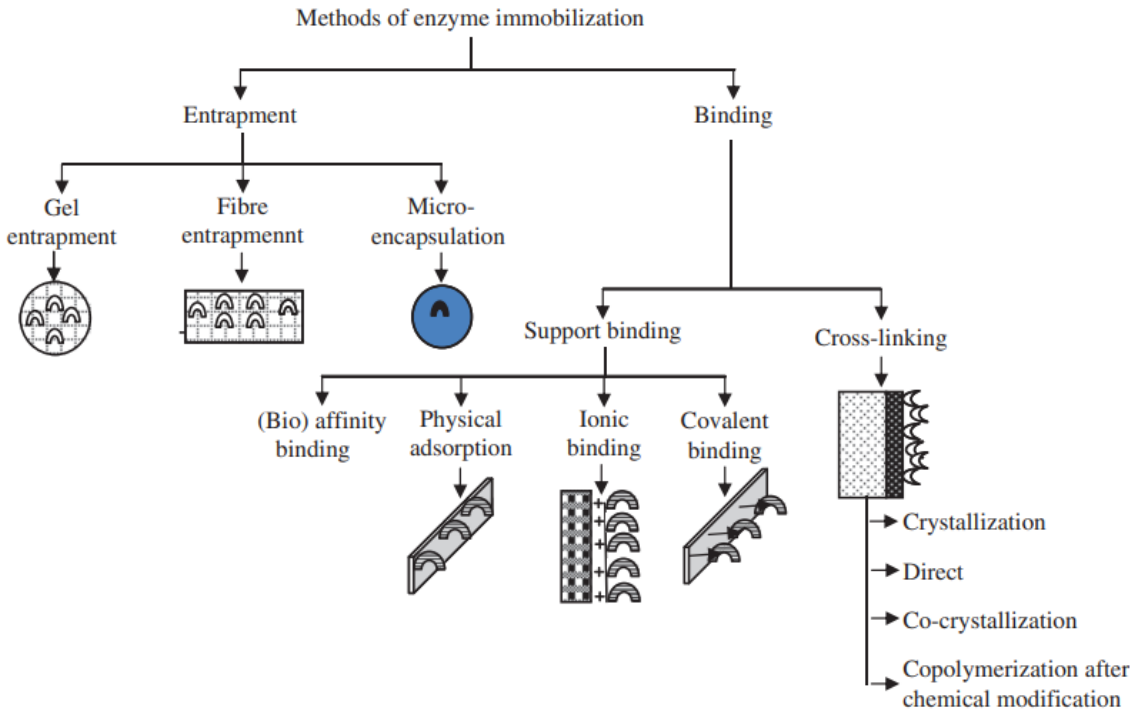

Figure 2.11: Protein immobilisation strategies [50]

The chosen immobilisation method not only determines the orientation, reactivity, stability and accessibility [48] of the immobilised proteins, it also dictates the biological properties and characteristics of the immobilised microarray. Some immobilisation strategies result in the complete loss of protein activity, caused by random orientation and physical deformation. To maintain full biological working order of the immobilised proteins, a strategy that will not affect the structural integrity and the functional properties of the proteins must be selected [49].

The selectivity and sensitivity of a biosensor relies largely on the successful immobilisation of the bio-recognition element [48]. Therefore the immobilisation process must be controlled to ensure the successful and specific binding of correctly orientated antibodies. Correctly orientated immobilised protein assays result in an antigen binding capacity that is two to eight times higher than if the proteins are randomly orientated [51], so this is a crucial consideration when deciding on the method to use.

2.8.1 Physical immobilisation

Physical adsorption is by far the simplest method of immobilisation, but there are various drawbacks that limit the ability to use this method to successfully immobilise antibodies for biosensor applications. Proteins adsorb onto different surfaces using intermolecular forces, such as polar and hydrophobic interactions, and ionic

bonds [49]. The intermolecular forces that play a role in the adsorption process are largely dependant on what surfaces and proteins are involved, and typically result in randomly orientated protein layers. This is because molecules can form bonds in many different orientations that minimise repulsive relationships with the substrate surface. Steric blocking of active protein sites and steric hindrance, which is the slowing or prevention of chemical interactions, may occur due to high-density packing and this can interfere with the functional properties of the proteins.

Alongside the random orientation of proteins that have been physically immobilised with adsorption, some of the drawbacks of physical immobilisation include large amounts of noise and background signals due to non-specific protein interactions [49], and denaturation of the proteins [51]. This results in poor reproducibility which is counter-productive in biosensor applications.

2.8.2 Covalent Immobilisation

Covalent immobilisation involves the binding of proteins to a substrate by making use of accessible functional groups of exposed amino acids. Covalent immobilisation is a more stable method that results in better reproducibility, but can also result in incorrect protein orientation, which in turn can lead to the loss of binding ability.

Covalent bonds, primarily made between side-chain-exposed functional groups of proteins and appropriately modified supports on substrates, result in irreversible binding and high surface coverage. Although the outcome of chemical binding (by use of exposed side chains on amino acids) is often randomly orientated proteins, there are many defined procedures that result in reproducible and correctly orientated protein arrays, where denaturation is prevented. For site-specific covalent immobilisation, it is necessary to functionalise either the substrate surface, the molecules, or both [49].

The addition of the self-assembled monolayer (SAM) technique to the immobilisation method is known to provide stable covalent binding as it makes way for flexibility regarding terminal functionality, correctly orientated proteins and it aids in the prevention of non-specific binding in biosensor applications. Additionally, a SAM provides increased stability under harsh pH and temperature conditions and practicable reusability [51]. A SAM comprises of ordered molecular sites of different organic materials that amplify the bio-compatibility of a substrate's surface and prevent the denaturation of proteins during the immobilisation process.

2.8.3 Bioaffinity Immobilisation

The biotin-streptavidin immobilisation technique has been one of the affinity methods gaining the most interest due to its ability to greatly increase the stability and sensitivity of immunosensors. This is a simple, two-step, method that is typically unaffected by external factors such as pH, temperature and organic solvents. It includes the biotinylation of the surface, onto which the proteins are to be immobilised, using a cross-linker substance. This is followed by the addition of streptavidin before the proteins can be added [48].

The biotin-streptavidin strategy has proven to have good management of the orientation of the immobilised proteins, which is a vital factor in the development of a working biosensor. However, the downfall of this immobilisation strategy is that the proteins need to be labelled with biotin (biotinylated) before immobilisation [52]. This is an extremely expensive process to perform.

2.9 Conclusion

This chapter described Parkinson's disease and the correlation between the disease and its biomarker, Mortalin antigen. Studies have shown that the Mortalin antigen, present in the blood circulation system of all humans, is down-regulated in Parkinson's disease patients. Due to these concentration differences, Mortalin can be used as a diagnostic, prognostic and antecedent serological biomarker for Parkinson's disease.

Biosensors and their various constituents were also discussed. The different transducer methods, including optical, electrochemical and piezoelectric, were discussed and the decision to develop a ZnO nanowire-based nanogenerator was made. The decision to use a ZnO nanowire-based nanogenerator as the transducer method for the Mortalin biosensor was based on the fact that the costs, materials and instrumentation required for this method can be minimised compared to the other biosensing methods. ZnO nanowire-based nanoforce biosensors show fantastic potential in biosensor applications because they do not require any isolated power input and can be used to perform point-of-care testing.

The production processes for ZnO nanowire arrays were discussed and the electrochemical deposition process was chosen as it requires the lowest growth time and temperature when compared to the other methods. During this study, the parameters used for the electrochemical deposition of ZnO nanowire arrays will be optimised to produce well-orientated, homogeneous nanowire arrays consisting of nanowires with the smallest possible diameter. This will affect the sensitivity of the ZnO nanowire-based nanoforce biosensors.

Finally, antibodies, as a biological element for biosensor applications, were discussed along with their various immobilisation strategies. In this study, a few strategies will be tested to determine the most effective immobilisation of anti-Mortalin antibodies onto the surface of the nanoforce biosensor.

Chapter 3

Zinc Oxide Nanowire Growth

This chapter documents the synthesis of ZnO nanowire arrays, on silicon 100 (Si(100)) wafers, via electrochemical deposition. Each step of the process will be discussed in detail and all information regarding parts and materials used will be provided. The preparation of the Si wafer substrates will be discussed, followed by a discussion of the preparation of the electrochemical cell system that was developed. A simple temperature control system was implemented to control the temperature of the electrolyte. This control system assists with the optimised growth of the ZnO nanowire arrays and will be briefly discussed. A comparison of the nanowires synthesised under different growth parameters will be provided, and finally, the success of the ZnO nanowire deposition will be analysed using scanning electron microscopy (SEM), EDX (Energy Dispersive X-ray) and XRD (X-ray Diffraction).

3.1 Introduction

The controlled deposition of well aligned, homogeneous ZnO nanowire arrays for a nanowire-based nanoforce biosensor is essential. The uniformity of the nanowire array, the orientation of the nanowires, and the dimensions of the nanowires determine the sensitivity and repeatability of the biosensors. The deposited ZnO nanowire arrays form the primary component of the nanoforce biosensor transducer and, therefore, every step of the nanowire array synthesis process is to be optimised.

There are various ZnO nanowire synthesis methods that have been developed recently, including the vapour-liquid-solid (VLS) method, the hydrothermal growth method and the chemical vapour deposition method. In this study, the electrochemical deposition method for ZnO nanowire growth was studied and optimised in order to minimise growth time, temperature and the usage of materials.

3.2 Methodology and Equipment

This section will give a brief overview of a few of the essential techniques used and methods followed in the process of the deposition of well-aligned ZnO nanowire arrays on Si(100) substrates. The deposition of ZnO nanowires on Si substrate involves various intricate processes that need to be performed precisely in order to ensure the deposition of nanowires that are correctly orientated and have the desired dimensions.

3.2.1 Silicon wafer preparation

The Si wafers were cleaved with a diamond-tipped scribe. The wafers were first cut perpendicularly to the "primary flat" which is the side of the wafer that has a flat cut-out shape. This is because if the wafer is chipped at the edge of this "flat", it will automatically break in a perfectly straight line, perpendicular to the flat. Initially, long strips with a width of 10 mm were cut and these were then cut into smaller 10 mm $\times$ 10 mm sample sizes, using the diamond-tipped scribe. To clean the wafer samples, they were placed in a beaker, filled with the respective solutions, and put into an ultrasonic bath. An ultrasonic bath, with both temperature and time control, was used, running at 40 Hz and high power. The wafers were then dried on a temperature controlled hot plate to rapidly evaporate any solvents left over from the ultrasonic cleaning process.

From this point, it became vital to only handle the wafer samples with laboratory tweezers and gloves to prevent contamination of the samples with oily substances that are present on bare fingers.

All gold (Au) coating in this study was done using the Leica EM ACE200 vacuum coater (Leica Microsystems, Germany). The coating was done in increments of 10 nm to not put any strain on the conductive coater.

3.2.2 ZnO seed layer preparation and deposition

The solute was measured using a calibrated micro-scale and the solvents were measured using calibrated pipettes before being added to a beaker. A magnetic bead was placed inside the beaker and the beaker was placed on a temperature controlled magnetic stirrer.

Parafilm was used to seal the beaker to prevent the evaporation of any of the seed layer solution and an infrared thermometer was used to ensure that the magnetic stirrer was set to the correct temperature setting.

A spin coater, with an integrated speed controller and timer, was used for the deposition of the seed layer onto the Si wafers. The seed layer solution was deposited onto the wafers using a calibrated pipette.

The wafers were once again dried on the hot plate, before being placed in the furnace for annealing. A furnace, that can reach temperatures of over 700°C and that would not contaminate the samples with dust particles, was required for this annealing process.

3.2.3 ZnO nanowire electrochemical deposition

The electrolyte used in the electrochemical deposition process was mixed using a laboratory spatula after the solute was weighed using the micro-scale and the solvent was measured in a measuring cylinder.

The electrochemical (electrolytic) cells were made up of 30 ml vials, containing the samples and the electrolyte, and toothless crocodile clips (both seen in Figure 3.4) were used to hold the zinc rods and Si substrates in place for the electrochemical deposition of the ZnO nanowires.

A desktop power supply was used to supply voltage to the electrochemical cells and a temperature sensor (TSIC306, RS Components) was used to determine the temperature of the electrolyte solution during the electrochemical nanowire deposition process. The temperature control system used in this process is described later in Section 3.6.

3.2.4 ZnO nanowire analysis

The ZnO nanowire analysis was done to determine the dimensions and consistency of the nanowire arrays, to determine the elemental composition of the nanowires, and to observe the orientation of the nanowires in the arrays deposited using the electrochemical deposition process.

In order to visually observe the dimensions of the ZnO nanowires, the Zeiss MERLIN SEM (Carl Zeiss Microscopy, Germany) was used with the SmartSEM (Zeiss electron imaging) software. An In-Lens detector was used to pick up all the secondary electrons being emitted from the samples, due to the high energy beam voltage (EHT) that was set. The accelerating voltage (EHT) of the beam was set to 5 kV and the beam current (which determines the spot size of the beam) was set to 90 nA in all SEM applications during this study. The beam size affects both the brightness and resolution of the images produced.

The EDX analysis was also performed using the Zeiss MERLIN SEM unit and Oxford Aztec (Oxford Instruments, Oxfordshire OX13 5QX, UK) software.

Figure 3.1(a) shows the ZnO nanowire array samples on the aluminium stage that is inserted into the SEM unit (shown in Figure 3.1(c)). Figure 3.1(b) shows that the samples were typically mounted onto a glass slide using carbon double-sided adhesive tape, before being put onto the stage. This is to minimise the risk of breaking samples when removing them from the stage.

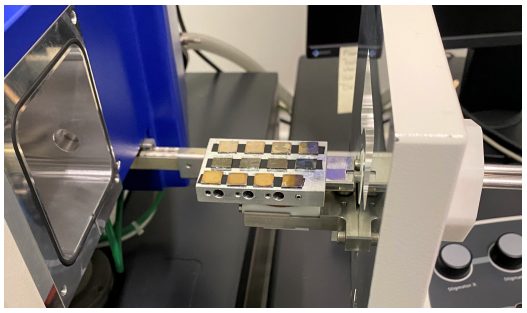

(a) Samples on aluminium stage

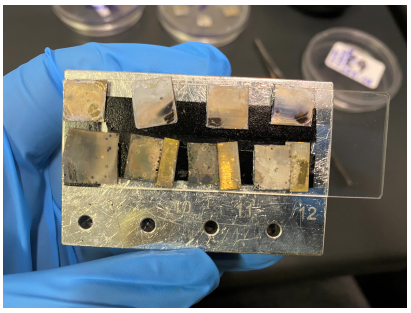

(b) Samples on aluminium stage with glass slide

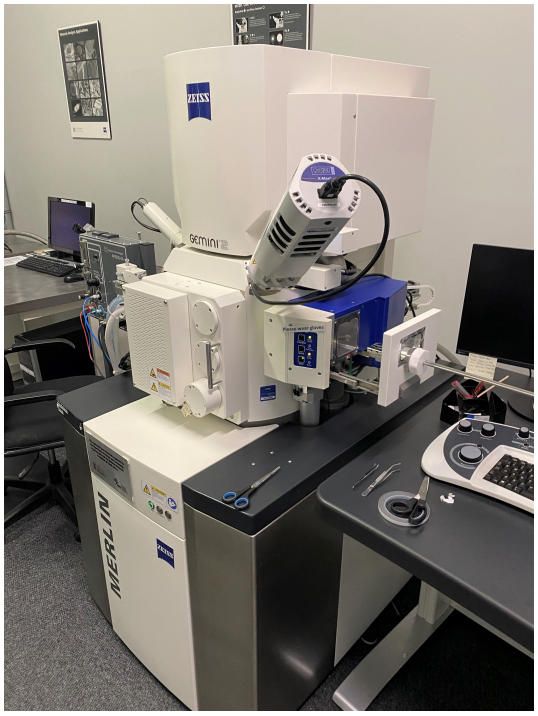

(c) Zeiss MERLIN SEM unit

Figure 3.1: Zeiss MERLIN SEM and samples

The XRD measurements were performed using a multi purpose X-ray Diffractometer D8-Advance (Bruker AXS, Germany), where the sample is mounted in the centre of the sample holder, on a glass slide. The measurements taken in this study were run within the 2θ range of 15° to 90° with a step size of 0.034°. A position sensitive detector (PSD), Lyn-Eye, was used to record the diffraction data at a typical speed of 0.5 seconds per step. To evaluate the data, the EVA (Bruker AXS, Germany) software was used with the ICDD database (1999). Figure 3.2 shows the x-ray diffractometer

used in this study.

Figure 3.2: X-ray Diffractometer D8-Advance

3.3 Silicon Wafer Preparation

P-type Si(100) wafers were cut into 10 mm $\times$ 10 mm sample sizes using the method discussed in Section 3.2. The Si samples were ultrasonically cleaned for 10 minutes in acetone, followed by a 10 minute sonication in a 1:1 volume ratio mixture of DI water and 70 % ethanol. This is done to remove any oil, dust, organic matter, or pieces of Si that has collected on the sample during and after cleaving. Remnants of the DI water and ethanol mixture were blown off the samples with nitrogen gas and the samples were left to dry on a hotplate at 150°C for 5 minutes.

A 40 nm layer of gold (Au) was deposited onto the samples using the Leica EM ACE200 (Leica Microsystems, Germany), as discussed in Section 3.2.

3.4 ZnO Seed Layer

A homogeneous and even seed layer, consisting of ZnO nanoparticles, was deposited onto the Si wafer samples using the sol-gel spin coating method.

The chemicals used to mix the ZnO seed layer solution are shown in Table 3.1. The ZnO solution was prepared with 2-methoxyethanol as the solvent, zinc acetate di-

hydrate ($Zn(CH_3COO)_2{\cdot}2H_2O$) as the precursor and monoethanolamine (MEA) as the stabiliser [53].

Table 3.1: Chemicals used in ZnO seed layer preparation.

Chemical Name	CAS Number	Supplier
2-Methoxyethanol	109-86-4	Sigma-Aldrich
Monoethanolamine	141-43-5	Sigma-Aldrich
Zinc acetate dihydrate	5970-45-6	Sigma-Aldrich

A 0.1 M ZnO solution is required and the required molar ratio between the zinc acetate dihydrate precursor and the MEA stabiliser is 1:1. When mixing 50 ml of the ZnO solution, the following steps were followed (calculations can be found in Appendix A):

1. Mix 1.1 g zinc acetate dihyrate into 50 ml 2-methoxyethanol.
2. Place on magnetic stirrer at 60°C for 15 to 20 minutes until the precursor crystals are completely dissolved.
3. Add 302.4 µl MEA to the solution.
4. Place on magnetic stirrer at 60°C for 2 hours. The white, cloudy solution should transform into a clear, homogeneous ZnO solution.
5. Store the solution for 24 hours before deposition.

A spin coater was used for the deposition of the ZnO sol-gel solution onto the Si wafer samples. A dry-start spin coating method was followed and 15 µl of the solution was dropped onto a sample spinning at 3000 rpm for 30 seconds. The samples were then left to dry on a hot plate at 200°C for 5 minutes. This process was followed four times to ensure that an even seed layer was deposited onto the Si samples.

The samples were annealed in a conventional furnace at 700°C for 10 minutes to remove the organic component and solvent of the sol-gel solution. Figure 3.3 shows a flow chart of the ZnO seed layer creation process.

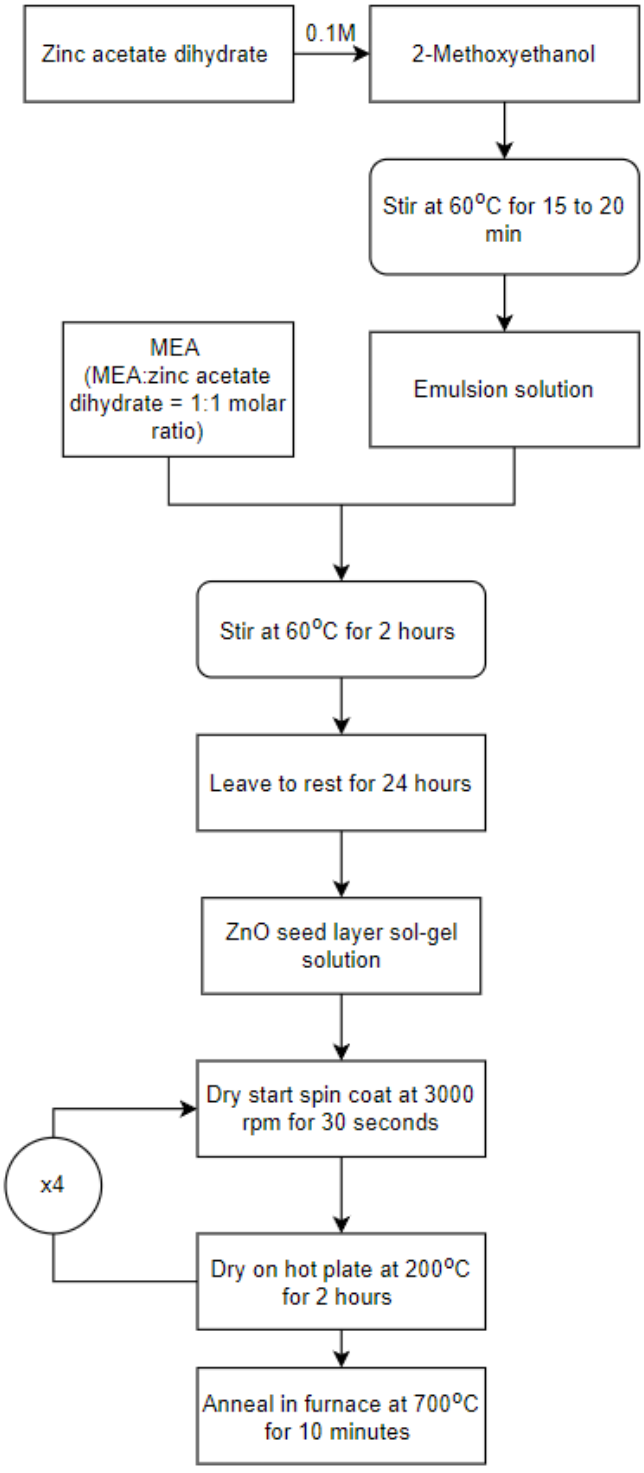

Figure 3.3: ZnO seed layer process

3.5 Electrochemical Deposition of ZnO Nanowires

The even and precise deposition of the ZnO nanowires is one of the essential components in the development of a ZnO nanowire-based nanoforce biosensor. An

electrochemical deposition method was chosen to be perfected for this project because there are multiple advantages in using this method:

1. The ZnO nanowire growth time is less than 1 hour.
2. The materials needed for the growth are minimal which reduces chemical waste.
3. The method is cost and time effective.
4. The equipment needed was readily available and not difficult to procure.

An electrochemical setup, with four electrochemical cells, was created for the electrochemical deposition of ZnO nanowires onto the prepared Si samples. Each cell has a volume capacity of 30 ml which minimises the use of materials that form the electrolyte. The small volume of the cells also allows for the temperature of the cells to be easily controlled during the deposition process. Figure 3.4(a) shows an example of the electrochemical (electrolytic) cells used for the growth of each sample and (b) shows the electrochemical deposition setup used for the simultaneous growth of four samples. In Figure 3.4(b), the fifth vial, containing the temperature sensor used for the temperature control system, can also be seen.

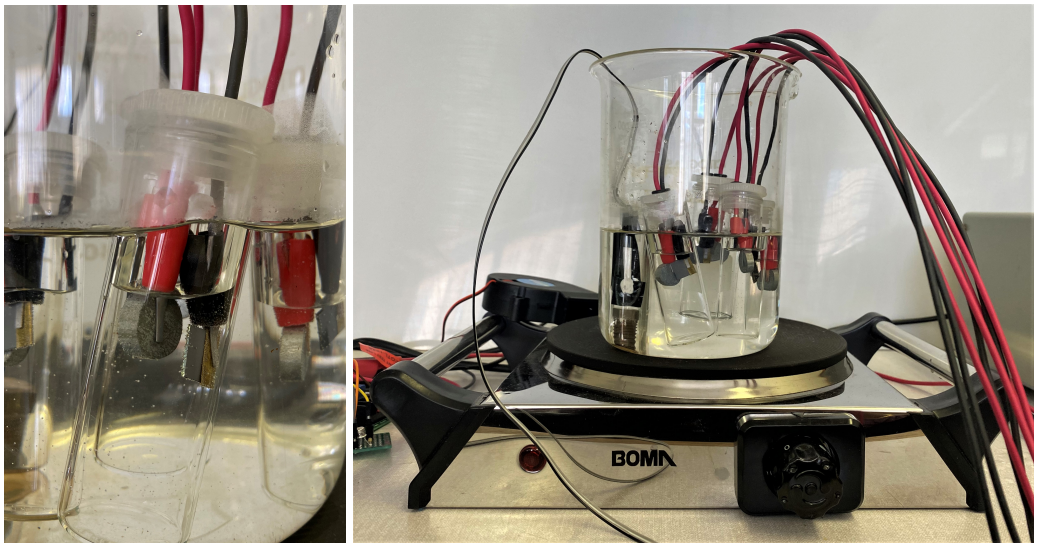

(a) Electrochemical (electrolytic) cell

(b) Electrochemical deposition setup

Figure 3.4: Final electrochemical deposition setup

The electrolyte solution was made up of DI water and zinc nitrate hexahydrate (Sigma-Aldrich, CAS 10196-18-6) and has a molar concentration of 1 mM. Because there are four cells in the electrochemical setup, 100 ml of the electrolyte solution

was made by mixing 0.0298 g of zinc nitrate hexahydrate in 100 ml of DI water. Approximately 25 ml of the electrolytic solution was placed in each cell. Due to the direction of material flow in an electrolytic cell as discussed in Section 2.6.3, a zinc rod (Sigma-Aldrich, CAS 7440-66-6) is attached to the positive terminal and acts as the cathode and the Si sample, onto which the ZnO nanowires are to be deposited, acts as the anode of the system and is attached to the negative terminal of the electrochemical (electrolytic) cell. The electrochemical cells were controlled at 70°C, by placing the cells in a temperature controlled water bath, and a voltage of 1 V was applied over the terminals of the cell. The supplied voltage was terminated after 1 hour.

Each sample was removed from its respective cell, rinsed with DI water and left to air dry. This rinsing was done in order to remove any extra remnants, salts or broken fragments of nanowires that accumulated on top of the perfectly orientated ZnO nanowire array, deposited during the time in the electrochemical cell. Finally, the ZnO nanowire-Si samples were placed in a furnace at 350°C for 30 minutes to sterilise the samples and prepare them for the antibody immobilisation procedure.

3.6 Electrochemical Cell Temperature Control System

A simple temperature control system was implemented in order to regulate the temperature of the electrochemical cells at 70°C. The regulation of the temperature of the electrolyte in the electrochemical cell is vital, during the deposition process of ZnO nanowires, because the temperature of the electrolyte affects the dimensions of the ZnO nanowires deposited onto the Si wafer during the electrochemical deposition process.

When designing the temperature control system for the electrochemical deposition process, various aspects and specifications were to be considered. These aspects include the following:

- How does the ambient temperature affect the system?
- How stable does the temperature need to be?
- Will there be any large disturbances affecting the temperature of the electrolyte?
- What is the most efficient method of controlling the temperature of the electrolyte?
- How fast does the electrolyte need to be able to reach the desired temperature?

3.6.1 Temperature control concept 1

Initially, the electrochemical cells were placed onto a hot plate set at 70°C, in a cell holder, shown in Figure 3.5. In this setup, the hot plate was set at 70°C, but due to the holder being used, the cells were only making contact with this input temperature through the bottom surface with a surface area of 490 mm^2. This resulted in the average temperature of the electrolyte being 52.58°C in a laboratory with an ambient temperature of 23°C.

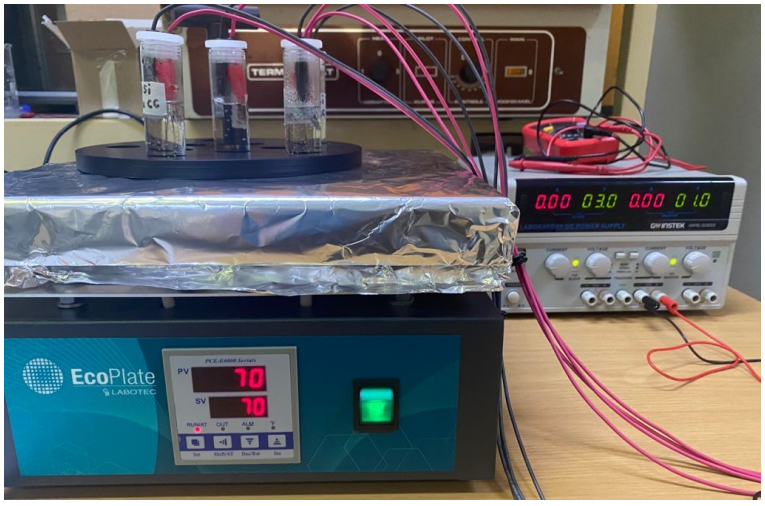

Figure 3.5: Electrochemical Deposition Setup 1

3.6.2 Temperature control concept 2

In order to more effectively control the temperature of the electrolyte solution, a water bath was included into the system to maximise the surface area of the electrochemical cell that comes in contact with the heating component. The inclusion of the water bath increased the surface area of the vile, in contact with the heating component, to 4418 mm^2. Using the commercial magnetic stirrer hot plate seen in Figure 3.6, the water in this bath was regulated to approximately 70°C, and due to the efficient heat transfer properties of the glass walls of the cells, the electrolyte was successfully regulated at 70°C too.

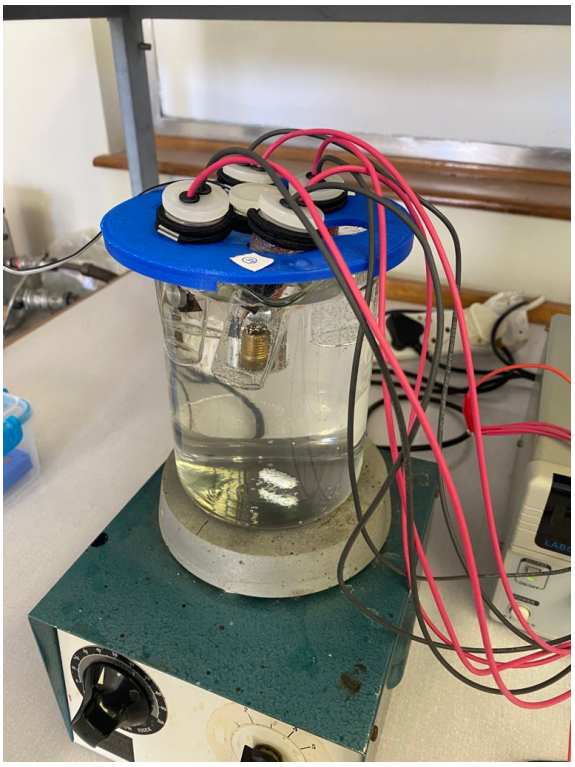

Figure 3.6: Electrochemical Deposition Setup 2

Although the temperature of the electrolyte was able to be controlled using this setup, the hot plate seen in Figure 3.6 did not have any built-in temperature control mechanisms and the heat setting of the hot plate was required to be manually controlled during the electrochemical deposition process. This was not ideal due to the time-consuming nature of the manual control of the temperature of the hotplate. Therefore, it became necessary to design and implement an automatic temperature control system that could effectively control the temperature of the electrolyte.

3.6.3 Automatic temperature control concept 1

When designing the automated temperature control system for the ZnO nanowire electrochemical deposition setup, the requirement of efficiency was a high priority during this study, due to the amount of times that growth of the ZnO nanowires was to be repeated. Therefore, an induction heater was considered as the heating element for the water bath containing the electrochemical cells. Induction heating is the process by which electrically conductive materials are heated by means of electromagnetic induction. This is done by the transfer of heat through some electromagnetic coil, in which an electromagnetic field is created. If a conductive material is placed within reach of this electromagnetic coil, it will be heated. Therefore, this concept involves placing the water-bath beaker, containing a conductive metal plate, on an electromagnetic bifilar coil. Through the principles of induction heat-

ing, the metal plate would be heated, in turn heating the water inside of the water bath. By controlling the power sent to the bifilar coil, it would be possible to control the amount of energy sent through the coil, therefore controlling the temperature of the water.

Figure 3.7(a) shows the induction module that was procured for the implementation of this concept. This is a low-voltage induction module requiring a DC power supply of 12 to 48 V and is rated with a maximum current of 20 A for a maximum power supply of 1000 W. Figure 3.7(b) shows the various bifilar coils that were made out of wires of different current ratings for this implementation.

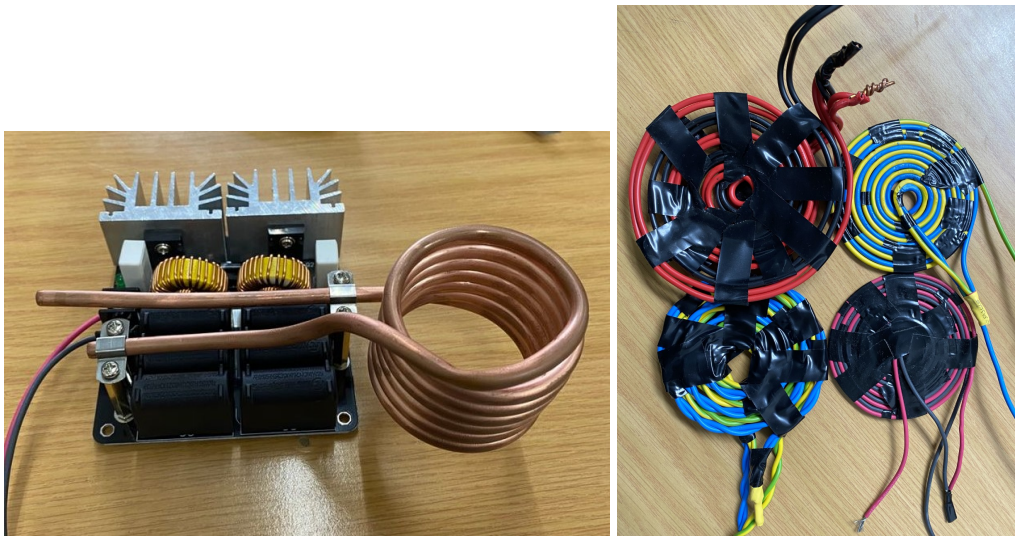

(a) Induction heating module (b) Bifilar coils

Figure 3.7: Induction heating concept

After extensive trial-and-error testing with commercial wiring, it was deduced that the current being sent through the wiring was exceeding the limits of each available option. This means that the wiring was being heated and the insulation on the wiring was being melted in every case. Therefore, it was concluded that a suitable bifilar coil was to be manufactured out of copper tubing for the successful implementation of this induction heating system and this concept was deemed impractical under the time constraints of this project.

3.6.4 Automatic temperature control concept 2

The final concept for the automated control of the temperature of the electrochemical cells, in which the electrochemical deposition of ZnO nanowires onto Si substrates took place, includes the control of the power supplied to a basic kitchen hot plate.

The power supplied to a 220 V hot plate is to be regulated such that the temperature of the water bath, and in turn the temperature of the electrolyte in the electro-

chemical cells, can be regulated at approximately 70°C. To do this, a solid state relay (SLA-12VDC-S L-C, MicroRobotics, Stellenbosch) was used to control the 240V AC power supplied to the hot plate with a PWM duty cycle of 60% implemented. A TSIC306 temperature sensor (RS Components) was used to transmit the temperature of the water bath back to the micro-controller (Arduino UNO). A simple 12 V fan was also included in the system to cool down the hot plate, once the desired temperature was reached, as the materials out of which the hot plate was produced retain heat. Figure 3.8 shows the electronic connections used for the implementation of this temperature control system and the Arduino code can be found in Appendix B.

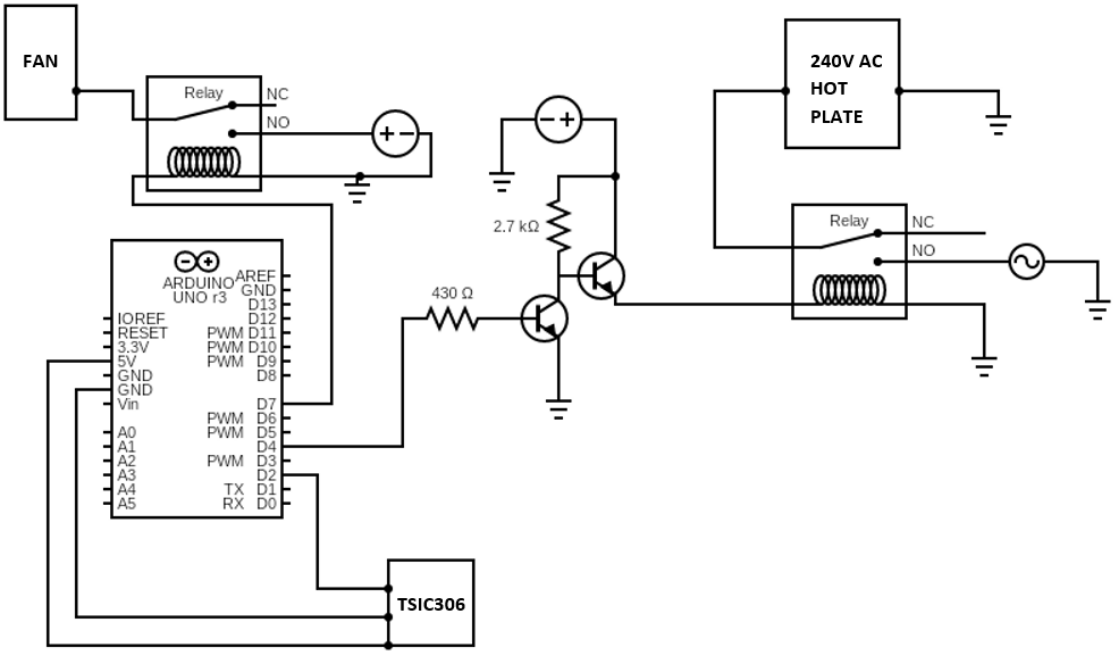

Figure 3.8: Schematic of electronic setup for the automatic temperature control system

Figure 3.9 shows the final setup of the ZnO nanowire electrochemical deposition system including the hot plate temperature control system.

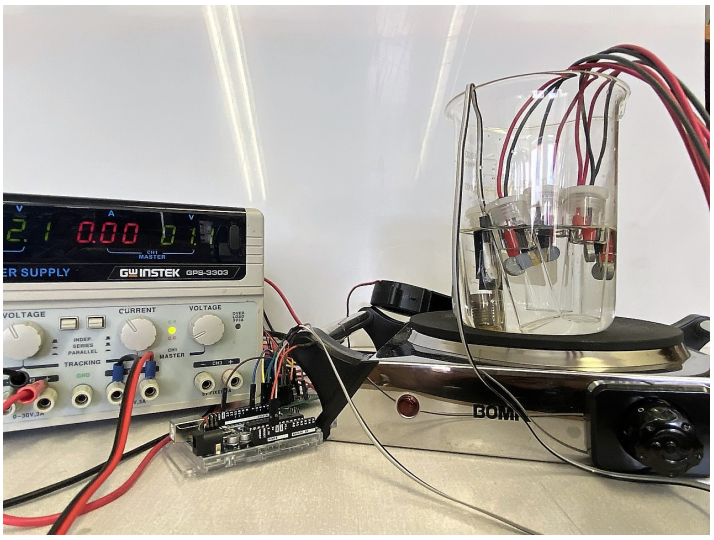

Figure 3.9: Final electrochemical deposition setup with temperature control system

3.6.5 Electrochemical cell temperature control system results

Using the system described in Section 3.6.4, the temperature of the electrolyte in the electrochemical cells was successfully controlled between 69.8 and 70.4°C (as seen in Figure 3.10). The desired temperature was achieved in approximately 7 minutes. This is not as fast as the anticipated heating time with the successful implementation of the induction heating concept, but this time was still deemed as appropriate for the application of the temperature control system in this study.

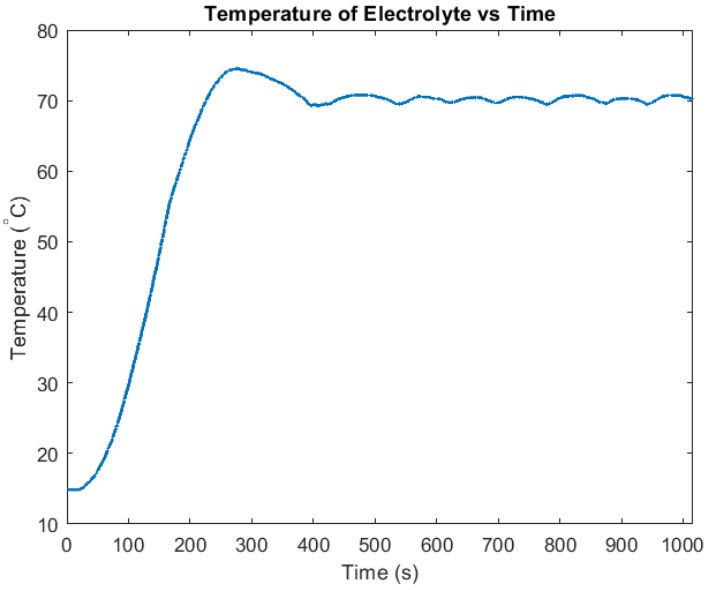

Figure 3.10: Temperature control system results

Figure 3.10 shows that the temperature of the electrolyte was stable at 70°C (±0.4°C) for an extended period of time. This means that the temperature control for the

electrochemical (electrolytic) cells was successfully implemented.

3.7 Analysis of ZnO Nanowires

The ZnO nanowires, electrochemically deposited following the methods discussed in Sections 3.3 to 3.5, were characterised by the following methods:

1. Visual analysis - to determine whether the deposition process was successful at first glance.
2. SEM (Scanning Electron Microscopy) imaging - to determine the dimensions (including the diameters and lengths) of the nanowires.
3. EDX (Energy Dispersive X-ray) spectroscopy - to determine the elemental composition of the nanowires.
4. XRD (X-ray Diffraction) - to determine the orientation of the nanowires in the nanowire arrays.

3.7.1 Visual analysis of samples

When the electrochemical deposition optimisation process in this study first began, it was difficult to determine whether nanowires were actually being deposited onto the Si substrates without performing SEM image analysis. As useful as the images acquired during SEM analysis are, the process of using a SEM imaging device is expensive and requires planning far in advance. Therefore, a visual representation at "first glance" became a useful strategy to determine whether an electrochemical deposition run may have been successful, or not.

Figure 3.11 shows samples before (a) and after (b) ZnO nanowires were deposited via electrochemical deposition. The samples numbered '15'-'18', in Figure 3.11(a), are seed layer coated samples that were also placed in the electrochemical cells. However, the polarity of the voltage for the deposition process was switched. Therefore, no ZnO nanowires were deposited onto these samples. The samples numbered '25'-'28', in Figure 3.11(b), underwent an electrochemical deposition process with correct polarity and therefore, ZnO nanowires were successfully deposited onto these samples. As can be seen, samples in Figure 3.11(a) have a shiny appearance, whereas the samples in Figure 3.11(b) have a white, cloudy, layer on them. This cloudy appearance indicates the deposition of ZnO nanowires on the substrate.

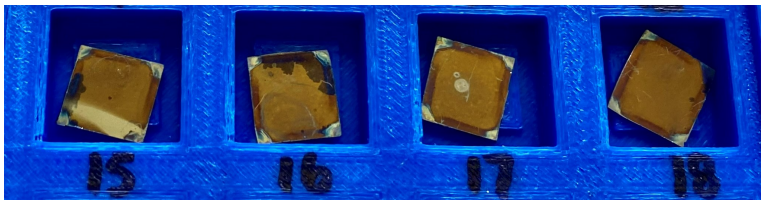

(a) Si substrate with no ZnO nanowires deposited

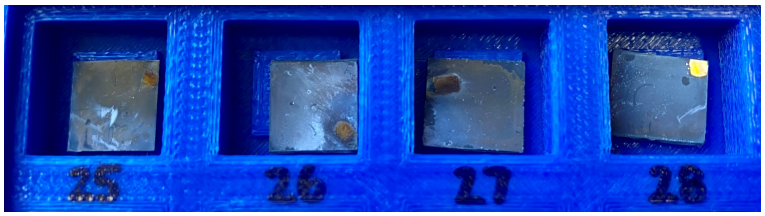

(b) Si substrate with ZnO nanowires deposited

Figure 3.11: Visual analysis of Si samples (a) with and (b) without nanowires deposited

As can be seen in Figure 3.11(b), on samples '25' and '26', the cloudy layer can also be inconsistent in colour and thickness on different areas of the sample. Figure 3.12 shows a masked sample (masking to be discussed later, in Chapter 4) that was grown under optimised parameters with thoroughly cleaned equipment. As can be seen, the portion of the sample (top) with the cloudy layer is also completely smooth and the layer is consistent all throughout the sample. This indicates the presence of a homogeneous array of ZnO nanowires.

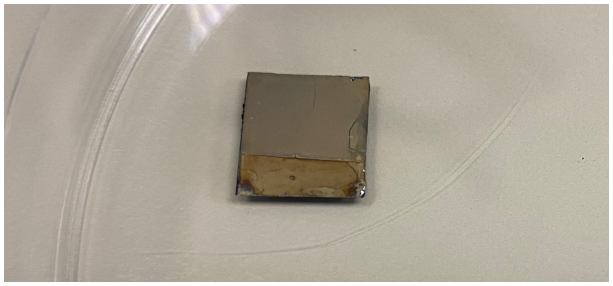

Figure 3.12: Sample 'B' grown under optimised parameters

3.7.2 SEM image analysis of nanowires during optimisation process

Using the MERLIN SEM by Zeiss with the parameters and specifications discussed in Section 3.2.4, highly magnified images of the ZnO nanowires, deposited onto various materials, were acquired.

These SEM images proved to be invaluable in the analysis of the ZnO nanowires deposited during this study, because they provided a visual representation of the dimensions and orientations of the electrochemically deposited nanowires. The correct diameters, lengths and orientations of the ZnO nanowires, as mentioned in pre-

vious sections in this chapter, are vital components in achieving the required sensitivity of the nanoforce biosensors being developed.

In a previous study on a ZnO nanowire-based nanoforce biosensor, performed by Tom [54], it was determined that ITO (indium tin oxide) coated glass slides were the ideal substrate to use for the deposition of ZnO nanowires. This was due to the fact that the ITO coating on the slides acts as a "seed layer" for the growth of the ZnO nanowires, and it was not necessary to deposit an additional ZnO-based seed layer onto the substrate (as would be required on a Si substrate). The possibility of being able to eliminate the seed layer deposition step of the ZnO nanowire synthesis process was an attractive thought, because the ZnO seed layer deposition process is complex and time-consuming. This process can lead to badly orientated ZnO nanowires being deposited onto the substrate, in the event that the steps are not carried out correctly.

To test the theory of ITO-coated glass slides being the ideal substrate onto which correctly orientated ZnO nanowires can be deposited, the following test was performed:

A Si wafer sample, coated with a ZnO seed layer (following the process described in Section 3.4), and a commercially-bought ITO-coated glass slide (Sigma-Aldrich, CAS 50926-11-9) sample were both placed in the same electrochemical deposition setup (as described in Section 3.5). It was ensured that the samples were correctly orientated in the electrochemical cells to confirm the likelihood of the deposition of well aligned ZnO nanowire arrays. This means that the face of the glass slide sample with the ITO coating, and the top side of the Si wafer, were placed facing the Zn rod in the electrochemical cell. All parameters aside from the growth substrate were kept constant during this test.

Figure 3.13 shows the results of this test. As can be seen, the nanowires grown on the Si substrate (shown in Figure 3.13(a)) are better aligned with the c-axis (the axis perpendicular to the growth substrate) than the nanowires grown on the ITO-coated glass substrate (shown in Figure 3.13(b)).

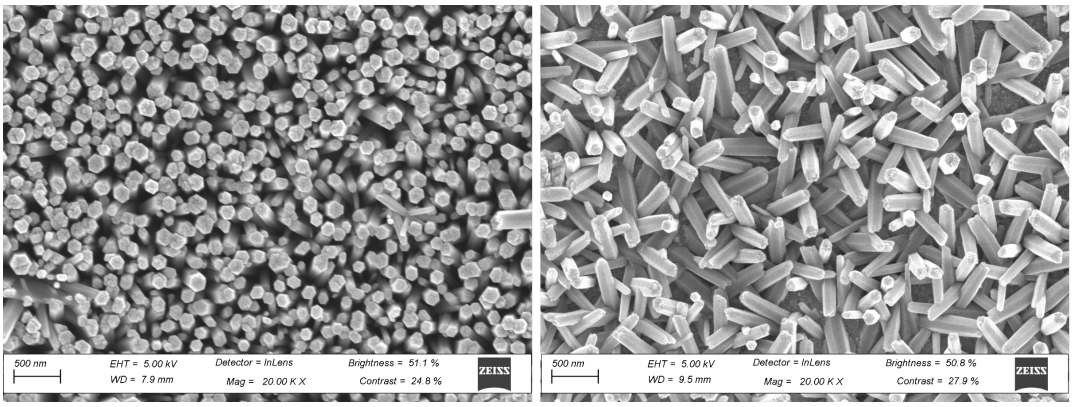

(a) ZnO nanowires deposited on Si substrate (b) ZnO nanowires deposited on ITO-coated glass substrate

Figure 3.13: The effect of the substrate material on ZnO nanowires

The alignment of the nanowires, in the electrochemically deposited nanowire array, holds a higher priority than the ease of manufacturing when it comes to the development of a ZnO nanowire-based nanoforce biosensor. Therefore, in this study, Si substrates with self-deposited ZnO seed layers will be used.

The next tests that were performed in optimising the parameters of the ZnO nanowire electrochemical deposition process, were tests to determine the correct temperature of the electrolyte. For the increased sensitivity of the ZnO nanowire-based nanoforce biosensor, ZnO nanowire arrays consisting of nanowires with the smallest possible diameters, are required. Figure 3.14 shows arrays of nanowires deposited on Si substrates with electrolytes at approximately 80°C (Figure 3.14(a)) and 70°C (Figure 3.14(b)).

Just by a visual representation, it can be seen that the temperature of the electrolyte makes a vast difference in the diameters of the ZnO nanowires deposited onto the Si wafers during the electrochemical deposition process. Using ImageJ (Fiji, 2011) on the SEM images, the mean diameters were calculated as 166 nm and 72 nm for nanowires deposited at 80°C and 70°C respectively.

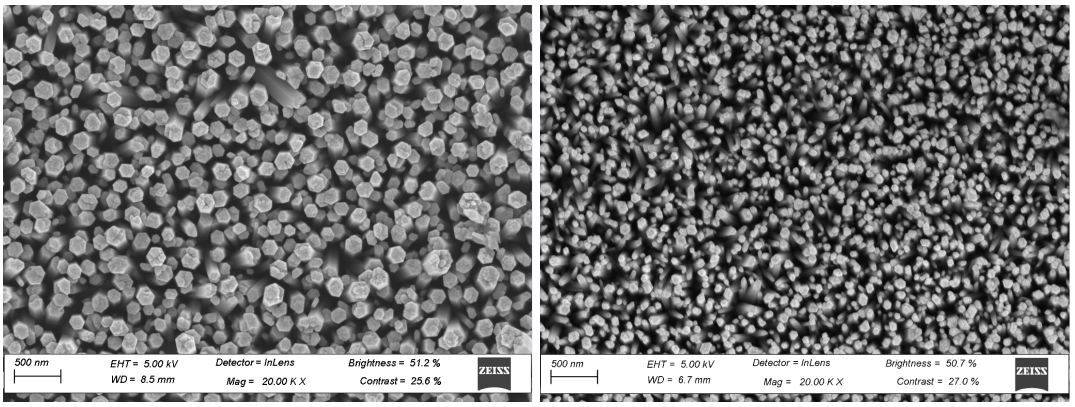

(a) ZnO nanowires deposited in an electrolyte at 80°C

(b) ZnO nanowires deposited in an electrolyte at 70°C

Figure 3.14: The effect of electrolyte temperature on ZnO nanowires

Further testing is required to ensure that the composition of the nanowires deposited at 70°C is appropriate. However, due to the requirement of smaller diameters to improve the sensitivity of the ZnO nanowire-based nanoforce biosensor, 70°C will be used as the electrolyte temperature in this study.

A reoccurring event that became apparent as an issue during the optimisation of the electrochemical deposition of ZnO nanowires on Si substrate, was the growth of perfect nanowire arrays that were polluted with artefacts found lying on top of the nanowire arrays after growth. Figure 3.15 shows an example of a perfect nanowire array with artefacts lying on top.

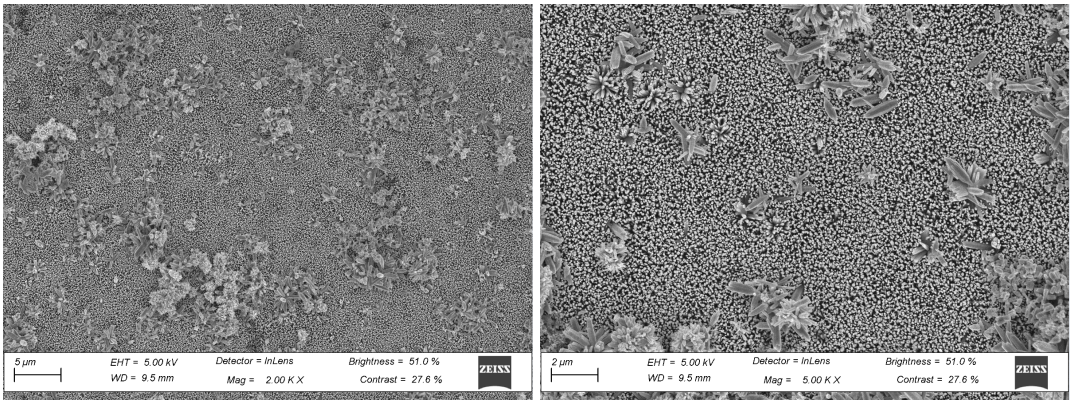

(a) ZnO nanowire array with artefacts at 2000 magnification

(b) ZnO nanowire array with artefacts at 5000 magnification

Figure 3.15: Perfect nanowire arrays polluted with artefacts

For the nanoforce biosensor application, these artefacts are not ideal, because they will affect the sensitivity of the biosensor and may cause interference during the antibody immobilisation stage. Therefore, various methods were tested to remove these artefacts so as not to waste any nanowire samples.

In previous studies, completed by Tom [54] and Neveling [42], it was mentioned that the nanowire arrays were "rinsed" with DI water and dried off with nitrogen gas following their respective growth methods. During the current study, due to the scarcity of nitrogen gas, this rinsing step only took place one week after the growth of the nanowire array samples. As shown in Figure 3.16, the rinsing of the nanowire arrays one week after growth did not make any significant difference in removing artefacts lying on top of the array. It is suspected that rinsing directly after growth would result in the removal of artefacts, but in this study no tests were performed to prove this theory.

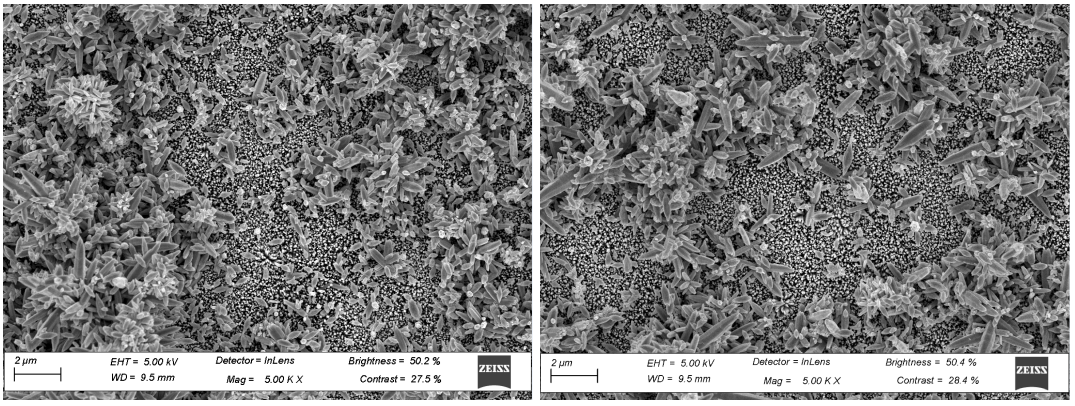

(a) ZnO nanowire array with artefacts, un- (b) ZnO nanowire array with artefacts, rinsed
rinsed

Figure 3.16: Results of rinsing to eliminate artefacts

3.7.3 SEM image analysis of nanowire arrays grown using optimised parameters

Once all of the growth parameters were optimised, it was possible to produce consistently even ZnO nanowire arrays. SEM image analysis was used to compare nanowire arrays of samples from the same batch (one batch consists of four samples) and to compare samples between different batches. This was done to ensure that the optimised parameters performed well for intra-batch and inter-batch depositions.

Figure 3.17 shows 'Sample A' and 'Sample B', both from 'Batch 1'. A visual representation shows the similarity between the two samples and using ImageJ (Fiji, 2011), it has been calculated that the mean diameter of the nanowires in the array of 'Sample A' is 71.2 nm (σ = 14.61) and the mean diameter of the nanowires in the array of 'Sample B' is 70.0 nm (σ = 13.39) .

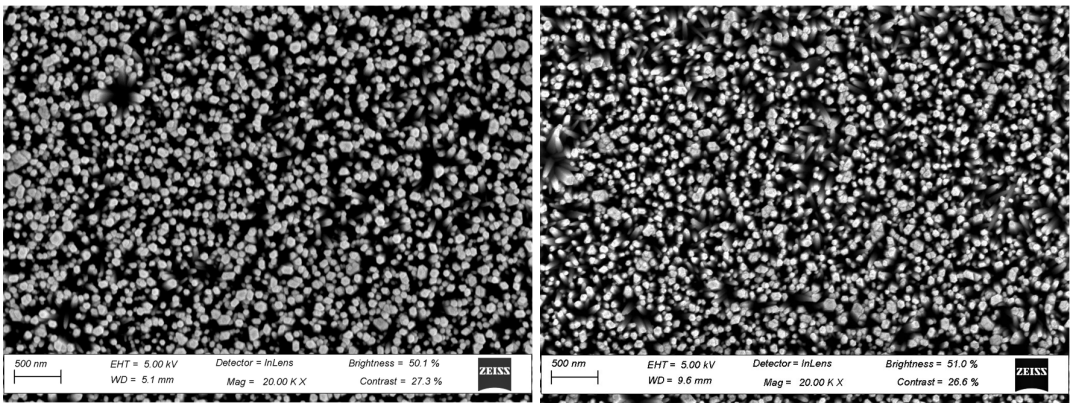

(a) Sample A, Batch 1 (b) Sample B, Batch 1

Figure 3.17: Intra-batch comparison of samples

Figure 3.18 compares samples 'A' and 'B' to samples 'C'-'H' all from different deposition batches. The mean diameters and the respective standard deviations of each sample (relative to 100 nanowires) are shown in Table 3.2.

Table 3.2: Mean diameters of nanowire array samples for inter-batch comparison

Sample Name	Mean Diameter (nm)	Standard Deviation (σ)
Sample A	71.22	14.61
Sample B	70.00	13.39
Sample C	70.11	13.96
Sample D	75.58	15.01
Sample E	68.86	15.71
Sample F	77.31	17.94
Sample G	69.09	12.11
Sample H	68.55	13.19

As it can be seen in Table 3.2, the mean diameters of the nanowires in the nanowire array samples range from 68.55 nm to 77.31 nm. The samples with the larger mean diameters also have the greatest standard deviation in their diameters, which means that there is more variance in the diameters of the nanowires in those array samples. Due to the range of the diameters of these nanowire samples and the diameters that were able to be achieved, this can be regarded as a successful optimisation of the ZnO nanowire electrochemical deposition process.

The final analysis performed using the SEM imaging technique was the analysis of the length of the ZnO nanowires deposited during the optimised electrochemical deposition process. Figure 3.19 shows the cross sectional view of 'Sample I' in which the length of the nanowires in the array can be seen. As shown, the length of all the nanowires in the array are consistent throughout the cross sectional area. There are other outlying nanowire protrusions that can also be seen, but these can be clearly

distinguished from the nanowires in the consistent ZnO nanowire array. Using ImageJ (Fiji, 2011), the mean length of the nanowires in the array was measured as 970.96 nm (σ = 43.17).

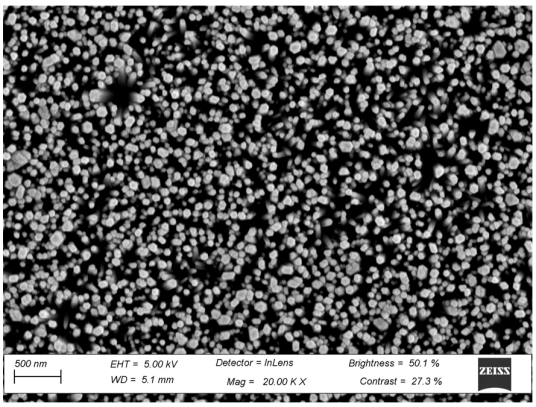

(a) Sample A, Batch 1

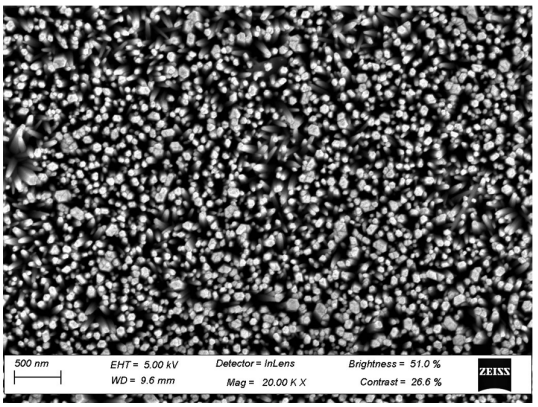

(b) Sample B, Batch 1

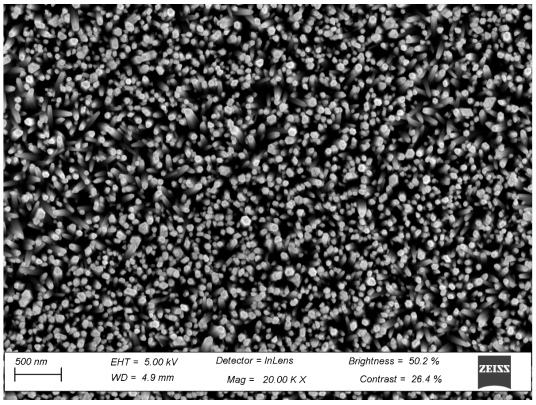

(c) Sample C, Batch 2

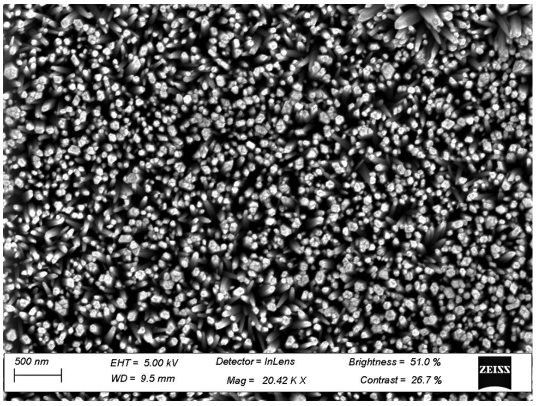

(d) Sample D, Batch 3

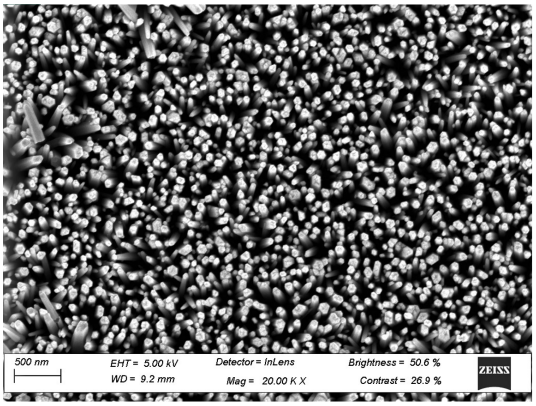

(e) Sample E, Batch 4

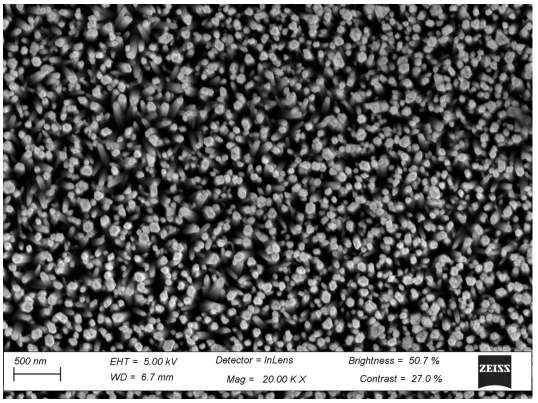

(f) Sample F, Batch 5

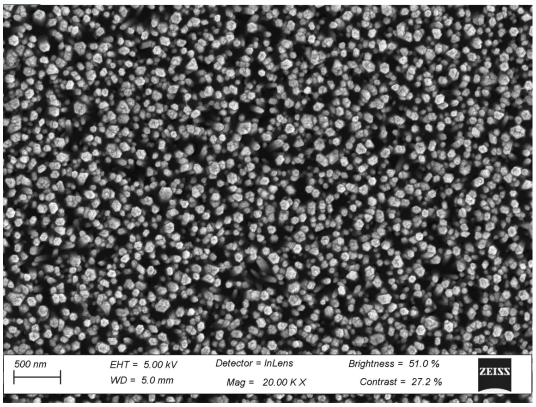

(g) Sample G, Batch 6

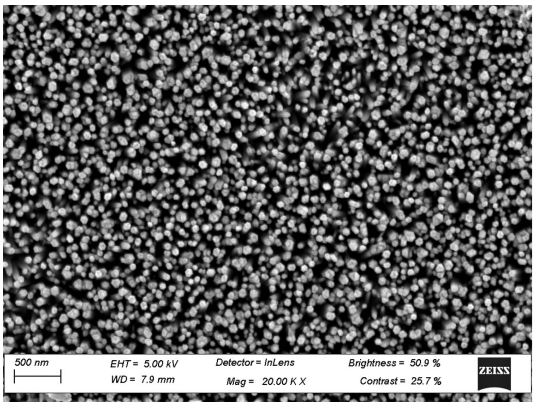

(h) Sample H, Batch 7

Figure 3.18: Inter-batch comparison of samples

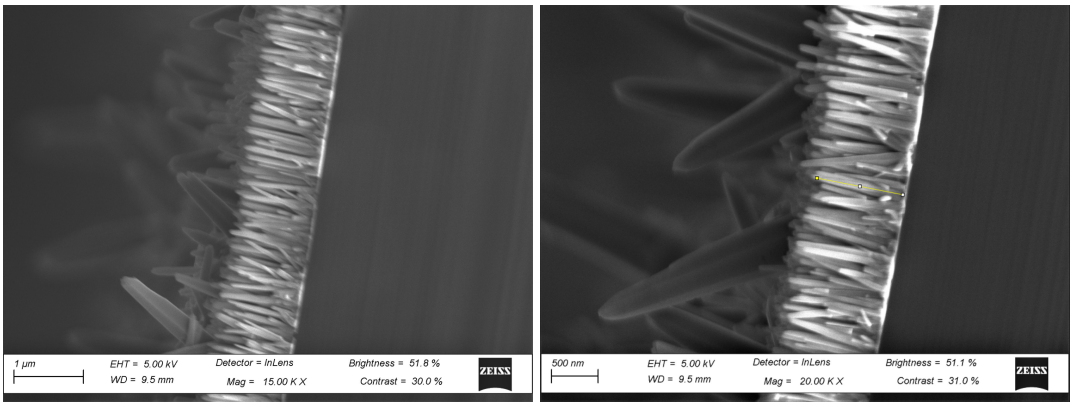

(a) ZnO nanowire array cross section (15k magnification)

(b) ZnO nanowire array cross section (20k magnification)

Figure 3.19: Side view of ZnO nanowire arrays on Si substrate

3.7.4 EDX/EDS Analysis of ZnO Nanowires

It is important to determine the elemental composition of the electrochemically deposited ZnO nanowires to ensure that there has been no contamination by other substances during the deposition process. Table 3.3 shows the EDX results of Samples 'B' and 'C' (all values shown represent the weight % of the element in the sample). As can be seen, for both samples, there are gold (Au) and silicon (Si) present. This is due to the substrate, onto which the ZnO nanowires are deposited, being a Si substrate that is gold-coated before the ZnO seed-layer is deposited.

Table 3.3: EDX results for ZnO nanowire array samples

Sample Name	Zinc (Zn)	Oxygen (O)	Gold (Au)	Silicon (Si)
Sample B	66.52%	19.85%	2.54%	11.09%
Sample C	66.45%	19.39%	2.36%	11.79%

The results in Table 3.3 show that the only elements present, other than the known elements of Au and Si, are Zn and O. The average weight percentage of Zn between the two samples is 66.49 wt% and the average weight percentage of O is 19.62 wt%.

3.7.5 XRD Analysis of ZnO Nanowires

The XRD analysis performed at iThemba Labs, Cape Town, on the ZnO nanowires arrays were used to determine the *c*-axis orientation and alignment of the nanowires. Due to the surface of the sample lying in the "scattering plane" of the XRD measurement equipment [42], an array of nanowires with perfect *c*-axis alignment (nanowires perpendicular to the growth substrate) would result in a single diffraction peak - the 002 peak - or peaks that are orders thereof. The presence of misaligned and ran-

domly orientated nanowires would result in an XRD patterns showing many peaks other than the 002 peak.

In this study, all XRD patterns obtained were indexed against the identified phases 'JCP2***' from the ICDD database.

Figure 3.20 shows the XRD pattern obtained of the ZnO nanowires deposited onto ITO-coated glass substrate (as shown previously in Section 3.7.2, Figure 3.13(b)) against the reference pattern of ZnO (zincite). This pattern shows that the distribution of ZnO nanowires on the ITO-coated glass substrate is quasi-random because all of the diffraction peaks of ZnO can clearly be observed in this pattern. The strong peak observed at the 002 peak for ZnO indicates that there is a slight anisotropy in the fibre alignment in favour of the *c*-axis. However, the presence of multiple peaks shows the random and non-ideal orientation of the ZnO nanowires deposited on the ITO-coated glass substrate. (Note: the peaks not indexed can be referenced to the presence of ITO).

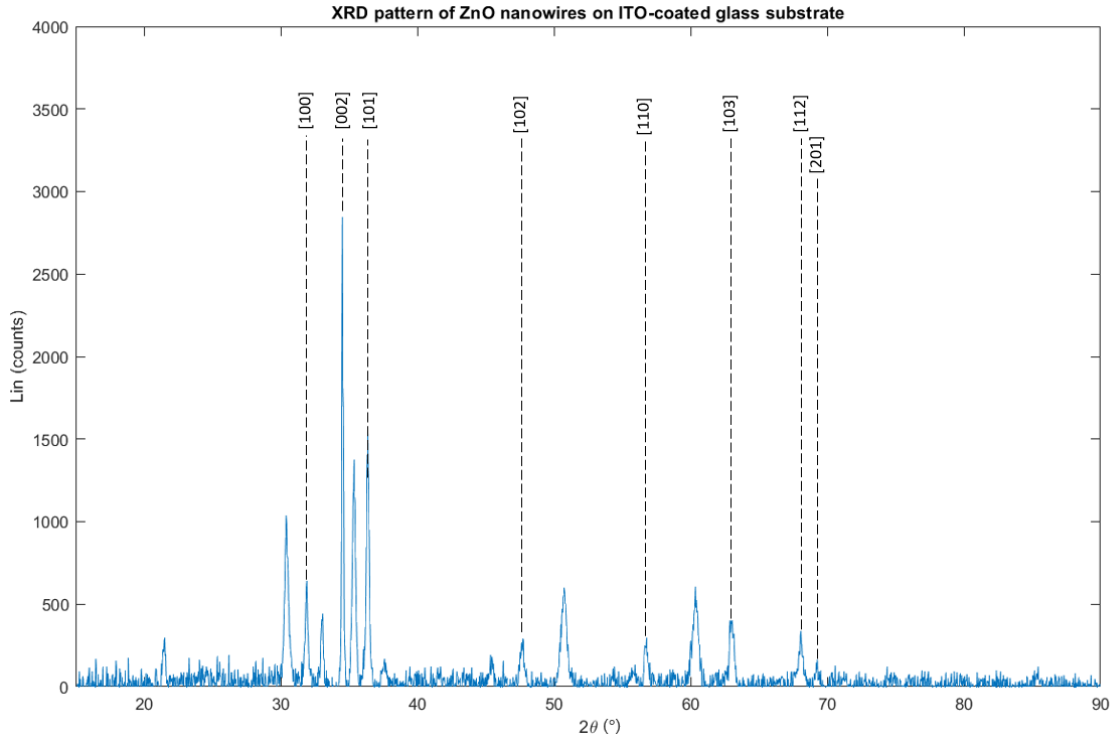

Figure 3.20: XRD pattern of ZnO nanowires on ITO-coated glass substrate

It is important to note that the Si(100) substrate, onto which the ZnO nanowires were deposited is an onerous material to perform XRD analysis on. Pure Si(100) wafers, measured with a PSD (position sensitive detector) in the absence of monochromators, can exhibit spike peaks (reflections) from the contaminated x-rays source. An example of this would be very sharp peaks on the principle, 400 peak of Si(100). Figure 3.21 shows the XRD pattern of a clean Si(100) wafer (with no Au coating,

seed layer, or ZnO nanowires deposited onto it) imposed onto the Si(100) reference index. In this figure you can clearly see a sharp peak next to the 400 peak of Si(100). Due to the unpredictability of how Si(100) wafers respond to XRD analysis, it was deemed important to analyse a clean wafer in order to compare this results to that of the XRD analysis of ZnO nanowires deposited onto the Si(100) wafer.

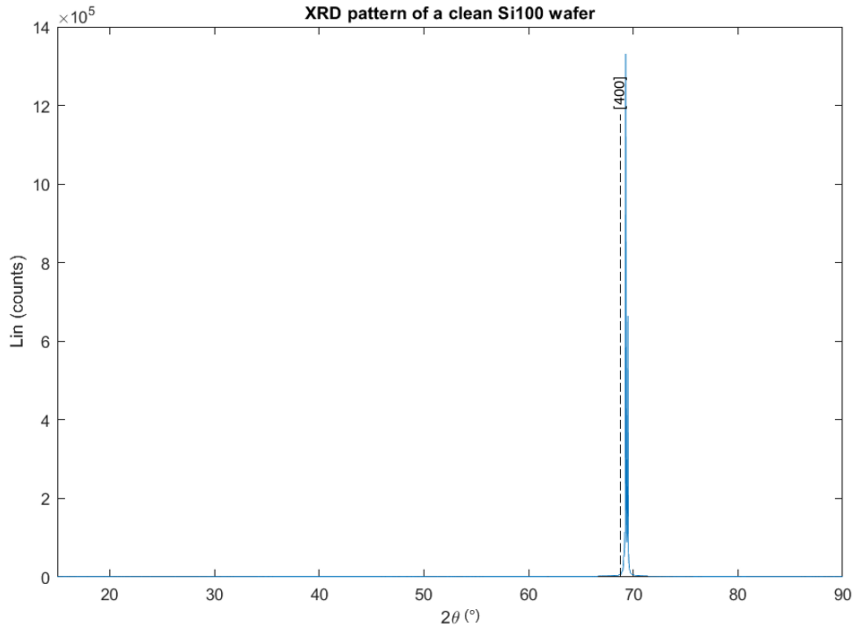

Figure 3.21: XRD pattern of clean Si(100) wafer

Figure 3.22 shows the almost-identical XRD patterns of Samples 'B' and 'C' with ZnO nanowires deposited, using the optimised electrochemical deposition parameters, onto Si(100) wafers. In these patterns, it can be seen that, along with the same spike that appears at approximately 68.7° in the XRD pattern of a clean Si(100) wafer (Figure 3.21), there are three new peaks that appear that can be attributed to the deposition of ZnO nanowires onto the Si(100) wafer. These peaks consist of a sharp peak at approximately 34.6°, a small peak at approximately 72.7° and a wider peak at 38.3°.

Upon comparing these peaks to the ZnO reference patterns, we see that the peaks at 34.6° and 72.7° match the 002 and 004 reflections of ZnO which indicates that the ZnO nanowires are almost perfectly aligned, perpendicular to the Si substrate (parallel to the *c*-axis). Due to the 004 peak being the second order diffraction of the 002 peak, these samples are a great example in which only one orientation is observed.

The wider peak, observed at approximately 38.3°, is characteristic of a thin film layer and corresponds to the Au(111) reflection. This can be attributed to the 40 nm layer of gold that is deposited onto the Si wafer, before seed layer deposition. Due

to the basal plane of both ZnO and Au(111) orientation having a hexagonal atomic arrangement, the Au(111) has assisted the growth of the ZnO nanowires along the *c*-axis by providing a hexagonal matrix for coherent growth.

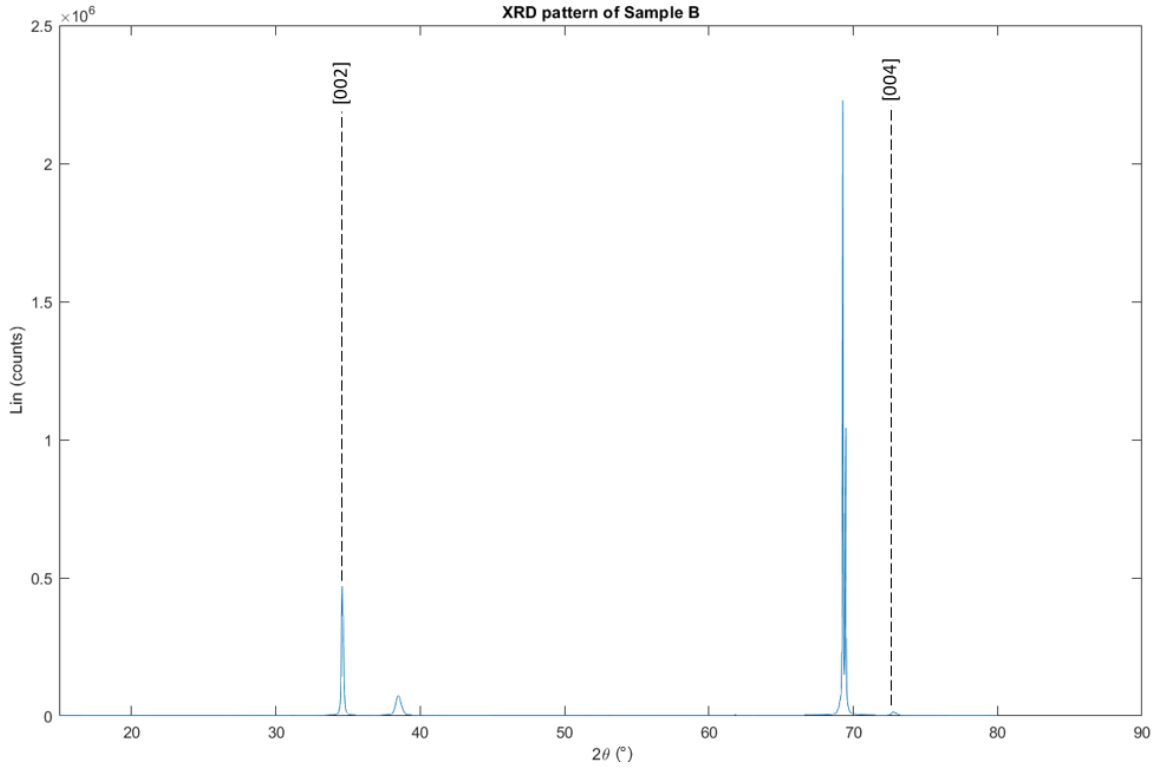

(a) XRD pattern of 'Sample B'

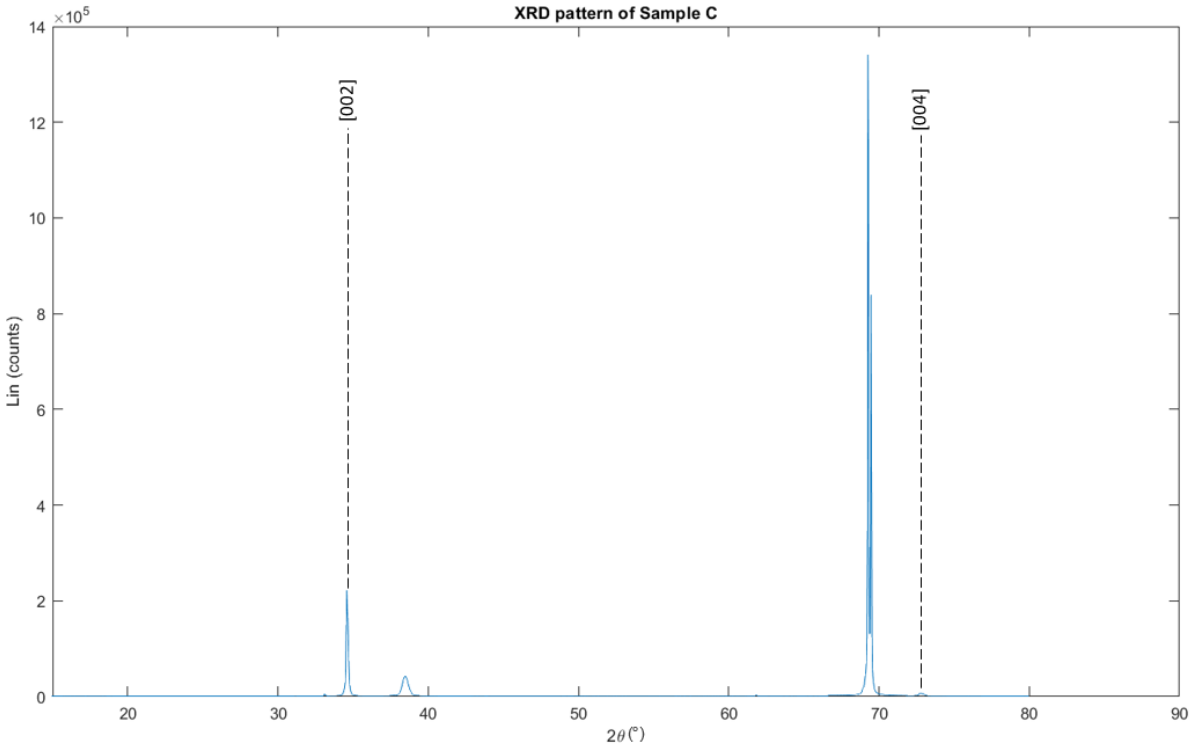

(b) XRD pattern of 'Sample C'

Figure 3.22: XRD patterns of ZnO nanowire arrays deposited onto Si(100) wafers

3.8 Conclusion

When producing ZnO nanowire arrays for a biosensor application, there are various factors that have an impact on a successful growth. The homogeneity of the nanowire array, the orientation of the nanowires (favoured to be perpendicular to the growth substrate, parallel to the *c*-axis), and the dimensions (the diameter and length) of the synthesised nanowires are three important factors that greatly affect the sensitivity of a nanoforce biosensor and are greatly impacted by the growth parameters implemented.

The optimisation of the electrochemical deposition of ZnO nanowires on a silicon (100) substrate was prioritised in this study for various reasons. Firstly, the electrochemical deposition incubation time is less than 1 hour and is controlled at an easily achievable temperature of 70°C. Secondly, this process is repeatable and the chemicals used for the growth of each sample are minimal. The instrumentation and equipment used in this process is also reusable which reduces unnecessary wastage.

The optimised growth parameters for achieving the successful growth of homogeneous nanowire arrays consisting of nanowires with a mean diameter of 71.34 nm and length of 970.96 nm are as follows:

- A 40 nm gold (Au) layer sputter coated onto the Si(100) wafers.
- The deposition of 4×15 µl of a ZnO sol-gel solution with a concentration of 0.1 M for an even seed layer.
- Annealing of the ZnO seed layer at 700°C for 10 minutes for the correct grain size.
- The incubation of the Si wafer samples for 1 hour at 70°C in an electrolyte with the concentration of 1 mM.

To achieve the correct temperature control for the electrochemical deposition, a simple temperature control system was implemented and was able to reach the required temperature of 70°C ($\pm$0.4°C) within 7 minutes.

The XRD analysis performed on ZnO nanowire arrays electrochemically deposited with the above-mentioned parameters showed that the nanowire arrays consisted primarily of nanowires orientated along the *c*-axis, the direction perpendicular to the growth substrate.

Chapter 4

ZnO Nanowire-based nanogenerator

This chapter offers an overview of the processes followed in developing and testing the ZnO nanowire-based nanogenerator that is the transducer mechanism of the Mortalin biosensor. A discussion of the development from ZnO nanowire array to nanogenerator will be provided. The initial testing of the nanogenerator will be discussed and the methods followed to determine the working order of the nanogenerator will be given. This will be followed by an explanation of the electronic components implemented in the system and how they were chosen. The design of a Sallen-Key low-pass filter, specific to this application, will be considered along with a simulation of this design and an overview of the final testing of the electronic components.

4.1 Introduction

The ZnO nanowire-based nanogenerator developed in this study are based on the findings discussed in Section 2.4.4. The nanogenerator consists of ZnO nanowire array (deposited onto a silicon substrate), as discussed in Chapter 3, layered with PMMA and gold. The gold coating on the silicon substrate, onto which the ZnO nanowires are deposited, and the gold layer deposited onto the ZnO nanowires act as the respective terminals over which an output voltage signal can be measured, upon disturbance of the nanowires. The ZnO nanowire transducer is connected to an electronic circuit, of which the primary functions are to amplify the collected signal, filter out noise from this signal, and to aid in the collection of data for later analysis and interpretation.

4.2 Development of a ZnO Nanowire-based Nanogenerator

The concept of the ZnO nanowire-based nanoforce biosensor is based on the piezoelectric properties of ZnO nanowires. This refers to the fact that when an external disturbance, such as an inflection of weight or a vibrational disturbance is acted upon a nanowire array, bending of the nanowires in the array will occur. Upon the lateral deflection or bending of the nanowires, a voltage drop occurs over the nanowires in the array. This voltage can be measured and analysed by an external electronic setup, which is made possible by the presence of a Schottky barrier - achieved by a metal-semiconductor interface.

Figure 4.1(a) shows a schematic of the ZnO nanowire-based nanogenerator developed during this study and (b) shows how the electronic connections are intended. As shown, the nanogenerator consists of the ZnO nanowire array deposited using an optimised electrochemical deposition method, as discussed in Chapter 3.

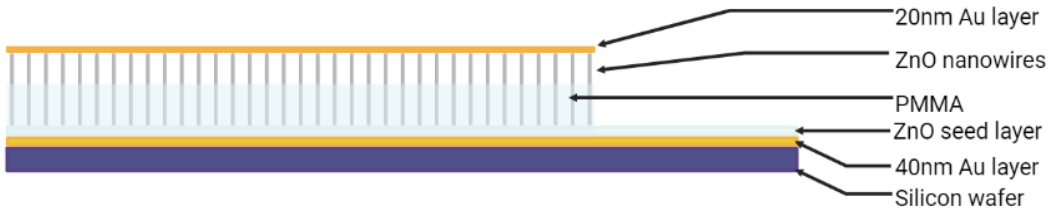

(a) Nanogenerator components

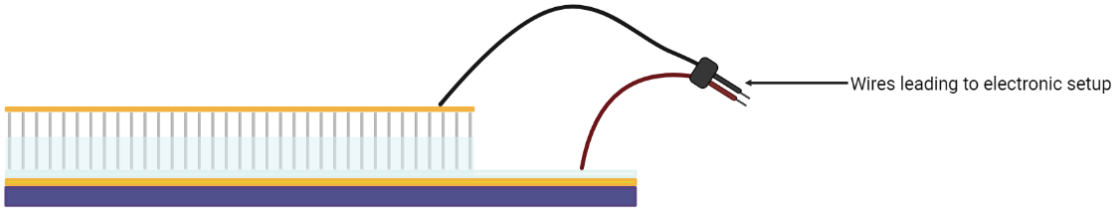

(b) Electronic connections on nanogenerator

Figure 4.1: Schematic of ZnO nanowire-based nanogenerator

In order to have two terminals exposed for the measurement of the voltage induced over the nanowires, a method was to be developed to deposit nanowires on one section of the Si substrates only. Initially, a photoresist masking method was considered. However, due to this specific application, photoresist was suspected to contaminate the samples, when used for masking. Additionally, the removal of photoresist from the samples includes the use of solvents such as NMP (1-methyl-2-pyrrolidone) and DMSO (dimethyl sulfoxide), which are likely to destroy or negatively impact the ZnO nanowire array. Therefore, the exposure of the bottom terminal was achieved by the addition of brass masks to the electrochemical deposition

setup. Using the brass masks, shown in Figure 4.2(a), it was possible to deposit ZnO nanowires to cover $\frac{2}{3}$ of the surface of the silicon substrate samples as shown on 'Sample B' in Figure 4.2(b). This masking allows for the Au layer under the nanowire array to be exposed, as this layer acts as the positive terminal for the measurement of the induced voltage.

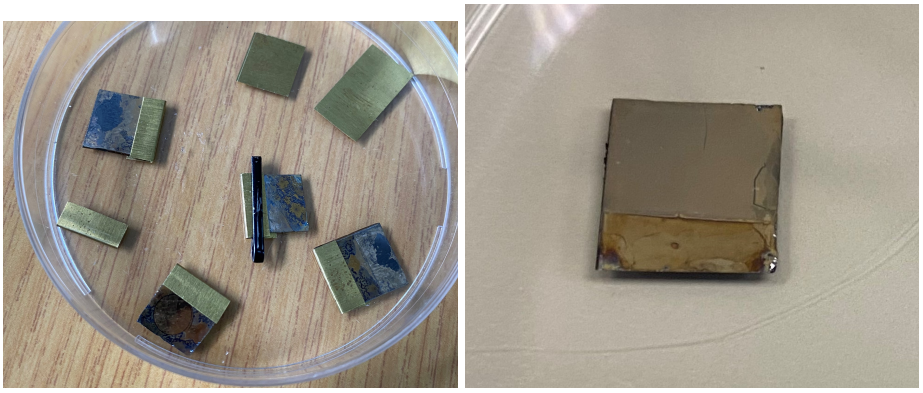

(a) Brass masks (b) Sample 'B' produced using brass masks

Figure 4.2: Masks used to prevent ZnO nanowire growth on sections of Si wafer sample

4.2.1 PMMA layer spin-coating

A layer of PMMA (seen in Figure 4.1) is required to be deposited between the nanowires in the array to prevent a short-circuit forming between the Au layers above and below the nanowire array in the nanogenerator. To do this, a solution of PMMA and acetone, with a viscosity appropriate to allow the solution to seep between (but not completely cover) the nanowires, was to be made. Solutions of various concentrations (shown in Figure 4.3) were developed in the process of optimising the coating process of the ZnO nanowire arrays with PMMA.

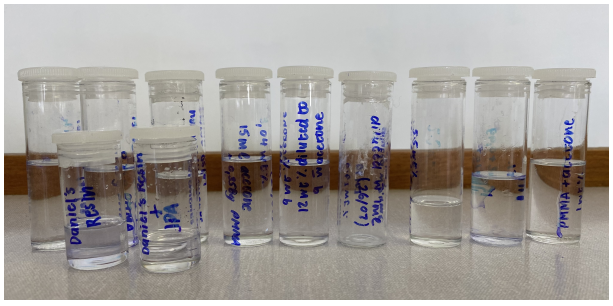

Figure 4.3: PMMA solutions

Along with the viscosity, the speed profile of the spin coater, during the process of the deposition of the PMMA-acetone solution onto the ZnO nanowire arrays, was to be optimised. Both wet and dry start operations were tested during this process, along with various starting and finishing speeds. One important consideration was

the fast evaporation of the acetone from the PMMA solution once the spin coater started spinning. Therefore, an operation that allowed for the even spreading of the solution (without the layer becoming too thick) before the evaporation of acetone, was to be developed. After numerous rounds of trial-and-error testing, the following process was developed:

A PMMA-acetone solution with a concentration of 3.0 wt% was made by mixing 0.358 g of PMMA (Sigma-Aldrich, 200336-50G) into 15 ml of acetone. This mixture was placed on a heat-controlled magnetic stirrer, set to 40°C, until it became a homogeneous solution. The masks were removed from each sample and 50 µl of this solution was deposited onto a ZnO nanowire array sample, stationary on the spin coater. The solution was left to seep into the nanowire array for 5 seconds before the spin coater was started at 3000 rpm for 15 seconds.

Figure 4.4 shows nanowire array samples throughout the PMMA spin-coating optimisation process and samples using the optimised parameters mentioned above.

Figure 4.5 shows nanowire array samples coated with PMMA, using the optimised method discussed above. Samples such as 'B' and 'C' were used for further nanogenerator (and later, biosensor) testing. In Figure 4.5 it can be seen that, using the optimised parameters, the PMMA layer lies between the ZnO nanowires and the tips of the nanowires are still exposed to be coated by the top Au layer.

Once the desired PMMA layer was achieved, the samples were coated with 20 nm of Au using the same conductive sputter coater mentioned in Chapter 3. Following this, the PMMA-Au layer, on the section of the sample without the deposited ZnO nanowires, was scraped off to expose the layer of Au lying underneath the nanowire array. This was done carefully, to ensure that this required layer of Au was not completely removed from the silicon substrate.

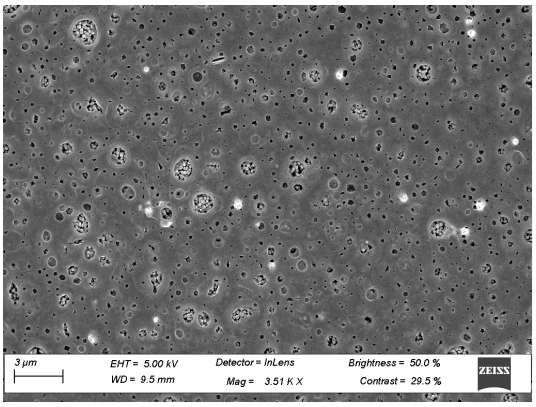

(a) Sample I, 6 wt% PMMA in acetone, wet start at 2000 rpm for 30 seconds

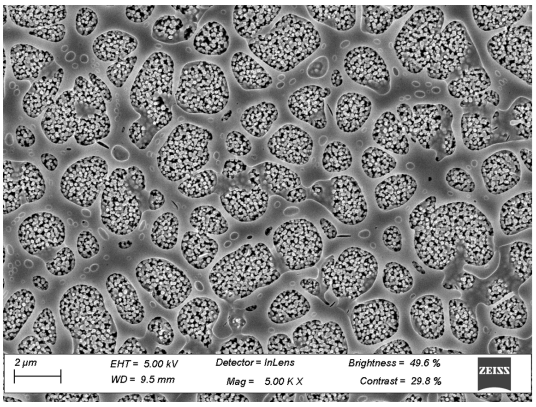

(b) Sample J, 3 wt% PMMA in acetone, dry start at 2000 rpm for 30 seconds

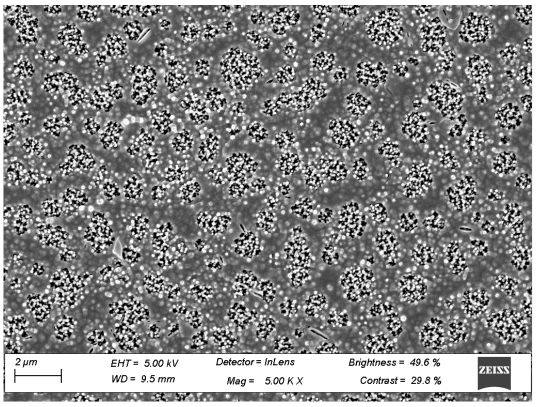

(c) Sample K, 3 wt% PMMA in acetone, wet start (no seeping time) at 2000 rpm for 30 seconds

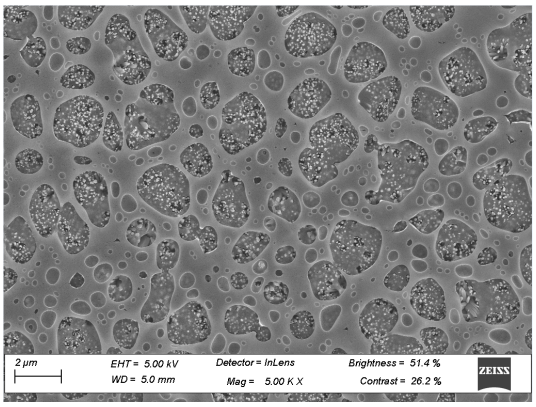

(d) Sample L, 3 wt% PMMA in acetone, wet start (10 seconds seeping time) at 2500 rpm for 20 seconds

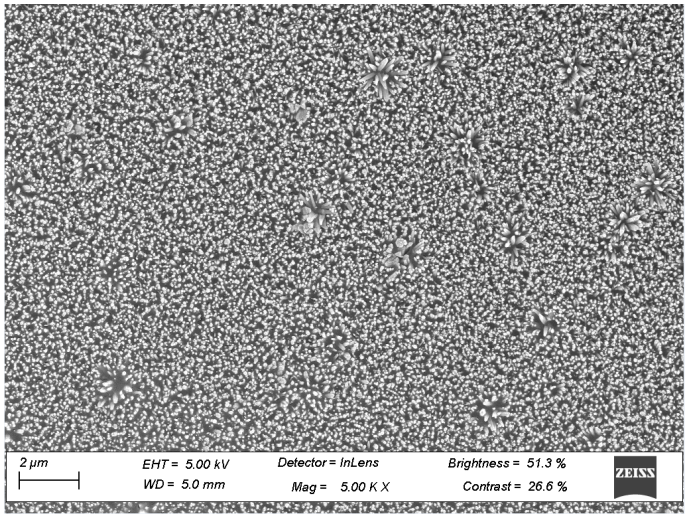

(e) Sample C, 3 wt% PMMA in acetone, wet start (5 seconds seeping time) at 3000 rpm for 20 seconds

Figure 4.4: PMMA coated samples during process optimisation

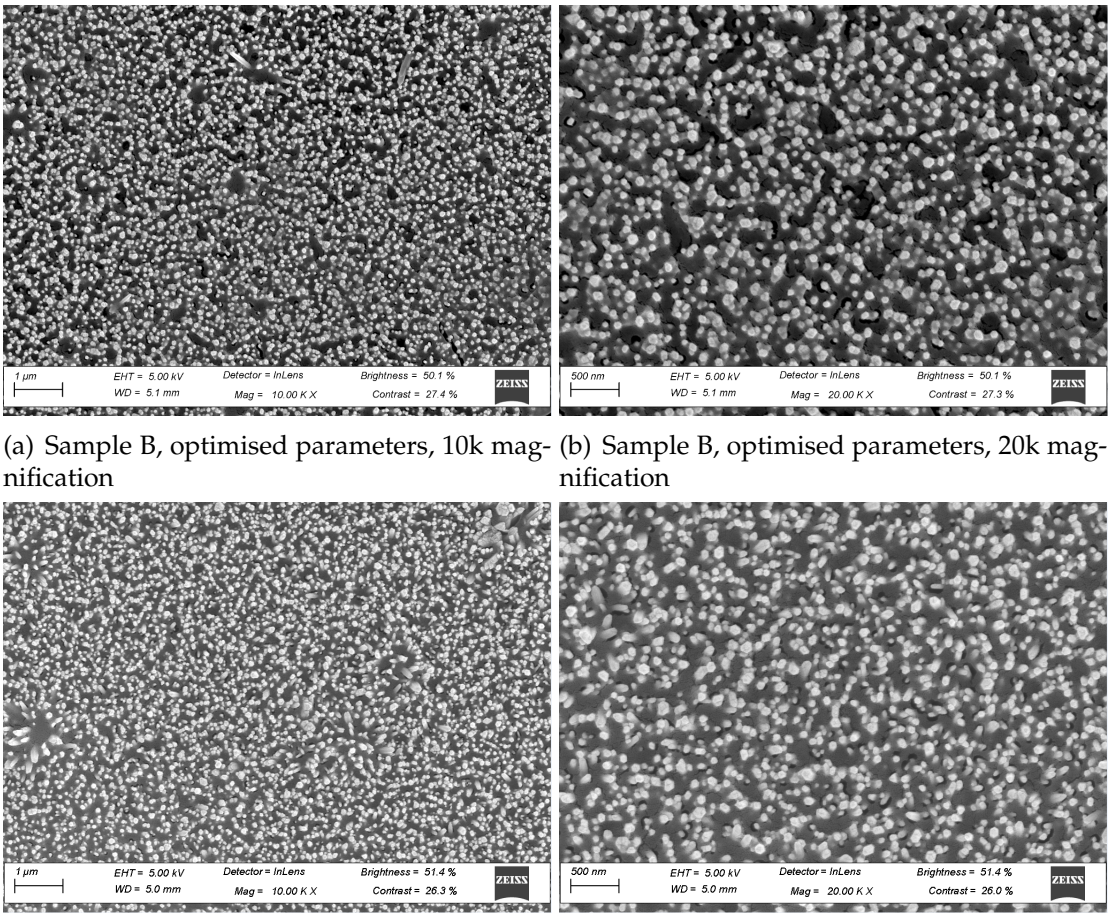

(a) Sample B, optimised parameters, 10k magnification

(b) Sample B, optimised parameters, 20k magnification

(c) Sample C, optimised parameters, 10k magnification

(d) Sample C, optimised parameters, 20k magnification

Figure 4.5: PMMA coated samples after process optimisation

A sample holder (shown in Figure 4.6) was designed to house the nanogenerator samples. The aims and requirements of this sample holder are:

1. To house and protect the nanogenerator samples
2. To establish a solid electronic connection between the nanogenerator sample and the electronic setup or measurement device
3. To provide an inlet for the biological sample during the biosensor testing stage.

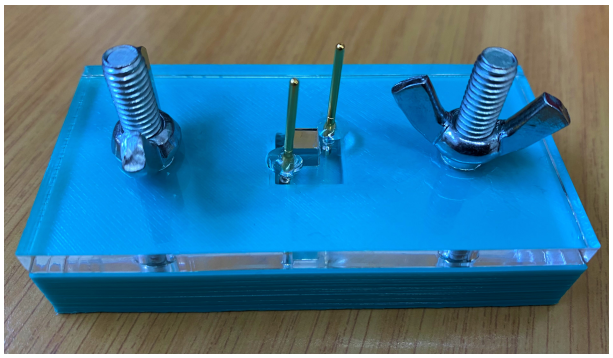

Figure 4.6: Sample holder

The sample holder, shown in Figure 4.6, is made up of a 3D printed base (with an indent for housing the nanogenerator sample), a laser-cut PVC top with an inlet for the biological samples and spring pins that were setup to make connection with the Au layers above and below the ZnO nanowire array on the nanogenerator sample. Connections to the electronic setup or the measurement equipment will be made with the nanogenerator via these spring pins.

4.3 Initial Testing of the ZnO Nanowire-based Nanogenerator

The initial testing done on the ZnO nanowire-based nanogenerator samples was to verify the principle that, upon an external disturbance, such as an inflection of weight or a vibrational disturbance upon a nanowire array, the bending of the nanowires will result in a voltage being induced over the array. This voltage can be observed as a change in baseline voltage, from before to during the inflicted disturbance, or as a spike in the voltage measured over the terminals of the nanogenerator.

To do this, first, the nanogenerator samples were tested using a tapping method. A non-conductive tool, not sharp enough to damage the top Au layer on the nanogenerator, was used to tap a nanogenerator sample in the sample holder, while a digital multimeter (Keysight 34401A) was connected to the spring pins to measure the voltage over the nanowire array in the process. Figure 4.7 shows the baseline voltage of a sample (blue) and how the baseline is affected when the sample is continuously being tapped by the tool (orange). It can be seen that the voltage measured over the sample peaks in the negative and positive directions upon the tapping disturbance.

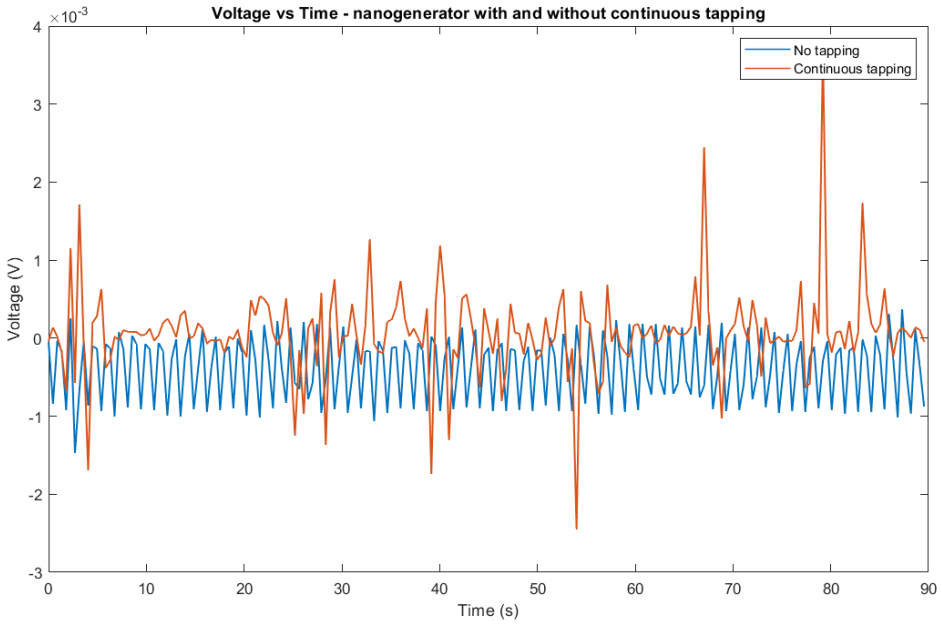

Figure 4.7: The voltage over a nanogenerator sample before and during continuous tapping disturbance

Due to the measuring frequency of the digital multimeter being too slow, only discrete measurements (as opposed to continuous measurements) were being taken using the instrument. This resulted in the data from these tests not being an accurate representation of how the nanogenerator would be affected by an external disturbance, as this disturbance was also not continuous, but rather sporadic. Therefore, another method of testing the working of the nanogenerators was to use a continuous disturbance that, even when being measured discretely, will have a continuous effect on the baseline voltage measured over the nanowire array.

This new disturbance was inflicted upon the nanogenerator using a continuous flow of nitrogen gas. Figure 4.8 shows how the voltage over a sample was affected when small, non-continuous, long and short bursts of gas were blown onto them. The downwards spikes in voltage represent the moments at which the nitrogen gas-disturbance occurred.

Figure 4.9 shows how the baseline voltage over the same sample was affected when a constant burst of nitrogen gas was blown onto the sample. In this test, the nitrogen disturbance was added at approximately 95 seconds and held over the sample until the end of the test run. As it can be seen, during this continued disturbance, the baseline voltage of the nanogenerator decreased significantly.

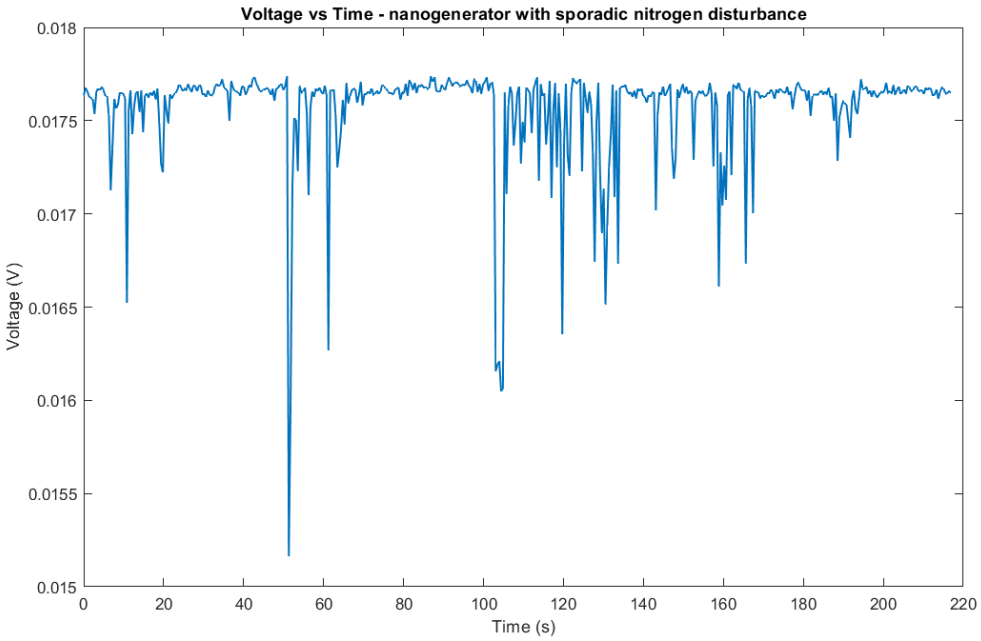

Figure 4.8: The voltage over a nanogenerator sample being sporadically disturbed by nitrogen gas

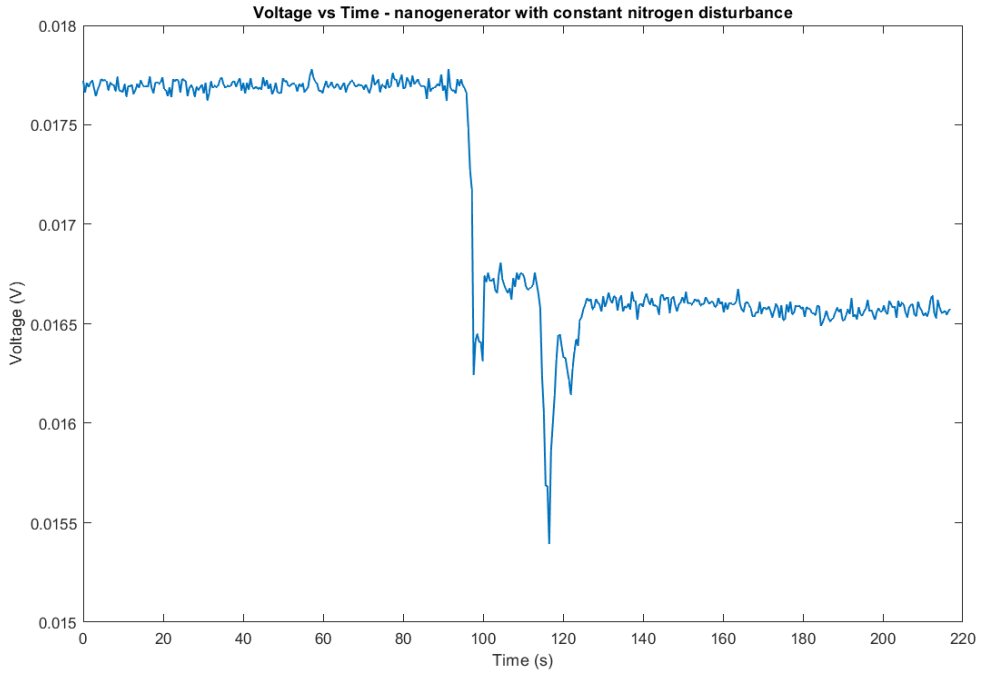

Figure 4.9: The voltage over a nanogenerator sample being constantly disturbed by nitrogen gas

In the next test (results shown in Figure 4.10, the nitrogen disturbance was added, for the first time, at approximately 30 seconds and removed at 65 seconds and for the second time, it was added closer to the sample at 80 seconds and removed at

105 seconds. Figure 4.10 shows how the voltage over a nanogenerator decreases when the external nitrogen gas disturbance is inflicted and returns back to the initial baseline when the disturbance is removed. This correlates with the information gathered about the working principle of ZnO nanowire-based nanogenerators, as discussed in Section 2.4.4. An important aspect to take note of here is that the change in the baseline voltage only exists while the disturbance is taking place. As it can also be seen in Figure 4.10, when the gas was held closer to the sample (therefore with increased pressure), during seconds 80 and 105, the voltage change was even greater.

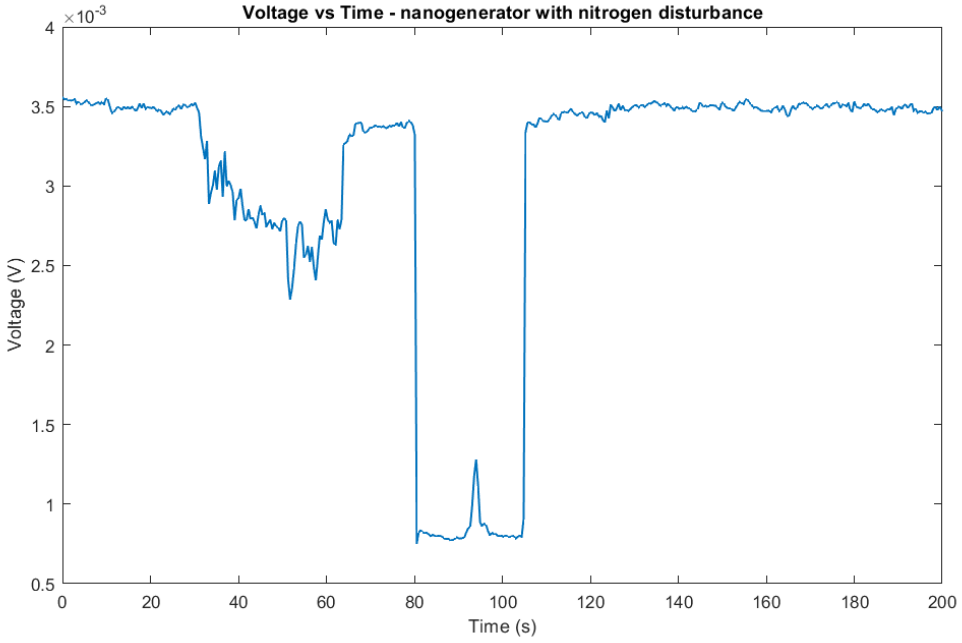

Figure 4.10: The voltage over a nanogenerator sample being disturbed by nitrogen gas

4.4 Electronic Design

Electronic circuitry is required to transform the data from the ZnO nanowire-based nanogenerator and biosensor into results that are readable to a user. The voltage signals that can be measured over the ZnO nanowire array, upon disturbance of the ZnO nanowires, are small signals that often include large amounts of noise and parasitic data. This may result in these signals being difficult to interpret. Therefore, the main objective of the implemented electronic circuitry is to amplify the magnitude of the piezoelectric voltage signal produced by the ZnO nanowires upon disturbance, and to filter out any noise from this signal. The result of this electronic circuit implementation should be clear, readable responses with definitive peaks and changes in magnitude.

4.4.1 Electronic Components

To amplify the signal detected over the ZnO nanowire array, an instrumentation amplifier was used. Initially, a differential amplifier was considered for use in the amplification stage of the implemented electronic circuitry. However, the application of a differential amplifier has a low input resistance, when using an inverting amplifier configuration. Increasing the input resistance to the differential amplifier would result in a great increase of the noise in the system. Therefore, an instrumentation amplifier was considered due to the fact that it has two voltage buffer stages, resulting in a greater input resistance, with less noise. Another advantage of using an instrumentation amplifier is that the gain can be changed just by changing one resistor, R_g. The instrumentation amplifier selected for use in this study is the Texas Instruments INA331 (Mouser Electronics, INA331AIDGKTG4) set with a gain of 5.

Along with the instrumentation amplifier, a filter was required to filter the very high frequency noise out of the signal resulting from the ZnO nanowire-based nanogenerator and biosensor applications. In this study, an active Sallen-Key biquad low-pass filter was employed. An active filter was selected because, not only does it filter out the noise from the signal, it also further amplifies the signal produced by the ZnO nanowire-based biosensor.

4.4.2 Sallen-Key Biquad Low-pass Filter

An active Sallen-Key biquadratic low-pass filter was designed to eliminate noise from (and further amplify) the signal detected from the nanogenerator upon disturbance of the ZnO nanowires. The Sallen-Key filter topology, as seen in Figure 4.11, is a popular topology, mainly attributed to the fact that in this configuration, the overall performance of the filter is least affected by the performance of the operational amplifier itself. This is because, in the Sallen-Key topology, the opamp is structured purely as an amplifier as opposed to being an integrator.

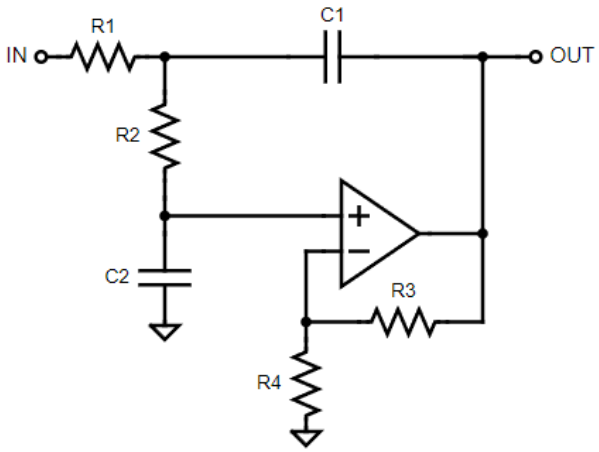

Figure 4.11: Sallen Key Topology

For the design of the implemented active Sallen-Key biquadratic low-pass filter, the transfer function can be derived as

$$\frac{V_o}{V_i} = \frac{\frac{\mu}{R_1R_2C_1C_2}}{s^2 + (\frac{1}{R_1C_1} + \frac{1}{R_2C_1} + \frac{1-\mu}{R_2C_2})s + \frac{1}{R_1R_2C_1C_2}} \tag{4.1}$$

where

$$\mu = 1 + \frac{R_a}{R_b} \tag{4.2}$$

By using this transfer function (4.1) and designing for a Butterworth characteristic, it was possible to determine the component values appropriate for this specific application. The second order normalised Butterworth polynomial

$$s^2 + 1.41421s + 1 \tag{4.3}$$

can be used to calculate the resistor values by equating the constants in (4.3) to those in the denominator of (4.1).

By doing this, and choosing $R_1 = R_2$, $C_1 = C_2 = 1\,\text{F}$ and $\omega_0 = 1\,\text{rad/s}$ (an assumption when designing for a Butterworth polynomial), we know that

$$\frac{1}{R_1R_2C_1C_2} = 1 = \frac{1}{R^2} \tag{4.4}$$

$$\therefore R = 1$$

and

$$\frac{1}{R_1C_1} + \frac{1}{R_2C_1} + \frac{1-\mu}{R_2C_2} = 1.41421 \tag{4.5}$$

$$\therefore \mu = 1.5858$$

For the purpose of stability, choose

$$R_1 + R_2 = \frac{R_aR_b}{R_a + R_b} \tag{4.6}$$

.

There is a special case of the Sallen Key low-pass filter where, if the gain is set to 2, the capacitor, as well as the resistor values will be the same.

$$\therefore 2 = \frac{R_aR_b}{R_a + R_b} \tag{4.7}$$

$$\therefore R_a = 5.4142 \text{ and } R_b = 3.1716$$

Due to the assumption that $\omega_0 = 1\,\text{rad/s}$, scaling is required in order to select component values for a filter that is specific to the actual application. The scaling equations, used for this purpose, are given by

$$R^{'} = K_mR \tag{4.8}$$

$$L^{'} = \frac{K_m}{K_f}L \tag{4.9}$$

$$C^{'} = \frac{1}{K_mK_f}C \tag{4.10}$$

$$\omega^{'} = K_f\omega \tag{4.11}$$

By using these scaling equations, and designing for an actual cutoff frequency (f_c) of 1 kHz, the final component values were calculated as

$$R_1 = R_2 = 470\,\Omega \tag{4.12}$$

$$R_a = 2700\,\Omega \tag{4.13}$$

$$R_a = 1500\,\Omega \tag{4.14}$$

The complete calculations followed during the design of this Sallen-Key biquad low-pass filter can be found in Appendix C.

Figure 4.12 shows the final Sallen-Key biquad low-pass filter designed for this system as well as the implementation of the instrumentation amplifier.

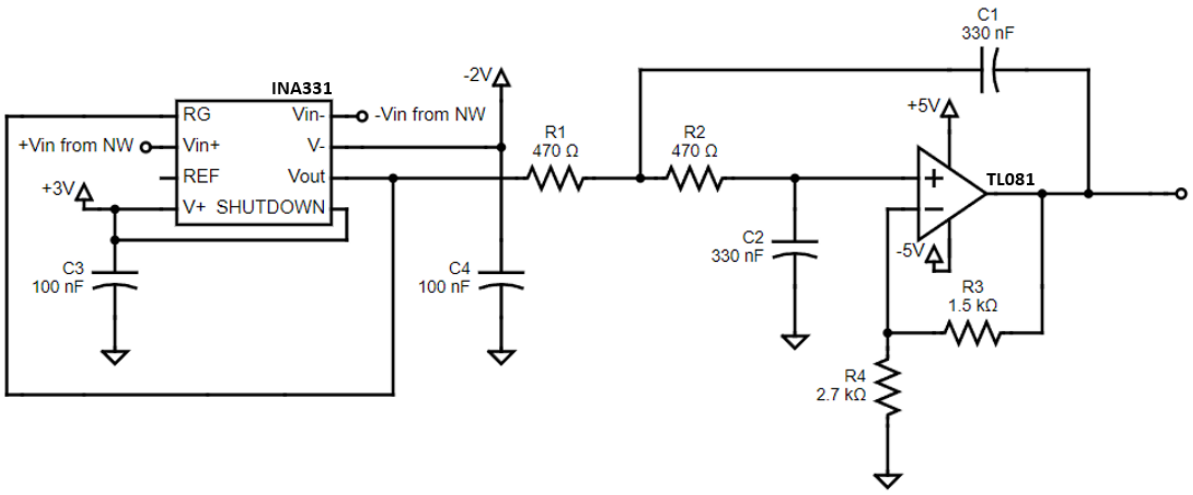

Figure 4.12: Circuit diagram of final electronic system

4.5 Electronics Simulation

LTSpice (Analog Devices, 2021) was used to simulate the electronic circuitry designed for the use of filtering and amplifying the signal, sent out of the ZnO nanowire biosensor developed in this study. It is important to note that, when simulating active filters in LTSpice, the results of the AC analysis are often not consistent with the results of the real-life application. However, the simulation is still useful in confirming the fundamental operation of the electronics designed.

Figure 4.13(a) shows the Sallen-Key biquad low-pass filter circuit that was simulated in LTSpice and Figure 4.13(b) shows the results of the AC sweep.

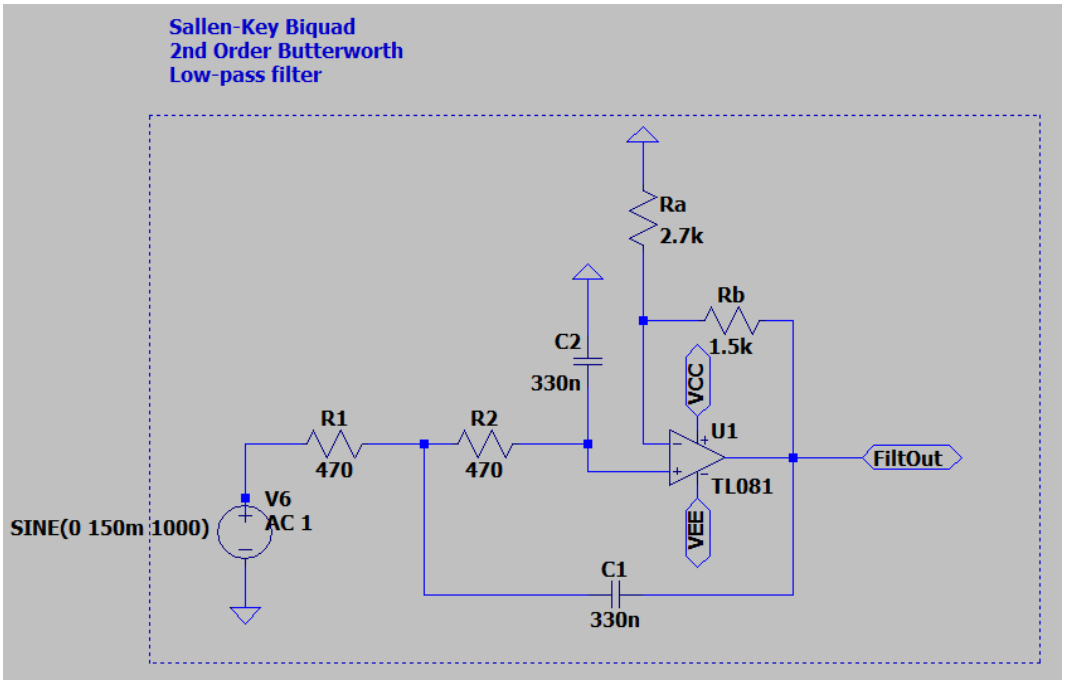

(a) Sallen-Key biquad low-pass filter simulation

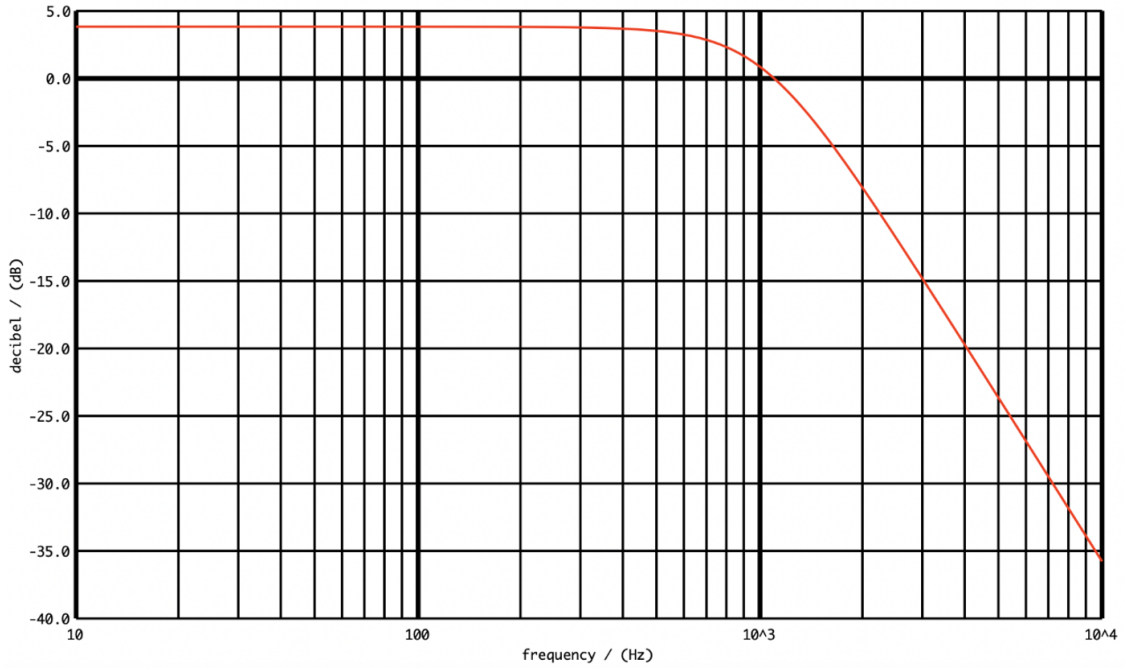

(b) AC Analysis of Sallen-Key biquad low-pass filter

Figure 4.13: Sallen-Key biquad low-pass filter simulation

As shown in the results of the simulation above (Figure 4.13(b)), as the frequency of the input increases, the amplitude of the output signal from the Sallen-Key filter decreases. If this is the case, it means that the filter operates as expected and eliminates the noise experienced due to high frequency signals. The Sallen-Key biquad filter implemented in this simulation was designed for a cut-off frequency of 1 kHz as discussed in Section 4.4.2 above. In the result of the simulation, shown in Figure

4.13(b), it can be seen that the cut-off frequency (which occurs at the point at which the initial gain has decreased by 3 dB) is precisely 1 kHz, as designed for. Therefore, the design can be considered successful and ready to be implemented.

4.6 Electronics Implementation and Results

To implement the electronics in a simple and compact way, Eagle (Autodesk, 2020) was used to create a printed circuit board (PCB) onto which the electronic components could be soldered. The PCB designed for these electronics can be seen in Figure 4.14.

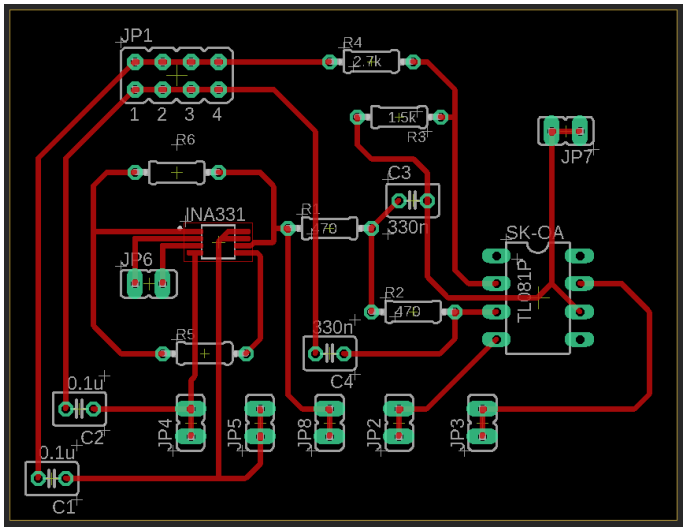

(a) Eagle layout of PCB design

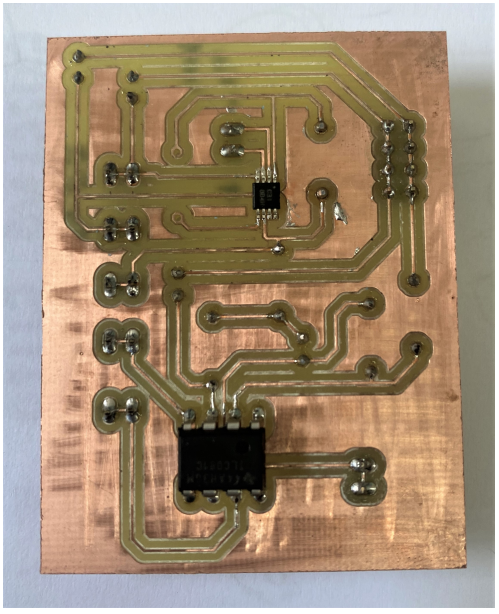

(b) PCB front with integrated circuits

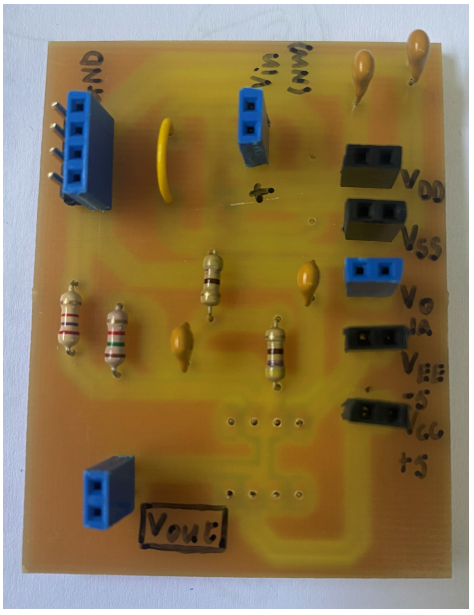

(c) PCB back with electronic components and labels

Figure 4.14: PCB designed for electronic implementation

To test the electronics implemented in this study, a wave generator was used to add a sinusoidal waves (with known, varying frequencies) to the input of the active Sallen-Key biquad filter while observing the output using the Keysight 34401A digital multimeter. Figure 4.15 shows the Bode plot that resulted from these tests with frequencies ranging from 1 Hz to 15 kHz.

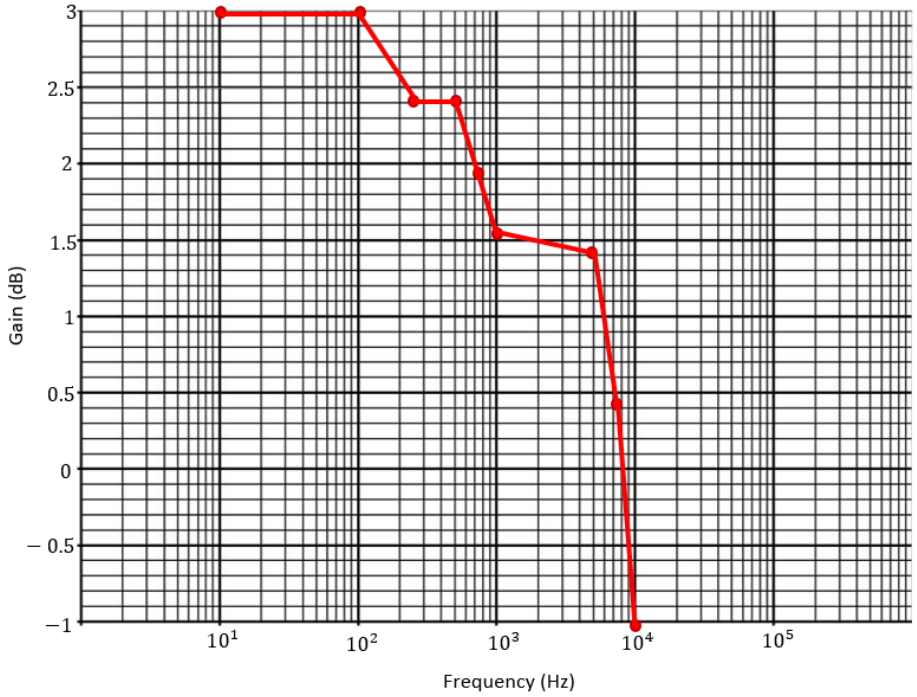

Figure 4.15: Bode plot of real electronic system results

Figure 4.15 shows that the cutoff frequency of the actual system is approximately 8 kHz. This is 8 times higher than the cutoff frequency for which the design was successfully completed as shown in Section 4.5 above.[1] Despite this fact, this electronic system will still be tested in the biosensor application, because the behaviour of the biosensor output will differ significantly from that of the signal generator used during the testing of the filter.

[1] As it is shown in Figure 4.15, the cut-off frequency of the actual system resulted as 8 kHz as opposed to the 1 kHz cutoff frequency for which the system was designed. The electronics tests were completed in September 2021, however the analysis of the acquired data was performed while the author of this study was in Munich, Germany, completing a research internship. Therefore, the electronics were unable to be further adjusted for documentation of a correctly working system in this thesis. As the analysis was done remotely, a LTSpice simulation was performed to assist in understanding the discrepancies between the results from the simulation of the design and the actual implementation. When the required 330 nF capacitors were replaced by 33 nF capacitors (in the simulation), the resulting gain Bode plot from the AC sweep (seen in Figure C.1 in Appendix C) shows a cutoff frequency of 10 kHz. Therefore, it is suspected that 33 nF capacitors were mistakenly used in the implementation of the electronic system.

4.7 Conclusion

The ZnO nanowire arrays deposited onto silicon(100) substrates, as described in Chapter 3, were transformed into ZnO nanowire-based nanogenerators for the detection of the voltage signal produced by the nanowire array upon the infliction of an external disturbance. This was done by controlling the deposition of the nanowires onto only $\frac{2}{3}$ of the surface of the silicon substrate, depositing PMMA between the nanowires to insulate the Au-layers above and below the nanowire arrays, and establishing a means of detecting the signal by creating a Schottky barrier.

An even PMMA layer was created by depositing a PMMA-acetone solution (with a 3 wt% PMMA concentration) onto samples, stationary on the spin coater, before letting the solution seep into the nanowire array for 5 seconds. The spin coater was then set to run at 3000 rpm for 20 seconds. This process resulted in the body of the nanowires being evenly coated with PMMA, and the tips of the nanowires still being exposed for the integration of the Schottky barrier. The nanowire arrays were then coated with a 20 nm layer of Au, to achieve this Schottky barrier.

A sample holder was designed with the purpose of housing and protecting the nanogenerator samples, establishing a solid connection between the nanogenerator and the electronic system and to provide an inlet for the biological samples during the biosensor application.

Various tests, including tapping tests and gas pressure tests, were performed on the nanogenerator samples to confirm the working principle of the ZnO nanowire-based nanogenerator. These tests showed that upon the infliction of an external disturbance on the nanowire arrays, the voltage recorded over the nanowire array increased or decreased from the initial baseline voltage. The constant infliction of pressurised nitrogen gas showed a significant decrease in the voltage and when the gas was removed, the voltage returned to the baseline.

An electronic system, consisting of an instrumentation amplifier and an active Sallen-Key biquadratic filter, was designed to amplify the signal detected over the nanogenerator and to reduce the noise in this signal. The instrumentation amplifier was implemented with a gain of 5 and the Sallen-Key filter was designed for a cut-off frequency of 1 kHz. The implemented circuit, however, resulted in the system having a cutoff frequency of 8 kHz. Regardless, this electronic system will still be tested in the biosensor application because the behavior of the biosensor output will differ significantly from that of the signal generator used during the testing of the filter.

Chapter 5

Anti-Mortalin Antibody Immobilisation

This chapter discusses the antibody immobilisation techniques tested and used in the immobilisation of anti-Mortalin antibody onto gold (Au) coated silicon substrates and Au-coated ZnO nanowire arrays. The immobilisation methods tested include covalent immobilisation, using a 3-MPA SAM with EDC/NHS as well, as the immobilisation using a Cysteamine SAM with a Glutaraldehyde cross-linker. Furthermore, this chapter covers the analysis of the immobilised antibodies using fluorescent microscopy and discusses the process followed to ensure the successful binding of Mortalin antigen to the immobilised anti-Mortalin antibodies, for the biosensor application.

5.1 Introduction

The next stage of this study involved the immobilisation of anti-Mortalin antibodies onto the top surface of the ZnO nanowire arrays on the nanogenerators. To do this, an immobilisation strategy, with the ability of immobilising anti-Mortalin antibodies onto gold, sputter coated by the Leica EM ACE200 vacuum coater used for all gold deposition in this study, needs to be developed.

Two different covalent antibody immobilisation strategies are to be tested:

1. The development of a 3-MPA self-assembled monolayer (SAM) with EDC and NHS cross-linking.
2. A Cysteamine-based SAM with Glutaraldehyde cross-linking.

These methods will be tested for the immobilisation of anti-Mortalin antibodies onto Au-coated Si substrates and Au-coated ZnO nanowire arrays and the most efficient and successful strategy will be selected for the biosensor application.

5.2 Methodology and Equipment

The following equipment was used while carrying out the antibody immobilisation methods tested in this study:

Calibrated pipettes of various sizes were used to measure specific amounts of the antigen, antibodies, buffers and other reagents used in this study. Any reagents that were in powder or crystal form were weighed on a calibrated microscale and stored in 1.5 ml, 2 ml or 5 ml Eppendorf tubes, to avoid contamination.

The antibody immobilisation stages, including the incubation of the nanogenerator samples onto which the antibodies were to be immobilised in the various solutions (to be discussed later in this chapter), took place in 24-well cell culture plates. This is because the Au-coated silicon and ZnO nanowire array samples fit perfectly into these wells and the volume of the solution for incubation could be easily controlled in the wells.

Figure 5.1 shows the equipment used for the immobilisation of anti-Mortalin antibodies onto Au-coated ZnO nanowire arrays.

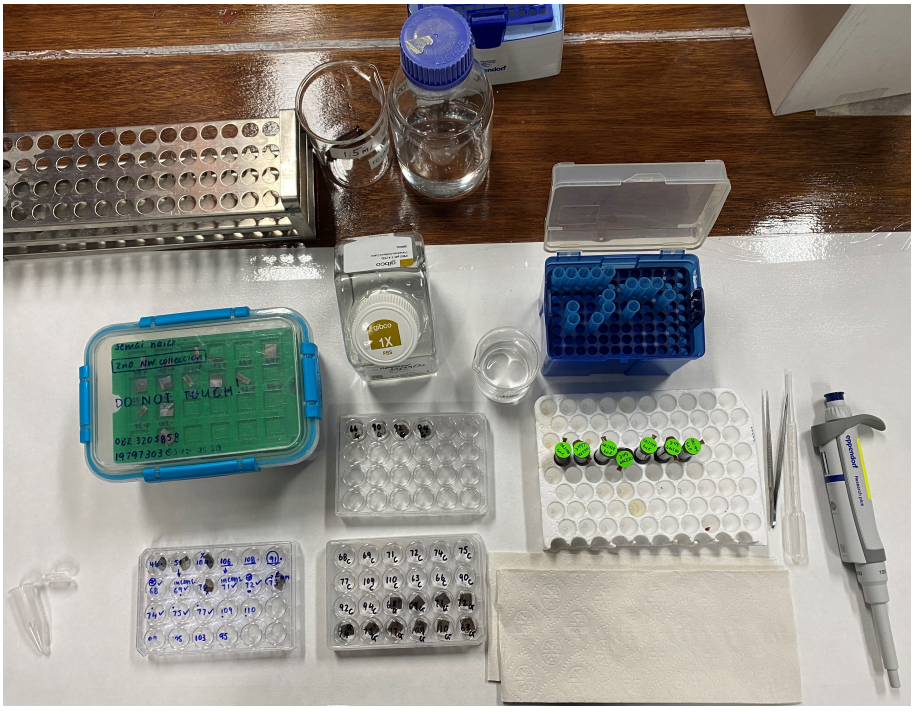

Figure 5.1: Anti-Mortalin antibody immobilisation setup

The success of the antibody immobilisation methods was analysed using the Zeiss Axio Observer 7 (Carl Zeiss, Germany) fluorescent microscope. All images were obtained with the light source intensity set to 33.33% in order for the images to be comparable during the analyses.

The ChemiDoc XRS+ (Bio-Rad Laboratories) was used to verify the anti-Mortalin antibody and Mortalin antigen binding, by performing the process of Chemiluminescence imaging.

5.3 Immobilisation of anti-Mortalin Antibody Onto Gold Coated Silicon Substrates

The initial antibody immobilisation tests were done to verify that the anti-Mortalin antibody can be immobilised onto a plain Au-coated silicon substrate, before attempting to immobilise the antibodies onto the Au-coated ZnO nanowire arrays. This was first done using the EDC (N-(3-Dimethylaminopropyl)-N'-ethylcarbodiimide hydrochloride)/NHS (N-Hydroxysuccinimide) protocol and then finally the Cysteamine/Glutaraldehyde protocol was attempted.

According to du Toit [55], the immobilisation of antibodies onto a Au-coated surface includes three stages:

1. The functionalisation of the Au with a polymer that contains a free thiol group, with the ability to react with the gold to form a self-assembled monolayer (SAM) using a poly-ethylene glycol (PEG) product such as 3-Mercap-topropionic acid (3-MPA), or a reagent such as Cysteamine;
2. The activation of the functional groups on the SAM layer using cross-linking reagents, such as EDC/NHS or Glutaraldehyde;
3. The binding of antibodies to the SAM layer developed on the Au layer.

5.3.1 Immobilisation using EDC/NHS

A protocol for the immobilisation of antibodies using EDC/NHS was optimised by du Toit [55] and will be followed in this study.

First, the Au-surface was to be functionalised with carboxyl groups with the use of thiolated 3-MPA containing a carboxyl functional group. The carboxyl groups are then to be activated by EDC and stabilised with NHS, before they react with the amine functional group present on the anti-Mortalin antibody.

The following steps were executed during the immobilisation of anti-Mortalin antibody, onto Au-coated Si(100) samples, using the EDC/NHS protocol in this study (Table 5.1 shows a summary of the various chemicals that were used in this process):

1. Gold coated Si(100) samples were baked in a furnace at 300°C for 30 minutes to sterilise them, and remove any organic matter, in preparation the the antibody immobilisation.
2. A solution of 3-MPA (Sigma-Aldrich, 107-96-0) in 70% ethanol, with a concentration of 10 mM, was mixed.
3. 400 µl of this 3-MPA solution was added onto each sample (placed into the cell culture plate wells) and the samples were left to incubate in the fridge overnight.
4. A 2-(N-morpholino)ethanesulfonic acid (MES) buffer was developed by mixing MES (Sigma-Aldrich, CAS 145224-94-8) in DI water to achieve a concentration of 1.95 g/100 ml. The pH of this solution was controlled to pH = 5.8 with the use of sodium hydroxide (NaOH).
5. The samples were rinsed twice with 70% ethanol.
6. The samples were rinsed twice with the MES buffer.
7. A solution of EDC (Sigma-Aldrich, CAS 25952-53-8), NHS (Sigma-Aldrich, CAS 6066-82-6) and MES was made with EDC and NHS at concentrations of 4 mg/ml and 6 mg/ml respectively.
8. 400 µl of this EDC/NHS solution was added onto each sample (placed into the cell culture plate wells) and the samples were left to incubate for 15 minutes.
9. Anti-Mortalin antibody (Biocom Africa, AB2799) was mixed into phosphate buffered saline (PBS) with a dilution of 1:200.
10. The samples were rinsed twice with the MES buffer.
11. The samples were rinsed twice with a PBS solution.
12. 400 µl of the antibody/PBS solution was added onto each sample (placed into the cell culture plate wells) and the samples were left to incubate in the fridge overnight.

Table 5.1: Chemicals used in antibody immobilisation with EDC/NHS.

Chemical Name	CAS Number	Supplier
3-MPA (3-Mercaptopropionic acid)	107-96-0	Sigma-Aldrich
MES (2-(N-morpholino)ethanesulfonic acid)	145224-94-8	Sigma-Aldrich
EDC (N-(3-Dimethylaminopropyl)-N′-ethylcarbodiimide hydrochloride)	25952-53-8	Sigma-Aldrich
NHS (N-Hydroxysuccinimide)	6066-82-6	Sigma-Aldrich

5.3.2 Immobilisation using Cysteamine and Glutaraldehyde

The next antibody immobilisation strategy that was employed in this study was the use of Cysteamine SAM technologies with a Glutaraldehyde cross-linking layer, with the purpose of strengthening the covalent bonds between the Cysteamine SAM and the anti-Mortalin antibodies.

The following steps were executed during the immobilisation of anti-Mortalin antibody, onto Au-coated Si(100) samples, using Cysteamine and Glutaraldehyde (Table 5.2 shows a summary of the various chemicals that were used in this process and the stoichiometric calculations can be found in Appendix D):

1. Au-coated Si(100) samples were baked in a furnace at 300°C for 30 minutes to sterilise them, and remove any organic matter, in preparation the the antibody immobilisation.

2. A solution, with a concentration of 0.01 M, of Cysteamine hydrochloride (Sigma-Aldrich, CAS 156-57-0) in PBS was mixed.

3. The Au-coated Si samples were rinsed twice with a PBS solution.

4. 400 µl of this Cysteamine/PBS solution was added onto each sample (placed into the cell culture plate wells) and the samples were left to incubate in the fridge for 2 hours.

5. A 1.5% Glutaraldehyde (Sigma-Aldrich, CAS 111-30-8) in PBS solution was mixed.

6. The samples were rinsed twice with a PBS solution.

7. 400 µl of this Glutaraldehyde/PBS solution was added onto each sample (placed into the cell culture plate wells) and the samples were left to incubate in the fridge for at least (but not restricted to) 1 hour.

8. Anti-Mortalin antibody (Biocom Africa, AB2799) was mixed into phosphate buffered saline (PBS) with a dilution of 1:200.

9. The samples were rinsed twice with a PBS solution.

10. 400 µl of this antibody/PBS solution was added onto each sample (placed into the cell culture plate wells) and the samples were left to incubate in the fridge overnight.

11. Samples were stored in a PBS buffer, ready for testing.

Table 5.2: Chemicals used in antibody immobilisation with Cysteamine/Glutaraldehyde.

Chemical Name	CAS Number	Supplier
Cysteamine hydrochloride	156-57-0	Sigma-Aldrich
Glutaraldehyde	111-30-8	Sigma-Aldrich

5.3.3 Confirmation of anti-Mortalin Antibody Immobilisation onto Au-coated silicon substrates

To confirm the successful immobilisation of anti-Mortalin antibody on the Au-coated silicon substrates, fluorescent microscopy was performed using the Zeiss Axio Observer, as discussed in Section 5.2. In order to use this confirmation method, a secondary antibody, with a fluorescent marker, had to be immobilised onto the primary anti-Mortalin antibody layer. In this study the goat anti-mouse polyclonal secondary antibody IgG, equipped with H and L (Alexa Fluor ®488) (Abcam, ab150113) was used.

The following protocol was used for the immobilisation of the secondary antibody onto the samples:

1. The goat anti-mouse polyclonal secondary antibody was mixed into PBS with a dilution of 1:150.

2. The samples were rinsed twice with a PBS solution.

3. 400 µl of this secondary antibody-PBS solution was added onto each sample, placed into the cell culture plate wells, and the cell culture plate was wrapped in foil. This stage was performed in a dark room to prevent the Alexa Fluor ®488 from being bleached.

4. The samples were left to incubate in the fridge for 5 hours.

5. The samples were rinsed twice with a tris-buffered saline and tween (TBS-T) solution.

Following this protocol, the samples were placed on glass slides and into the sample holder of the Zeiss Axio Observer fluorescent microscope. With every batch of samples analysed, a Cysteamine control sample (with no primary and only secondary antibodies immobilised) was included in order to have a baseline for the comparison of the fluorescence of the immobilised samples.

Figure 5.2 shows a Cysteamine control sample (a), along with an Au-coated sample including antibodies immobilised using the EDC/NHS and Cysteamine/Glutaraldehyde strategies in Figure 5.2(b) and (c) respectively. As can be seen, there is no significant difference between the cysteamine control sample and the sample with Anti-Mortalin antibodies immobilised using EDC/NHS. Contrastingly, the sample with Anti-Mortalin antibodies immobilised using Cysteamine/Glutaraldehyde (c) shows a significantly increase fluorescence when compared to the Cysteamine control sample (a). Therefore, in this study, the Cysteamine/Glutaraldehyde antibody immobilisation samples will be employed. This is also advantageous because the Cysteamine/Glutaraldehyde includs fewer process steps and can be performed in a shorter time frame.

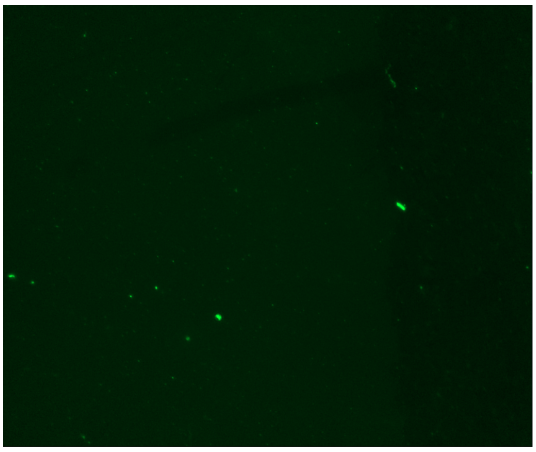

(a) Cysteamine control

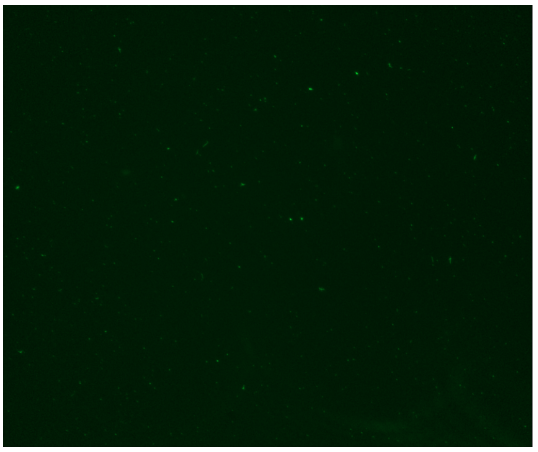

(b) Anti-Mortalin antibodies immobilised onto Au-coated silicon using EDC/NHS

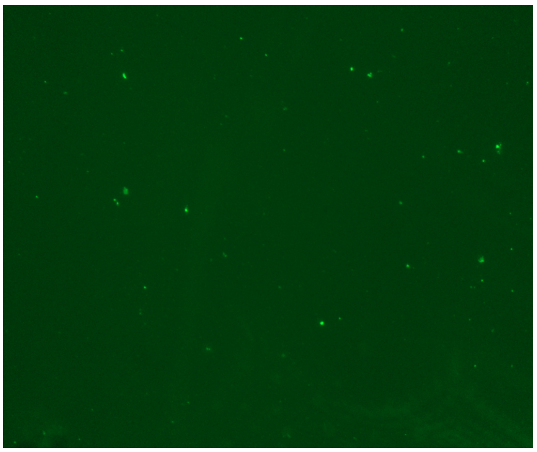

(c) Anti-Mortalin antibodies immobilised onto Au-coated silicon using Cysteamine/Glutaraldehyde

Figure 5.2: Immobilisation of anti-Mortalin antibody onto Au-coated silicon substrate using EDC/NHS versus Cysteamine/Glutaraldehyde

Further tests were performed on Au-coated Si(100) samples to determine the dilution of anti-Mortalin antibody that will completely saturate the entire area of the sample. This was done by following the Cysteamine/Glutaraldehyde protocol discussed in Section 5.3.2, with an adjustment in Steps 8 to 10 to include some samples incubated in an anti-Mortalin antibody/PBS solution with a dilution of 1:150. Figure 5.3 shows the results of this test acquired during fluorescent microscopy. As it can be seen, there is no significant difference between the fluorescence of the sample with antibodies in a 1:150 dilution (Figure 5.3(a)) and that with a 1:200 dilution (Figure 5.3(b)). Therefore, in order to minimise unnecessary use of the expensive antibodies, a dilution of 1:200 will continue to be used in this study.

(a) Cysteamine control

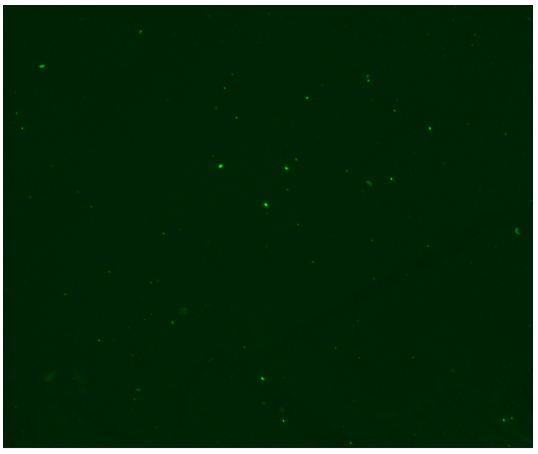

(b) Anti-Mortalin antibodies (dilution 1:150 in PBS) immobilised onto Au-coated silicon using Cysteamine/Glutaraldehyde

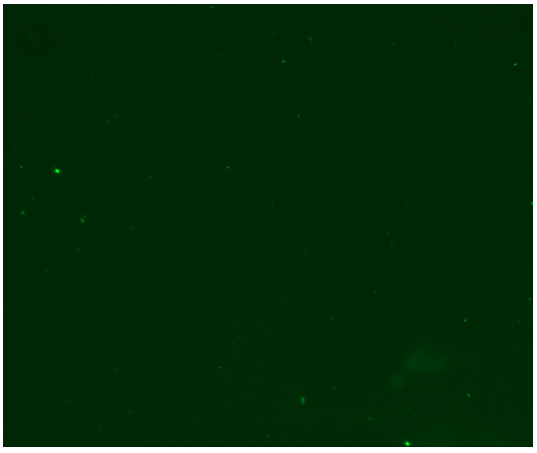

(c) Anti-Mortalin antibodies (dilution 1:200 in PBS) immobilised onto Au-coated silicon using Cysteamine/Glutaraldehyde

Figure 5.3: Testing the immobilisation of different anti-Mortalin antibody dilutions onto Au-coated silicon substrate using Cysteamine/Glutaraldehyde

5.4 Immobilisation Onto ZnO Nanowire Arrays

Once it was confirmed that anti-Mortalin antibodies can be immobilised onto the silicon samples with a layer of gold sputter-coated using the Leica EM ACE200 (Leica Microsystems, Germany), a trial of tests began to immobilise anti-Mortalin antibodies onto Au-coated nanowire arrays. As the top surface of the nanowire arrays are not as even as the surface of Au-coated silicon wafers, the concentration of the reagents may need to be adjusted for the successful immobilisation of antibodies for the biosensor integration.

5.4.1 Immobilisation of antibodies onto ZnO nanowire arrays using Cysteamine and Glutaraldehyde

The same process discussed in Section 5.3.2 was followed to immobilise anti-Mortalin antibodies onto a set of ZnO nanowire array samples. All process steps from Step 1 to Step 10 were followed precisely. However, the Au-coated silicon substrate samples were replaced by Au-coated ZnO nanowire array samples and extra care was taken not to scratch or damage any part of the nanowire array.

Figure 5.4 shows the results of this immobilisation procedure. As can be seen in the results, the Cysteamine sample fluoresces significantly (although less than the sample with anti-Mortalin antibodies immobilised), indicating that non-specific binding of the antibodies has occurred. Therefore, it is necessary to consider the inclusion of a BSA-blocking stage.

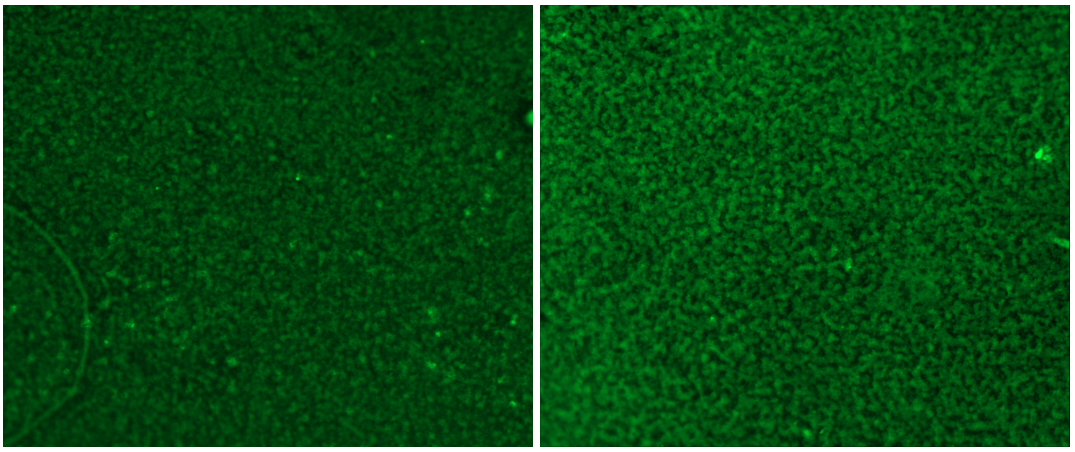

(a) Cysteamine control on ZnO nanowires

(b) Anti-Mortalin antibodies (dilution 1:200 in PBS) immobilised onto Au-coated ZnO nanowires

Figure 5.4: Anti-Mortalin antibodies immobilised onto Au-coated ZnO nanowires

A BSA-blocking stage is useful for the purpose of saturating excess protein-binding sites on the surface of the substrate onto which the biological sample is to be added for the biosensor application. A further discussion of this can be found in Section 6.2.

5.5 Supplementary Tests

This section discusses two supplementary tests that were completed as part of the antibody binding confirmation process. The first test has the purpose of determining the effects of the auto-fluorescence of Glutaralderhyde and the second test is with the purpose of confirming the binding of the anti-Mortalin antibody to the Mortalin

antigen protein that is of interest in the biological samples that will be deposited during the biosensor testing.

5.5.1 Glutaraldehyde auto-fluorescence

Glutaraldehyde is a widely used fixative that forms part of the aldehyde fixative group - largely known for their reactions with amines and proteins to generate fluorescent products [56][57]. Compared to other aldehydes, Glutaraldehyde typically induces particularly high auto-fluorescence [57]. Therefore, it was necessary to determine the auto-fluorescence of the Glutaraldehyde used in the immobilisation of anti-Mortalin antibodies onto ZnO nanowire arrays, in the event that it may be necessary to eliminate its fluorescence from the final results to determine the true antibody binding.

The following protocol was followed during the test to determine the auto-fluorescence of Glutaraldehyde on ZnO nanowires:

1. Au-coated ZnO nanowire array samples were baked in a furnace at 300°C for 30 minutes to sterilise them, and remove any organic matter.
2. A solution with a concentration of 0.01 M of Cysteamine hydrochloride (Sigma-Aldrich, CAS 156-57-0) in PBS was mixed.
3. The samples were rinsed twice with a PBS solution.
4. 400 µl of this Cysteamine/PBS solution was added onto each sample (placed into the cell culture plate wells) and the samples were left to incubate in the fridge for 2 hours.
5. A 1.5% Glutaraldehyde (Sigma, CAS 111-30-8) in PBS solution was mixed.
6. The samples were rinsed twice with a PBS solution.
7. 400 µl of this Glutaraldehyde/PBS solution was added onto each sample (placed into the cell culture plate wells) and the samples were left to incubate in the fridge for at least (but not restricted to) 1 hour.

These samples were then placed under the Zeiss Axio Observer along with a Cysteamine control sample. Figure 5.5 shows the results of this test and as it can be seen, there is no fluorescence emitted by the sample coated in Glutaraldehyde (Figure 5.5(b)) compared to the Cysteamine control sample (Figure 5.5(a)). Therefore, the effects of the auto-fluorescence of the Glutaraldehyde were considered negligible in this study.

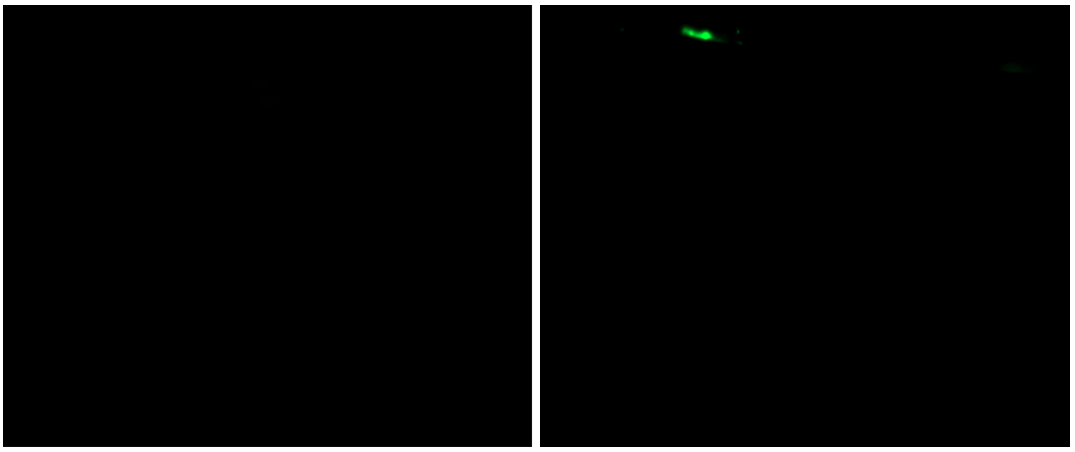

(a) Cysteamine control sample (b) Glutaraldehyde coated sample

Figure 5.5: Testing the auto-fluorescence of Glutaraldehyde coated onto ZnO nanowire array samples

5.5.2 Antibody-Antigen binding

The working principle of the ZnO nanowire-based nanoforce biosensor relies on the successful binding of the Mortalin antigen (contained in the biological sample) to the anti-Mortalin antibodies immobilised onto the surface of the nanogenerator biosensor. Therefore, a Chemiluminescence test was performed using the ChemiDoc XRS+ (Bio-Rad Laboratories) on anti-Mortalin antibody samples spots with and without Mortalin antigen deposited.

The following steps were followed in this test:

1. Two samples of nitrocellulose membrane were cut with an area of 10 mm $\times$ 10 mm.
2. 2 µl of Mortalin antigen (Biocom Africa, AB79145) was dropped onto one sample (Sample 1) and left to dry.
3. Another 2 µl of Mortalin antigen was dropped onto Sample 1 and left to dry.
4. A 5% (5 g/100 ml) solution of Bovine Serum Albumin (BSA) (Sigma-Aldrich, CAS 9048-46-8) in TBS-T was mixed.
5. Sample 1 and 2 were placed in separate cuvettes and each cuvette was labelled accordingly.
6. 400 µl of the BSA/TBS-T solution was placed in each cuvette and the samples were left to incubate for 1 hour.
7. The samples were rinsed twice with a TBS-T solution.

8. Anti-Mortalin antibody (Biocom Africa, AB2799) was mixed into TBST with a dilution of 1:250.

9. 400 µl of the antibody/TBS-T solution was placed in new cuvettes, along with the samples, and they were left to incubate in the fridge overnight.

10. Anti-mouse IgG, HRP-linked secondary antibody #7076 (Cell Signaling Technology, #7076) was mixed into TBS-T with a dilution of 1:250.

11. 400 µl of the secondary antibody/TBS-T solution was placed in new cuvettes, along with the samples, and they were left to incubate in the fridge for 3 hours.

Samples 1 and 2 were then placed in the ChemiDoc XRS+. The hypothesis is that, on Sample 1 (with the Mortalin antigen) antigen-antibody binding will have taken place and due to Chemiluminescence, there will be an emission of light as the result of the binding reaction. Sample 2, however, should not emit any light in the ChemiDoc and should appear clear.

Figure 5.6 shows the results of the test in the ChemiDoc. As shown, Sample 1 (on the left) emits light due to the binding of the antigen to the antibody and Sample 2 (on the right) cannot be seen due to no light being emitted. This confirms that the anti-Mortalin anti body and the Mortalin antigen will successfully bind on the surface of the biosensor.

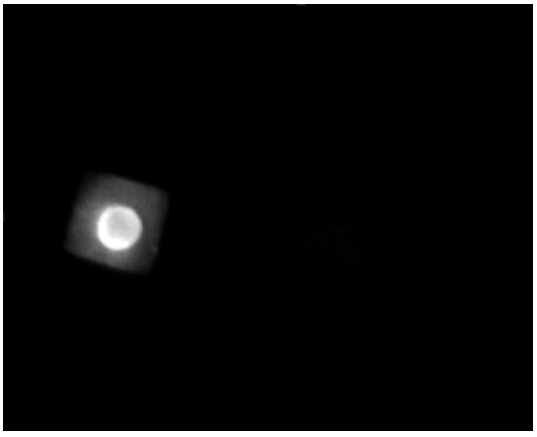

Figure 5.6: Results from Chemiluminescence test

5.6 Conclusion

For the ZnO nanowire-based nanoforce biosensor application of the ZnO nanowire nanogenerator, anti-Mortalin antibodies had to be immobilised onto the nanogenerators developed in Chapter 4. Two strategies for the immobilisation of anti-Mortalin antibodies onto Au-coated Silicon samples were tested. Both strategies made use of SAM and cross-linking technologies. The first method made use of a 3-MPA SAM

and used both EDC and NHS for the cross-linking stage and the second method used a Cysteamine SAM with a Glutaraldehyde cross-linker.

With the immobilisation of a goat anti-mouse polyclonal secondary antibody and the use of a fluorescent microscope, it can be concluded that the Cysteamine/Glutaraldehyde immobilisation strategy is the most effective for the immobilisation of anti-Mortalin antibodies onto Au-coated surfaces. This also provides an extra advantage, because the Cysteamine/Glutaraldehyde strategy requires less time and reagents than the EDC/NHS protocol.

Anti-Mortalin antibodies were also successfully immobilised onto Au-coated ZnO nanowire array samples, using the Cysteamine/Glutaraldehyde protocol. However, there is significant non-specific binding that takes place during this immobilisation, which required the addition of a BSA-blocking stage. This will be performed in the biosensor integration stage of this study.

Two supplementary tests were done as part of this study: 1) to determine the auto-fluorescence of the Glutaraldehyde utilised in the immobilisation protocal and 2) to determine the successful binding of Mortalin antigen to anti-Mortalin antibodies. Test 1 proved that there is minimal auto-fluorescence that occurs when the Glutaraldehyde is coated onto the ZnO nanowire array samples and these effects can therefore be deemed negligible. Test 2 showed the successful binding of Mortalin antigen to anti-Mortalin antibodies through the emission of light from the sample on which the binding occurred.

Chapter 6

ZnO Nanowire Biosensor

This chapter discusses the integration of the ZnO nanowire arrays with the anti-Mortalin antibody immobilisation strategy and the electronic system to develop the final biosensor system. The biosensor testing setup is briefly discussed, followed by a discussion of the full testing procedures followed for the confirmation of the working of the Mortalin biosensor.

6.1 Introduction

To transform the general-application nanogenerators, developed and discussed in Chapter 4, into ZnO nanowire based biosensors for the detection of Mortalin, a prospective biomarker for Parkinson's disease, anti-Mortalin antibodies are to be immobilised onto the ZnO nanowire array of the nanogenerator and the electronic system developed is to be integrated. As explained in Section 2.4.4, piezoelectric nanogenerators rely on the fact that, upon an external disturbance, such as a mass being applied to a nanowire array, bending will occur in the nanowire arrays. When this lateral bending takes place, a voltage drop occurs over the nanowires in the array.

In the biosensor application of ZnO nanowire-based nanogenerators, we rely on this phenomenon as we base the working principle of the biosensor upon the fact that, if anti-Mortalin antibodies are immobilised onto the nanowire array of the nanogenerator, and a biological sample (containing the Mortalin antigen of interest) is added onto this biosensor, the antibody and antigen will bind, causing an increase in mass on the nanogenerator. This increased mass should cause a change in the baseline voltage measured over the nanoforce biosensor.

6.2 Biosensor Integration

All developments throughout this study have been aimed towards the development of a biosensor that detects Mortalin, a novel biomarker for Parkinson's Disease.

For the integration of the nanogenerator and antibody immobilisation technique into a ZnO nanowire-based nanoforce biosensor, utilising the protocol discussed in Section 5.3.2 (i.e. the immobilisation of anti-Mortalin antibodies onto Au-coated nanowire arrays using Cysteamine and Glutaraldehyde), anti-Mortalin antibodies are to be immobilised onto ZnO nanowire based nanogenerators. Figure 6.1 shows a diagram of the biosensor once the antibodies are immobilised onto the biosensor (a) and how the Mortalin antigens are anticipated to bind to these immobilised antibodies.

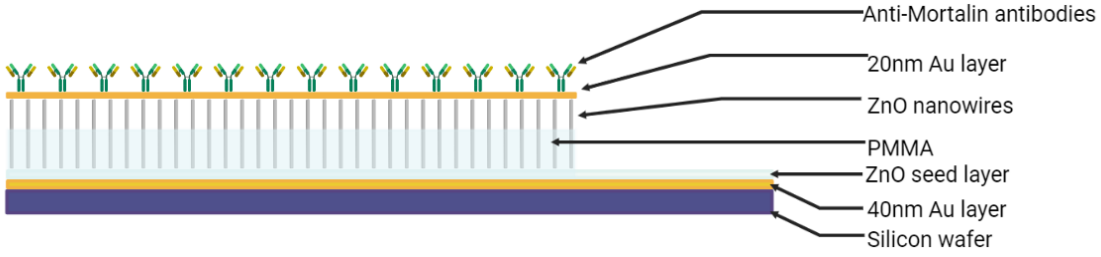

(a) Schematic of ZnO nanowire-based nanoforce biosensor

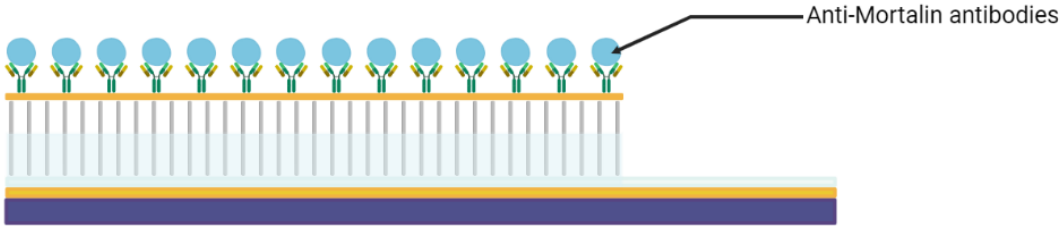

(b) Schematic of ZnO nanowire-based nanoforce biosensor with Mortalin antigen

Figure 6.1: ZnO nanowire based nanoforce biosensor - nanogenerator and antibody integration

As discussed in Section 5.4.1, significant non-specific binding took place during the immobilisation of anti-Mortalin antibodies onto Au-coated ZnO nanowire arrays. Therefore, the process of immobilising the anti-Mortalin antibodies onto ZnO nanowire-based nanogenerators was adjusted to include a BSA-blocking stage as follows:

1. ZnO nanowire array samples were baked in a furnace at 300°C for 30 minutes to sterilise them, and remove any organic matter, in preparation the the antibody immobilisation.

2. PMMA was deposited between the nanowire arrays as discussed in Section 4.2.1.
3. The samples were sputter-coated with a layer of Au with a thickness of 20 nm.
4. A solution with a concentration of 0.01 M of Cysteamine hydrochloride (Sigma-Aldrich, CAS 156-57-0) in PBS was mixed.
5. The nanogenerator samples were rinsed twice with a PBS solution.
6. 400 µl of this Cysteamine-PBS solution was added onto each sample (placed into the cell culture plate wells) and the samples were left to incubate in the fridge for 2 hours.
7. A 1.5% Glutaraldehyde (Sigma, CAS 111-30-8) in PBS solution was mixed.
8. The samples were rinsed twice with a PBS solution.
9. 400 µl of this Glutaraldehyde-PBS solution was added onto each sample (placed into the cell culture plate wells) and the samples were left to incubate in the fridge for at least (but not restricted to) 1 hour.
10. Anti-Mortalin antibody (Biocom Africa, AB2799) was mixed into phosphate buffered saline (PBS) with a dilution of 1:200.
11. The samples were rinsed twice with a PBS solution.
12. 400 µl of this antibody-PBS solution was added onto each sample (placed into the cell culture plate wells) and the samples were left to incubate in the fridge overnight.
13. A 5% (5 g/100 ml) solution of Bovine Serum Albumin (BSA) (Sigma-Aldrich, CAS 9048-46-8) in PBS was mixed.
14. The samples were stored in this BSA-PBS solution to prepare of biosensor testing.

To determine the effectiveness of the BSA-blocking stage, confirmation testing was performed (as discussed in Section 5.3.3) by immobilising anti-mouse polyclonal secondary antibody IgG (Abcam, ab150113) onto the samples and analysing them under the fluorescent microscope. Figure 6.2 shows the results of this test. As can be seen, there is no longer any significant non-specific binding that takes place on the Cysteamine control sample, as was observed in Figure 5.4. This means that the inclusion of the BSA blocker was successful in the elimination of non-specific binding of proteins on the biosensor surface.

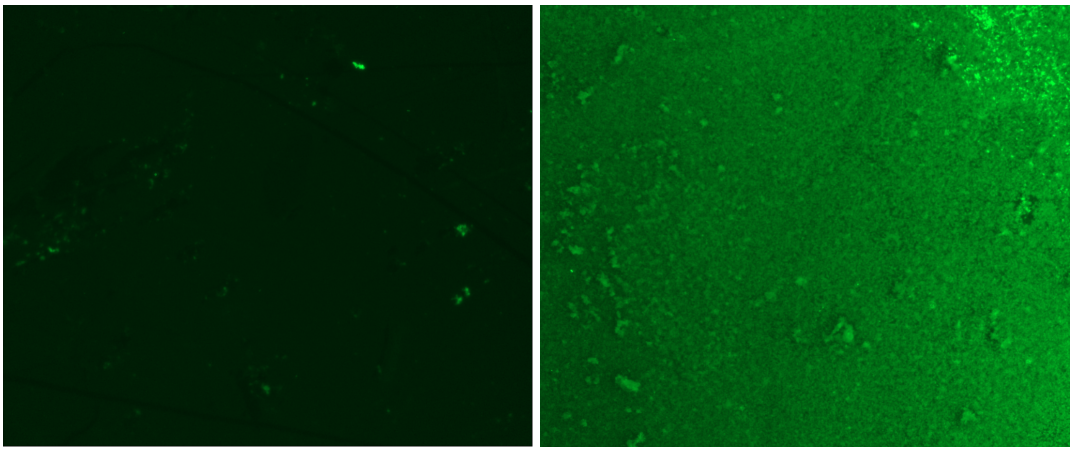

(a) Cysteamine control with BSA on ZnO nanowires

(b) Anti-Mortalin antibodies (dilution 1:200 in PBS) immobilised with BSA onto Au-coated ZnO nanowires

Figure 6.2: Anti-Mortalin antibodies immobilised onto Au-coated ZnO nanowires with BSA-blocking stage

The nanogenerator-antibody system developed by immobilising anti-Mortalin antibodies (using the methods discussed in Chapter 5) onto the ZnO nanowire-based nanogenerators developed (according to the methods in Chapters 3 and 4) are the basis of the ZnO nanowire-based nanoforce biosensors. This system, in conjunction with the electronics developed and discussed in Chapter 4, make up the full extent of the ZnO nanowire-based nanoforce biosensor and perform the following vital functions of a biosensor, as mentioned in Section 2.3.1:

1. The immobilised anti-Mortalin antibodies act as the biological element that actively and specifically bind to the Mortalin antigen contained in the biological sample.

2. The ZnO nanowire-based nanogenerator acts as the transducer that emits a quantifiable voltage signal upon the binding of the anti-Mortalin antibody to the Mortalin antigen, which causes the nanowires to bend.

3. The instrumentation amplifier and Sallen-Key biquad filter electronic system works to convert the signal from the nanogenerator into interpretable results by amplifying the signal and reducing the noise observed in the output of the system.

Figure 6.3 shows the full setup of the biosensor system with the nanogenerator, complete with antibodies immobilised and the full electronic system. This is the setup that was used for the biosensor testing. Initially, the electronic system was not included and the Keysight 34401A digital multimeter was connected directly to the

spring pins on the sample holder to measure the output of the biosensor. The electronic system was then connected to the system for further tests and the results were compared.

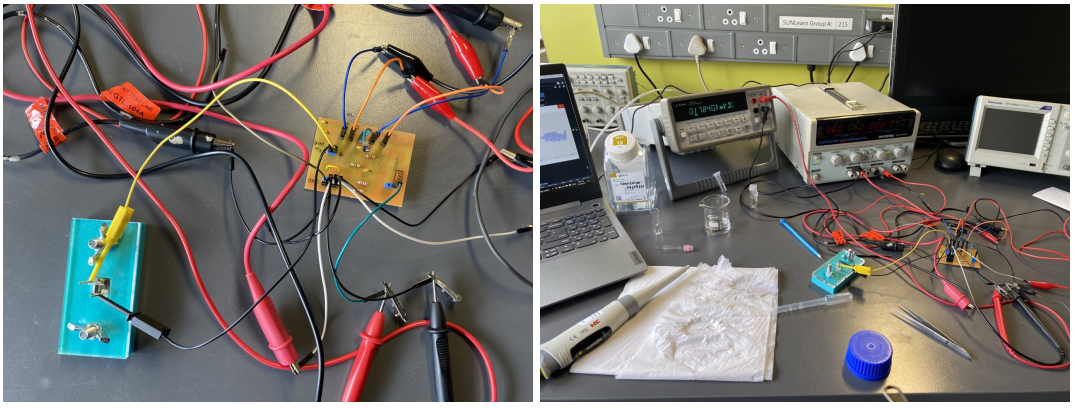

(a) Full biosensor system

(b) Full biosensor system with biological sample

Figure 6.3: Full Mortalin antigen nanoforce biosensor system with electronic integration

6.3 Biosensor Testing

Various tests were performed to determine the working efficiency of the ZnO nanowire-based nanoforce biosensors. Firstly, tests were performed to ascertain that the biosensor samples produce some result when a solution, with an arbitrary antigen concentration, is dropped onto the biosensor. This was done without the electronic integration to determine the raw data that was to be processed. Next, with the integration of the electronic system, the buffer (PBS) used for the mixing of Mortalin antigen concentration solutions was dropped onto the biosensor, to determine the baseline effects of this buffer on the biosensor. Finally, solutions with different (known) concentrations of Mortalin antigen in PBS were dropped onto the biosensor, to understand whether different Mortalin concentrations can be detected by the biosensors. It is anticipated that, with an increase in Mortalin concentration, the biosensor signal would be greater or have a larger difference between the initial and final baseline voltage values.

6.3.1 Biosensor testing without electronic integration

Initially, the developed ZnO nanowire biosensors were tested by dropping a solution of known concentration of Mortalin antigen in PBS onto the biosensor. This solution was used to mimic the biological samples that would be utilised in real-life biosensor applications.

For this test, a "biological sample" with an arbitrary concentration of 5 µg/ml of

Mortalin antigen in PBS was used to drop onto the biosensors. The biosensor was directly connected to the digital multimeter and the baseline voltage was established before 20 µl of the 'biological sample' was gently added onto the biosensor through the inlet of the sample holder. Figure 6.4 shows the resulting output from the two different biosensor samples, detected by the digital multimeter, during this test.

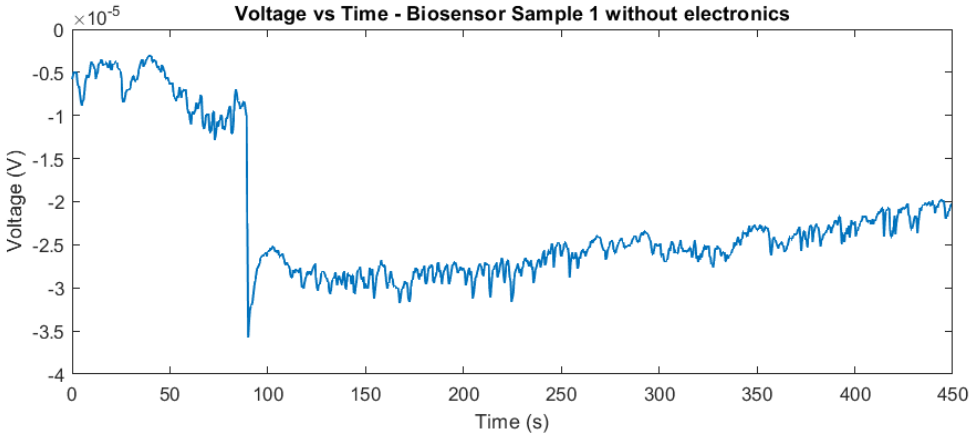

(a) 5 µg/ml solution of Mortalin antigen on biosensor Sample 1

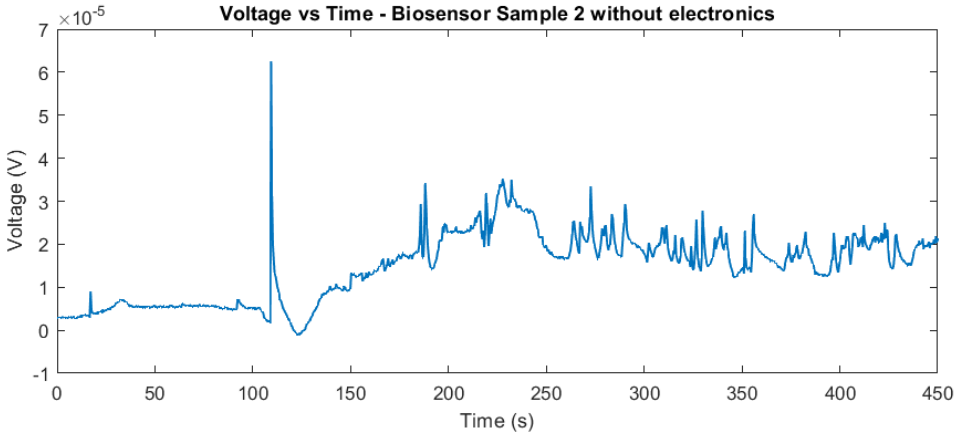

(b) 5 µg/ml solution of Mortalin antigen on biosensor Sample 2

Figure 6.4: Antigen-biosensor test results for tests performed without electronic system implementation

The Mortalin antigen-PBS solution was dropped onto the sample at approximately 100 seconds. This can be seen with the large spike in voltage at this point. During the binding of the Mortalin antigen to the anti-Mortalin antibody, Figure 6.4 (a) and (b) both show that there is a gradual shift from the baseline voltage until a final voltage will be established.

This is precisely the response that would be expected from the output of this ZnO nanowire-based nanoforce biosensor. Due to the immobilised anti-Mortalin antibodies, there is already an initial baseline voltage that can be established, caused merely by the weight of the on the ZnO nanowires in the array. During the antibody-antigen binding process, the voltage slowly increases or decreases due to the insta-

bility of the molecules during the binding process. Once the binding is complete, and the Mortalin antigen molecules are fully bound to the anti-Mortalin antibodies, a new baseline voltage (higher or lower than the initial baseline) will be established due to an increased weight on the nanowire array.

As seen in Figure 6.4(a), the baseline voltage over Sample 1 decreased by approximately 2.5×10^{-5} V, while in Figure 6.4(b) it can be seen that the baseline voltage over Sample 2 increased by approximately 2×10^{-5} V. The reason for the responses for each sample occurring in opposite directions may be due to differences that occur in the biosensor samples during the manufacturing stage. While the process for development of each sample is the same, each sample is handmade and slight inconsistencies can result in different responses. The Au-layer below the ZnO nanowire array is treated as the positive terminal for the electrical connections for both samples (as discussed in Section 4.2). However, as seen in the results in Figure 6.4, this may not have been correct for both samples. Therefore, it may be necessary to evaluate the results according to the change in voltage between the baseline and final value (as opposed to the final value itself) going forward. The change in voltage between the baseline and final voltages for both samples lie within the same range and can therefore be compared.

Figure 6.4 also shows that the raw data detected over the biosensor using the multimeter, without the implementation of the electronic amplification and filtering system, include extremely small-scale values and great amounts of noise. This means that it is difficult to compare the baseline and final voltage values by purely analysing the graphical representation of the data, and it also confirms the necessity of the implementation of the electronic system designed.

6.3.2 Biosensor testing with electronic integration

With the electronics set up and connected, as shown in Figure 6.3, further tests were performed on the biosensor samples to determine: 1) the baseline effects of the addition of PBS buffer to the samples; 2) the effect of a positive control on the biosensor; 3) the effect on the biosensor by adding "biological sample" solutions of Mortalin antigen in PBS with three different known concentrations and 4) the effect of the electronic system on the efficiency of interpreting the signal from the biosensor.

The 'biological sample' used for the testing of the ZnO nanowire-based nanoforce biosensors in this study is a solution that consists of Mortalin antigen mixed into a PBS buffer. Therefore, it was necessary to test the baseline effect of the PBS buffer (without any antigen), to understand whether or not any adjustments would need to be made to the final results to account for this effect. To do this, the biosensor system was set up with the full electronic implementation and with the output connected to

the digital multimeter and 20 µl of PBS was gently dropped onto the samples while the output was being recorded.

The results from the PBS drop tests show that the only response produced by the biosensor, upon the addition of PBS to the biosensor sample, is the recognition of the weight of the PBS. Once the PBS was added to the biosensor sample, the baseline voltage output from the sample did not change as there was no Mortalin antigen present in the PBS for binding to take place. This result indicates that the future results do not need to be adjusted on account of the PBS as it does not affect the baseline voltage of the biosensor.

The next test performed was to determine the effect of dropping a biological sample, containing a positive control protein, onto the biosensor. The ZnO nanowire-based nanoforce Mortalin biosensor was designed for specific binding between the immobilised anti-Mortalin antibody and the Mortalin antigen contained in the added biological sample. Should a biological sample, containing some other antigen, be dropped onto the biosensor, the biosensor should ideally not be affected by the presence of this protein, other than maybe recognising the initial weight of the biological samples (similar to the response to the addition of PBS, discussed above).

To perform this test, Recombinant Human C Reactive protein (CRP) was mixed into PBS to achieve a concentration of 5 µg/ml. This solution was gently dropped onto biosensor Samples 3 and 4 while they were connected to the full electronic setup and the digital multimeter was reading the voltage output response from the system.

Figure 6.5 shows the results of this test performed on two different biosensor samples. These results show that when the CRP-PBS solution was dropped onto the samples (at approximately 50 seconds), there was a slight downward spike in the voltage due to the weight of the solution. However, once the CRP-PBS was on the samples, the voltage did not shift from the baseline. Therefore it can be established that the positive control sample does not have any significant effect on the biosensor and no non-specific binding took place to have an effect on the output results of the biosensor.

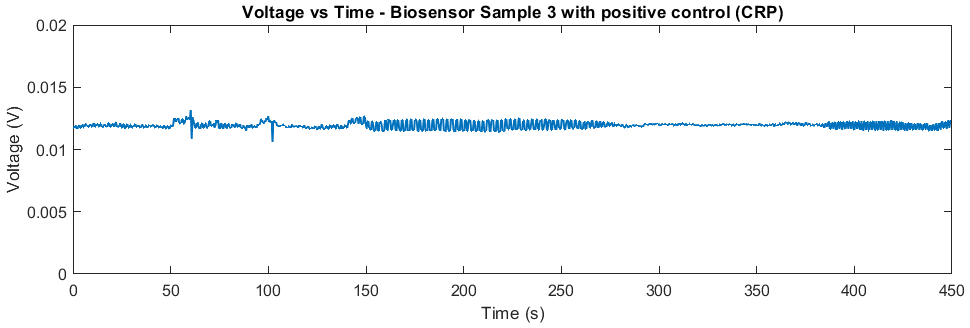

(a) Positive control (CRP) on biosensor Sample 3

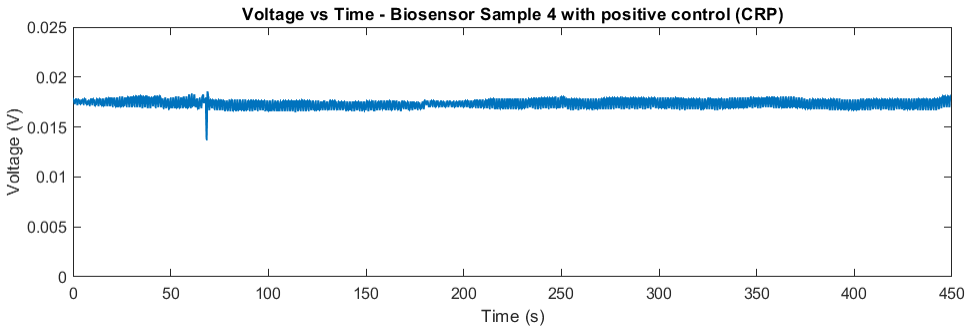

(b) Positive control (CRP) on biosensor Sample 4

Figure 6.5: Positive control (CRP) test results for tests performed with electronic system implementation

The final tests performed on the biosensor samples were those to determine the effect of adding biological samples, with different concentrations, onto the biosensor samples. This is to determine the ability of the biosensor to detect the concentration levels of Mortalin antigen in biological samples. As mentioned in Section 2.2.2, the concentration of Mortalin in the blood of people with Parkinson's disease is down-regulated compared to people without the disease. It was shown in Table 2.1 that the concentration of Mortalin in the blood of a person without Parkinson's disease is $3.13 \pm 0.48\,\mu g/ml$ and with Parkinson's disease is $1.98 \pm 0.53\,\mu g/ml$. Therefore, the three concentration solutions used for these tests were: 1) $1\,\mu g/ml$; 2) $3\,\mu g/ml$ and 3) $5\,\mu g/ml$.

For these tests, the biosensor system was set up with the full electronic implementation and with the output connected to the digital multimeter. $20\,\mu l$ the appropriate Mortalin antigen-PBS solution was gently dropped onto the samples while the output voltage was being recorded. Each test was performed within a constant duration of 450 seconds (7.5 minutes).

Figures 6.6 to 6.8 show the biosensor outputs for the addition of solutions at the different concentrations.

Figure 6.6 (a) and (b) show the biosensor results from antigen Test 1, where a Mortalin antigen-PBS solution of $1\,\mu g/ml$ concentration were dropped onto the biosen-

sor. In these results, one can see the true transient response from the biosensor. In Figure 6.6 (a), for example, the point at which the biological sample was dropped onto the biosensor Sample 5, at approximately 100 seconds, can be observed in the sharp peak. Between 100 and 200 seconds, the binding process can be observed as the voltage signal gradually decreases toward the new established baseline by 225 seconds.

The same response can be observed from biosensor Sample 6. However, as discussed in Section 6.3.1, it appears as if the polarity of the different biosensor samples have been switched. Along with this fact, the biosensors have different initial voltage baselines. Therefore, in order to compare the results, the change in voltage between the initial baseline and the new established baseline of each sample will be compared, as opposed to the absolute values of the voltage outputs. Sample 5 exhibits a change in voltage (ΔV) of 0.0171 V and Sample 6 exhibits a ΔV of 0.0043 V (all results are summarised in Table 6.1).

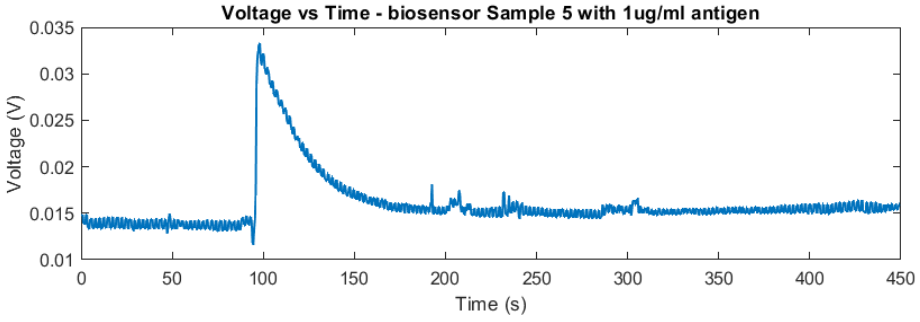

(a) 1 µg/ml Mortalin antigen in PBS on biosensor Sample 5

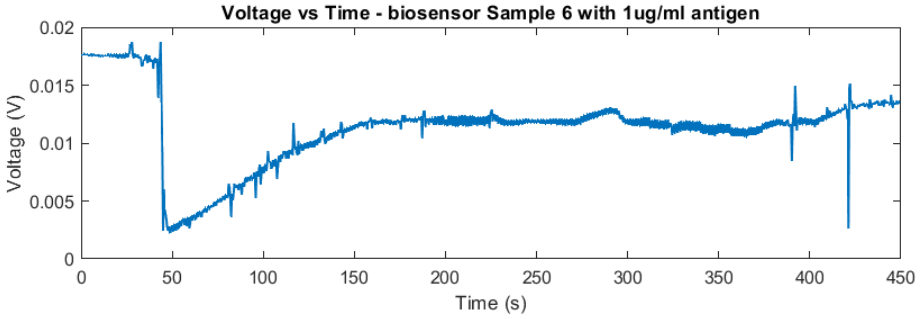

(b) 1 µg/ml Mortalin antigen in PBS on biosensor Sample 6

Figure 6.6: Mortalin antigen test results for 1 µg/ml Mortalin antigen in PBS on biosensor

Antigen Test 2, where a Mortalin antigen-PBS solution of 3 µg/ml concentration was dropped onto the biosensor, was performed on biosensor Samples 7 and 8. Figure 6.7 shows the results from the test performed on biosensor Sample 8. As it can be seen, the antigen solution was dropped onto the Sample 8 just after 50 seconds, causing a great increase in the voltage over the biosensor. At 75 seconds, the voltage detected over the biosensor starts to gradually decrease towards a new baseline voltage.

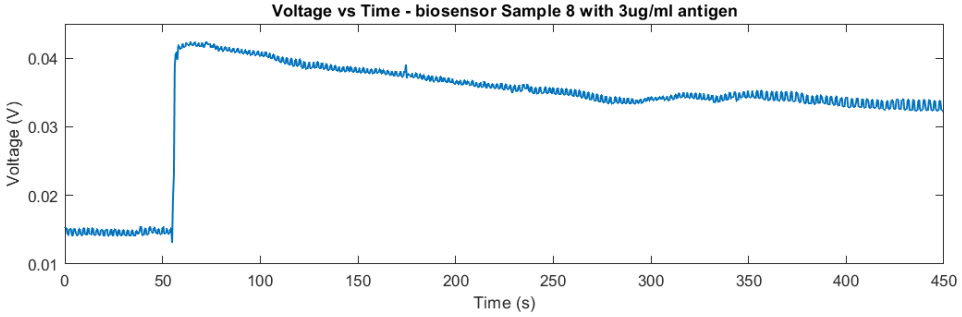

Figure 6.7: Mortalin antigen test results for 3 µg/ml Mortalin antigen in PBS on biosensor

Compared to antigen Test 1 performed with an antigen concentration of 1 µg/ml, the results from Test 2 do not settle at a new steady baseline before the end of the 450 second duration over which the results were recorded. It is suspected that, due to the higher concentration of the antigen solution dropped onto biosensor Sample 8, there are more antigen molecules available for binding to the anti-Mortalin antibodies immobilised onto the surface of the biosensor sample. Because of this, the binding process will take longer and the final voltage value will be reached at a later time (not recorded in the results shown in Figure 6.7). However, for the purpose of comparison in this study, the final voltage values detected in the results of Test 2, during the duration of the recording, will be used to calculate (ΔV).

The change in voltage (ΔV) between the baseline and final values for antigen Test 2 resulted as 0.0162 V for Sample 7 [1] and 0.0184 V for Sample 8. It can be seen that ΔV_7 is 0.002V lower than ΔV_8 and it can therefore be confirmed that the binding process in Test 3 does indeed last longer than the 450 second measurement duration.

Antigen Test 3, in which a Mortalin antigen-PBS solution with a concentration of 5 µg/ml was dropped onto the biosensor, was performed on biosensor Samples 9 and 10, with ΔV_9 resulting as 0.0215 V and ΔV_{10} resulting as 0.0226 V[1]. Figure 6.8 shows the voltage results recorded over biosensor Sample 9 during antigen Test 3. This result shows, even further, that with a higher antigen concentration, the anti-Mortalin antibody and Mortalin antigen binding process takes longer to complete and the final voltage takes longer to be reached.

[1] The transient data resulting from antigen Test 2 performed on Sample 7 and Test 3 performed on Sample 10 were unsuccessfully captured during the experiments. Therefore, to produce comparable results for these samples, the initial baseline was merely compared to the stable final voltage detected after the 450 second measurement duration. The graphical representation of these results (without the transient section) can be seen in Figures E.1 and E.2 in Appendix E

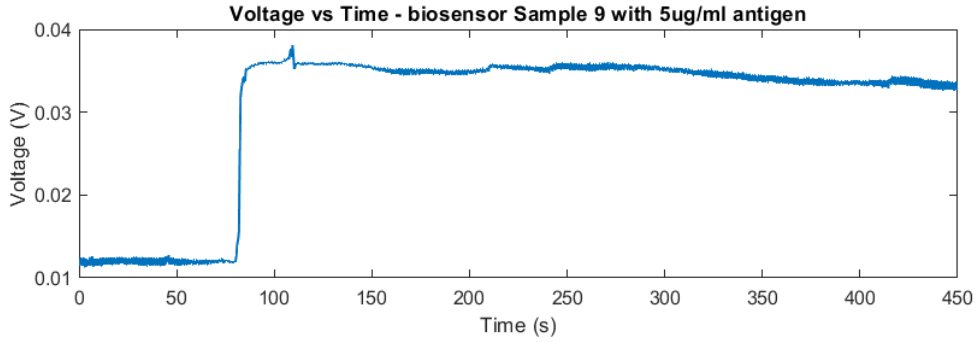

Figure 6.8: Mortalin antigen test results for 5 µg/ml Mortalin antigen in PBS on biosensor

Table 6.1 shows a summary of all the results produced during the biosensor testing and Figure 6.9 shows the graphical representation of this data. As can be seen, as the Mortalin antigen concentration in the 'biological sample' increased, the change in voltage (ΔV) between the initial baseline voltage and the final voltage increased. Figure 6.9 shows that the variation in the results produced by the biosensor upon the measurement of higher concentrations is lower than that when measuring low concentrations. This is to be expected as, when a biological sample with lower Mortalin antigen concentrations is added onto the biosensor, binding can take place at various, smaller sites on the surface of the biosensor, meaning that only these sections of the nanowire array are being disturbed - resulting in a lower ΔV. Biological samples with higher Mortalin antigen concentrations, consist of more Mortalin antigen molecules, allowing for binding on larger areas of the biosensor's surface, with a more even distribution. Therefore the number of nanowires disturbed increases and a greater voltage signal is produced.

Table 6.1: Mortalin antigen biosensor test results

Sample Number	**Antigen concentration in PBS (µg/ml)**	**ΔV(V)**
Sample 5	1	0.0017
Sample 6	1	0.0043
Sample 7	3	0.0162
Sample 8	3	0.0184
Sample 9	5	0.0215
Sample 10	5	0.0226

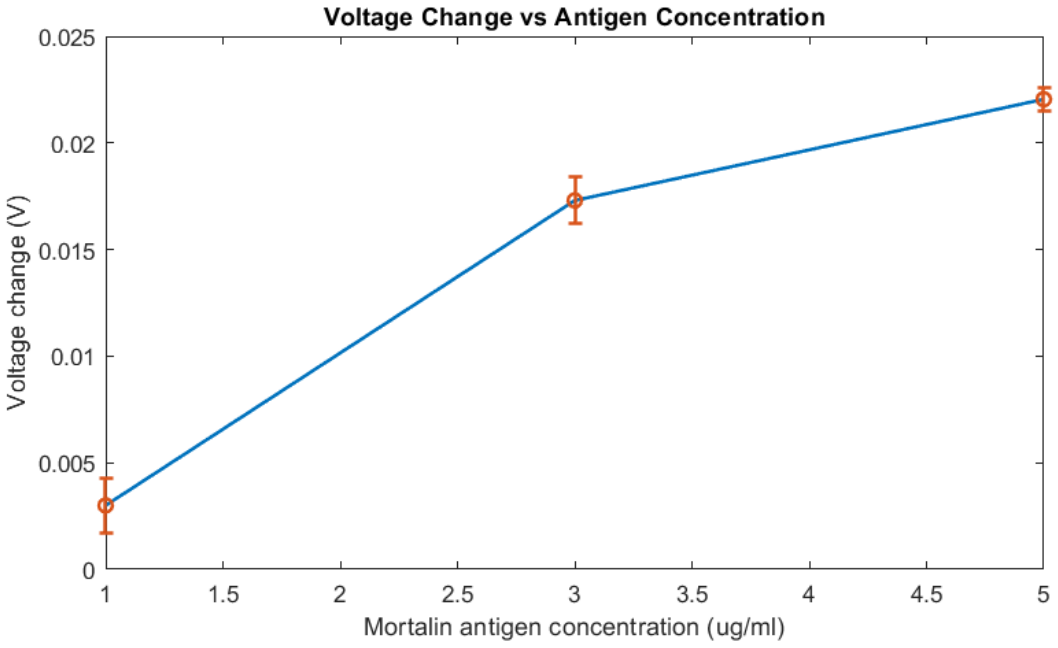

Figure 6.9: Mortalin antigen biosensor test results

When comparing the biosensor outputs with and without the electronic implementation, the effects of the electronics on the biosensor outputs are clear. In Figure 6.4 the biosensor output includes noise that makes the output difficult to interpret, compared to the outputs observed in Figures 6.6 to 6.8 where majority of the noise is eliminated and the baseline voltage can be easily determined and compared to the final voltage output. With the electronic implementation, however, there can still be a 30 Hz to 50 Hz wave observed that is superimposed onto the voltage output of the biosensor (see Figure 6.10). This is due to the fact that the electronic system was designed for a cutoff frequency of 1 kHz and successfully implemented for a cutoff frequency of 8 kHz. Regardless of the fact that the biosensor results with electronic implementation are interpretable, the implementation of an additional filter would assist in eliminating this 30 to 50 Hz noise. The implementation of the electronic system, along with eliminating a significant portion of the noise in the output signal, also successfully amplified the signal output by the biosensor, allowing for the digital multimeter to detect more stable results than without the amplification.

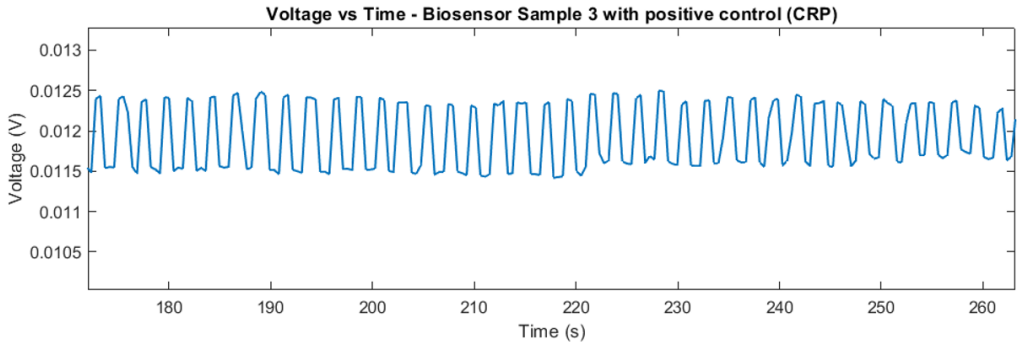

Figure 6.10: Magnified biosensor output (with electronic system implementation)

6.4 Results and Discussion

The ZnO nanowire nanogenerators, developed using the methods developed and discussed in Chapters 3 and 4, were further developed for a Mortalin biosensor application by immobilising anti-Mortalin antibodies onto the nanogenerator surface (using the strategy discussed in Chapter 5) and integrating the electronic system developed in Chapter 4.

With the addition of a BSA-blocking stage to the Cysteamine/Glutaraldehyde immobilisation strategy, anti-Mortalin antibodies were successfully immobilised onto the surface of the nanogenerators and non-specific binding was avoided. Integrating the antibodies and the electronic system, lead to the completion of the development of the nanoforce biosensor, ready for testing with biological samples.

The "biological samples" used for the testing of the Mortalin biosensors consisted of solutions of PBS and Mortalin antigen, at different concentrations. First, it was necessary to determine the effect of PBS on the biosensor samples to ascertain whether or not the baseline voltage was affected by the addition of PBS. The results of a test, in which pure PBS was added onto the biosensor samples, shows that the PBS did not have any significant effect on the biosensor samples and no such adjustment would be necessary.

A Mortalin antigen and PBS solution, with a concentration of 5 µg/ml, was deposited onto biosensor samples (without the connection of the electronic system) to ensure that Mortalin antigen can be detected by the Mortalin biosensors. After establishing a voltage baseline, the output of the biosensor, upon deposition of the biological sample, showed a voltage spike due to the weight of the solution, followed by a gradual shift in voltage toward a new final voltage, higher or lower than the baseline. Because the direction of this shift in response was different for each

sample, the change in voltage between the initial baseline voltage and the final was analysed, as opposed to the absolute voltage values.

The next test completed was to determine the effect of a positive control biological sample on the Mortalin biosensor. CRP was mixed into PBS to achieve a solution with a concentration of 5 µg/ml and this solution was deposited onto biosensor samples, while the output was measured by a digital multimeter. The voltage output of the biosensors during this test showed that the deposition of this positive control caused a small spike in voltage, due to the weight of the solution. However, there was no effect of the voltage baseline output by the biosensor due to the addition of the positive control solution. This means that no non-specific binding interaction took place between the anti-Mortalin antibodies (immobilised on the biosensor) and the CRP in the positive control solution.

The final tests performed on the Mortalin biosensor samples included the deposition of solutions of PBS and Mortalin antigen, at different concentrations, onto the biosensor with full electronic implementation. This was to understand how the biosensor response changes according to the Mortalin concentration in the biological samples. When a biological sample with the lowest Mortalin antigen concentration (1 µg/ml) was deposited onto the biosensor samples and the voltage output was recorded for 450 seconds (7.5 minutes), the full binding process was observed. The voltage baseline was established and upon the deposition of the biological sample, a voltage spike was observed, followed by a gradual shift towards a new fully established final voltage. However, when higher concentration Mortalin antigen solutions (3 µg/ml and 5 µg/ml) were deposited onto the biosensor, the full binding interaction was not able to be observed within the measurement duration of 7.5 minutes. This can be seen because the voltage outputs continue to change at the measurement cutoff point. The final values detected at this point were used for the comparison of the results.

The average voltage change values (ΔV) for the biosensors with biological samples of 1 µg/ml, 3 µg/ml and 5 µg/ml were 0.003 V (σ=0.0013), 0.0173 V (σ=0.0011) and 0.02205 V (σ=0.00055) respectively. This shows that the voltage change increases with an increase in Mortalin antigen concentration, and the variation between the results from different biosensors decreases with this concentration increase. Although these relationships exist, there is no clear proportionality.

The electronic integration in this biosensor system successfully achieved the amplification of, and the reduction of noise from, the output response of the biosensor. When comparing the graphical representation of the biosensor outputs with and without electronic implementation, this can clearly be seen and it can be concluded that the electronics were successful in converting the results into interpretable data.

The integration of an additional filtering stage (possibly designed for a 1 Hz cutoff frequency) may assist in further improving the biosensor outputs.

Chapter 7

Discussion

This chapter provides a discussion of all procedures followed throughout this study and the results obtained from each. The development of the ZnO nanowire-based nanoforce biosensor for Mortalin is discussed and the various constituents will be outlined.

7.1 Biosensor Outline

This study was based on the development of a ZnO nanowire-based nanoforce biosensor for the detection of Mortalin, a novel biomarker for Parkinson's disease. Presently, there are no existing biosensors for the detection of Parkinson's disease and all diagnosis is done clinically, resulting in diagnosis being completed after onset of the disease. Therefore, the development of a biosensor for Mortalin is useful as it may provide indication of the predisposition of Parkinson's disease in a patient, allowing for corrective and preventative lifestyle measures to be put into place, even before onset of the disease.

Mortalin is a protein that all people contain in their blood. However, studies have shown that there is a correlation between the concentration levels of Mortalin in the blood serum of patients with Parkinson's disease, versus healthy people. Mortalin concentration levels have been found to be down-regulated in the blood serum of patients with Parkinson's disease. Therefore, a ZnO nanowire-based nanoforce biosensor, for the detection of the concentration level of the Mortalin protein in blood serum or other biological samples, was developed.

The development of the ZnO nanowire-based nanoforce biosensor for Mortalin consisted of four main phases:

1. The growth/deposition of homogeneous, well-aligned ZnO nanowire arrays on an appropriate substrate, using an optimised method;

2. The progression of the homogeneous ZnO nanowire arrays into working nanogenerators (able to output a response upon deflection of the nanowires in the array) and the design and development of an electronic system aimed at amplifying and filtering this output response;

3. The immobilisation of anti-Mortalin antibodies onto the surface of Au-coated ZnO nanowire nanogenerators;

4. The integration of the ZnO nanowire-based nanogenerators with the antibody immobilisation strategies and the electronic system to complete the Mortalin nanoforce biosensor application.

7.2 ZnO Nanowire Array Deposition

The development of an optimised growth process for homogeneous, well-aligned ZnO nanowire arrays consisting of nanowires, orientated parallel to the c-axis and with the smallest possible diameters was required. An electrochemical deposition process was chosen for the deposition of ZnO nanowires onto the growth substrate for various reasons: 1) the electrochemical deposition method requires the least growth time compared to other methods; 2) multiple samples can be deposited in each growth batch and 3) the chemicals and reagents required for this process can be minimised to reduce wastage.

The first task to be completed was deciding on the appropriate substrate (between Silicon(100) wafers and ITO-coated glass) onto which the ZnO nanowires were to be deposited. The advantage of using ITO-coated glass slides is that they do not require the extensive substrate preparation procedures that need to be performed on the Si substrate before the electrochemical deposition process, resulting in an additional overnight waiting period. To choose the appropriate growth substrate for the electrochemical deposition of ZnO nanowires, the electrochemical deposition process was carried out on both ITO-coated glass slides as well as Si(100) wafers. This resulted in misaligned, badly orientated nanowires being deposited onto the ITO-glass slide samples and c-axis aligned nanowires being deposited onto the Si(100) substrate. The XRD analysis performed on the ZnO nanowire array deposited onto the ITO-coated glass substrates showed that the nanowire misalignment was perceived as a powder-like substance, whereas the results of the XRD analysis performed on the ZnO nanowire arrays grown on Si(100) indicated the presence of perfectly aligned nanowires. Therefore, Si(100) substrate was chosen as the growth substrate for this study and the successful alignment of the ZnO nanowires was prioritised over the time that could be saved by eliminating the substrate preparation procedures.

The Si(100) wafer preparation involved the ultrasonic cleaning of the Si samples in acetone, ethanol and DI water and the drying of the substrates on a hot plate. This was done to remove any organic compounds, oils and dust on the surface of the substrate. The more extensive Si sample preparation involved the development of a ZnO seed layer solution consisting of 2-methoxyethanol as the solvent, zinc acetate dihydrate as the precursor and monoethanolamine (MEA) as the stabiliser. The seed layer sol-gel solution was prepared the day before deposition. By depositing 4 x 15 µl of this prepared solution onto each Si sample, and annealing the samples at 700°C for 10 minutes, an even ZnO seed layer was achieved. The process of developing and depositing the ZnO seed layer onto the Si substrates is time consuming and has to be done in a precise manner, however, the successful implementation of this procedure does result in perfectly aligned ZnO nanowires in the deposited arrays.

The electrochemical deposition of the ZnO nanowire arrays on the ZnO seed layer-coated Si substrates involved the incubation of the substrates, along with zinc rods, in an electrolytic cell containing an electrolyte solution (1 mM zinc nitrate hexahydrate mixed in DI water). ZnO nanowires were deposited onto the Si substrate, during the 1 hour deposition duration, once the deposition process was initiated by supplying the cell with 1 V and controlling the temperature of the electrolytic cell at 70°C.

The control of the temperature of the electrolyte was achieved by implementing a temperature controlled water bath, into which the electrolytic cells were placed during the electrochemical deposition process. This water bath (containing an additional cell with a temperature sensor) was placed on a power-controlled hot plate. This implemented temperature control system was able to achieve the desired electrolyte temperature of 70°C ($\pm$0.4°C) in approximately 7 minutes and hold it for the duration of the electrochemical deposition process. This temperature rise time may have been improved with the implementation of an induction heating system, with minimal loss, as opposed to the hotplate system.

The above mentioned electrochemical deposition process, along with the integrated temperature control system, resulted in the deposition of well-aligned homogeneous ZnO nanowire arrays being deposited onto Si(100) wafer substrates. With the use of SEM imaging, it was determined that the resulting nanowire arrays consisted of ZnO nanowires with a mean diameter of 71.34 nm (σ = 14.49 nm) and a mean length of 970.96 nm (σ = 43.17 nm). The EDX analysis performed on the ZnO nanowire arrays showed that the mean weight percentage of Zn in the samples is 66.5% and of O is 19.6%. XRD analysis shows that the nanowire arrays deposited onto Si(100) wafers, using the optimised electrochemical deposition process and pa-

rameters, consist of almost-perfectly aligned nanowires as the XRD response shows peaks at the points matching the 002 and 004 reflections of ZnO. This indicates that the nanowires are perfectly aligned parallel to the c-axis and perpendicular to the growth substrate.

From the start of the mixing of the ZnO seed layer solution to the removal of the ZnO nanowire arrays from the electrochemical cells, this ZnO nanowire deposition process takes approximately 18 hours.

7.3 Progression of ZnO nanowire arrays into ZnO nanowire-based nanogenerators

The ZnO nanowire arrays were further developed into ZnO nanowire-based nanogenerators by limiting the growth area on the Si substrate (to expose the terminals for the electronic connections), depositing PMMA between the nanowires in the array (to insulate the terminals from each other) and coating the PMMA-coated ZnO nanowire array with a layer of gold (to create a Schottky barrier). The brass masking process successfully resulted in ZnO nanowires being deposited on only $\frac{2}{3}$ of the Si substrate with no contamination of the nanowire array. The PMMA deposition process mostly resulted in an even layer of PMMA between the nanowires in the nanowire array. Some ZnO nanowire array samples resulted in even layers of PMMA being deposited in some sections, while in other sections the PMMA layer was either too thick or contained air bubbles, therefore the PMMA deposition process is to be further developed. Nevertheless, the process followed in this study achieved that aim of insulating the bottom Au layer from the Schottky barrier.

A sample holder was designed with the purpose of housing the ZnO nanowire-based nanogenerator samples, providing an inlet for the biological samples during the biosensor testing stages and establishing a connection between the nanogenerator and the electronic system. An electronic system was designed and manufactured with the aim of amplifying and filtering noise from the output signal of the nanoforce biosensor. This electronic system consists of a small-signal instrumentation amplifier (set with a gain of 5) and an active Sallen-Key biquadratic filter designed to have a cutoff frequency of 1 kHz and an additional gain of 2.8. LTSpice was used to perform a simulation of the designed Sallen-Key filter, to confirm the success of the design and the simulation resulted in a cutoff frequency of precisely 1 kHz, as expected. The real electronic system implementation, however, resulted in an actual cutoff frequency of approximately 8 kHz. It is suspected that this discrepancy between the designed and actual cutoff frequencies is due to the use of incorrect capacitor values in the real implementation. An additional LTSpice simu-

lation indicates that 33 nF capacitors may have been used in the actual implementation, as opposed to the correct 330 nF capacitors in the design. Although the use of 33 nF capacitors results in a cutoff frequency of 8 kHz, the real biosensor system is anticipated to show output responses that differ immensely from the signals used to test this design. Therefore, this electronic system was implemented in the biosensor integration.

Various tests were performed on the ZnO nanowire-based nanogenerators to confirm the working of the nanogenerators due to the piezoelectric properties of the ZnO nanowires. Tapping tests, in which a non-sharp and non-conductive item was used to tap on the nanogenerator, while the output response was observed, showed that upon disturbance, the voltage response spikes up or down from the established baseline voltage. Due to the measurement instrument (the digital multimeter) only measuring discrete values, a test was performed to asses the response from the nanogenerator upon a continuous disturbance of the ZnO nanowire array. A continuous, constant stream of nitrogen gas was used to blow onto the nanogenerators, disturbing the nanowire arrays and producing some response. When sporadic bursts of the nitrogen gas were introduced to the nanogenerator, voltage spikes of different amplitudes were observed in the voltage response from the nanogenerator. When a constant stream of nitrogen gas was introduced to the nanogenerator samples, the voltage response shifted to a new, constant level. Upon the removal of the nitrogen gas disturbance, the nanogenerator voltage response returns to its initial baseline value. This confirms the theory that the piezoelectric nanowires only produce a voltage response upon disturbance.

7.4 Anti-Mortalin Antibody Immobilisation

The next phase of this study included the testing of the immobilisation of anti-Mortalin antibodies onto Au-coated Si substrates and Au-coated ZnO nanowire array samples. A protocol for the immobilisation of plain Au-coated Si samples was first developed to confirm the ability of the anti-Mortalin antibodies to be immobilised onto Au coated using the Leica EM ACE200. Initially, an immobilisation strategy using a 3-MPA SAM along with EDC/NHS cross-linking was tested. Upon analysis using fluorescence microscopy (with goat anti-mouse polyclonal secondary antibody IgG immobilised onto the samples), it was seen that this strategy was not successful in immobilising anti-Mortalin antibodies onto the Au-coated Si substrates. Therefore, a second immobilisation strategy using a Cysteamine SAM and a Glutaraldehyde cross-linker was employed. This strategy, with the parameters set to: Cysteamine in PBS with a concentration of 0.01 M; 1.5% Glutaraldehyde in PBS; and a 1:200 dilution of anti-Mortalin antibodies in PBS, the anti-Mortalin antibodies

were successfully immobilised onto the Au-coated Si substrate.

The same Cysteamine/Glutaraldehyde strategy was successfully used to immobilise anti-Mortalin antibodies onto Au-coated ZnO nanowire arrays. However, the fluorescent microscopy tests performed on these samples showed that there was non-specific binding taking place on samples without any immobilised antibodies. Therefore, it became necessary to implement a BSA-blocking stage in the immobilisation procedure. ZnO NW samples were incubated in a 5% solution of BSA in PBS before any secondary antibodies were immobilised and this resulted in the elimination of the non-specific binding. Therefore, in future tests, all samples were stored in a BSA/PBS solution after the immobilisation of the primary anti-Mortalin antibodies onto the biosensor surface.

7.5 Biosensor Integration

The full nanoforce biosensor integration was completed by immobilising anti-Mortalin antibodies (using the Cysteamine/Glutaraldehyde strategy, along with the BSA-blocker) onto the ZnO nanowire-based nanogenerators and integrating the system with the electronic setup.

First, the biosensor was tested without the electronic implementation to determine the raw response of the nanoforce biosensor. In all biosensor tests performed in this study, the biological samples were made of Mortalin antigen mixed into PBS with different, known concentrations. For this test, 20 µl of a biological sample solution with a concentration of 5 µg/ml was dropped onto the biosensor while the voltage response was being recorded. This response showed a baseline voltage established before a large spike in voltage upon the addition of the biological sample. After this addition, the response shows a gradual shift in the voltage toward a final, stable value. Regardless of the fact that, without the electronic implementation, the biosensor's response can be interpreted, the integration of the electronic system is vital to increase the effectiveness of the interpretation of the results by amplifying the values and reducing noise from the signal.

Due to the biological sample consisting of Mortalin antigen mixed in PBS, the effect of the PBS on the biosensor samples was to be determined - to ensure that there is no significant effect on the biosensor response due to the PBS alone. Upon the deposition of PBS onto the biosensor, a slight spike was observed due to the weight of the buffer. However, there was no shift from the baseline voltage on account of the PBS. Therefore it was deemed unnecessary to adjust any results due to the PBS buffer.

Next, a positive control biological sample of CRP mixed into PBS was tested on the biosensors. This was done to determine whether any non-specific binding would occur on the biosensor, between the anti-Mortalin antibodies and the CRP. The response of this test shows that, similar to the PBS test, there is a slight downward spike due to the weight of the solution. However, the baseline voltage is not affected by the addition of this positive control solution. This means that there is no non-specific binding that occurs on this biosensor and that any responses that occur, during tests using biological samples with Mortalin antigen, are strictly due to the binding of the Mortalin antigen to the anti-Mortalin antibodies.

The final, and most important, tests performed were to determine how the response of the biosensors are affected by biological solutions with different Mortalin antigen concentrations. A complementary result of these tests was the analysis of how effective the electronic system was in amplifying and filtering the biosensor responses.

Biological samples of Mortalin antigen in PBS with concentrations of 1 µg/ml (low), 3 µg/ml (medium) and 5 µg/ml (high) were tested on the ZnO nanowire-based nanoforce biosensor samples. These biological samples were dropped onto biosensor samples while the biosensor was connected to the full electronic system. The digital multimeter was recording the biosensor response for a measurement duration of 450 seconds (7.5 minutes). The results of the test performed with a biological sample of low Mortalin concentration shows that the full binding process is completed within the measurement duration of 450 seconds. This is determined due to a final voltage being fully established after the transient binding process. Compared to this, the results of the test performed with biological samples of medium and high concentrations show that the shift towards the final voltage value continues after the 450 second measurement duration. Therefore, in order to increase the accuracy of these test results, the measurement duration should be increased.

Due to the fact that the difference biosensor samples responded with voltage changes in different reference directions, the comparison of results was done by comparing the voltage change, between initial baseline value and final voltage value, experienced by each sample, as opposed to comparing the absolute voltage values that resulted at the end of each test.

The average voltage change values (ΔV) for the biosensors with biological samples of 1 µg/ml, 3 µg/ml and 5 µg/ml were 0.003 V (σ=0.0013), 0.0173 V (σ=0.0011) and 0.02205 V (σ=0.00055) respectively. This shows that with an increase in the concentration of Mortalin antigen in the biological sample, the change between the initial and final voltage in the biosensor response increased and the variation between the responses of different biosensors decreased. These results correspond to the expectation of the functioning of the ZnO nanowire-based nanoforce biosensors. With a

lower antigen concentration, fewer Mortalin antigen molecules are available for binding which means that antibody-antigen binding will take place at random sites on the biosensor surface, causing a disturbance in these sites only, and resulting in a low voltage change. Higher Mortalin antigen concentrations are anticipated to allow for more Mortalin antigen molecules to be available for an even distribution of binding on the biosensor surface. This increased binding leads to more nanowires being disturbed and a greater voltage change. While the change in voltage experienced by the biosensor increases as the Mortalin antigen concentration in the biological sample increases, this correlation is not directly proportional.

Some of the inconsistencies in the results may originate from badly-orientated anti-Mortalin antibodies being immobilised onto the ZnO nanowire nanogenerator. The surface of the nanowire array is not smooth and even, due to the spacing between the nanowires in the array. Therefore, antibodies may have been immobilised onto the sides of the nanowires, resulting in differently orientated antibodies, with their antigen binding sites unavailable for binding to take place. As discussed in Section 2.4.4, the direction of the bending of the nanowires determines the polarity of the voltage induced over the nanowires. There is no way to control this bending direction of the nanowires, therefore, this may affect the accuracy of the voltage measurements. Further, and more extensive, testing is required in order to determine the relationship between the biosensor response and the Mortalin antigen concentration.

When comparing the biosensor responses from tests performed with and without the electronic system implementation, it is clear that the electronic system was successful in amplifying and filtering the biosensor responses. The electronic system was able to minimise noise from the responses which assists in being able to determine the initial baseline and final voltages by merely analysing the graphical representation of the data, as opposed to having to perform an in-depth data analysis. The biosensor responses with the electronic implementation, however, do show the presence of noise with a frequency of 30 to 50 Hz. Therefore, the implementation of a filter designed for a lower cutoff frequency (such as 1 to 10 Hz) may further improve this system.

Chapter 8

Conclusion

The main objective of this study was to develop a a biosensor with the ability to detect the Mortalin protein concentration levels in biological samples. To do this, it was decided to develop a ZnO nanowire-based nanoforce biosensor. This involved four objectives. The first objective was to develop an optimised ZnO nanowire array deposition method. This was done by using an electrochemical deposition process to deposit well-aligned, c-axis orientated nanowires onto a ZnO seed layer-coated Silicon (100) substrate.

The second objective was to develop a ZnO nanowire-based nanogenerator. The ZnO nanowire arrays were deposited onto controlled areas of the Si(100) samples and were coated with PMMA to insulate the Au layer coated onto the Si sample. The PMMA coated nanowire arrays were coated with Au to complete the development of the nanogenerator by creating a Schottky barrier for the detection of the voltage response from the nanogenerators. The working of the nanogenerator was tested as successful by performing disturbance tests and analysing the voltage responses.

To accomplish the third objective of integrating the ZnO nanogenerators into nanoforce biosensors for Mortalin, anti-Mortalin antibodies were immobilised onto the surface of the nanogenerators. This was done using a Cysteamnine SAM and a Glutaraldehyde cross-linker. A 1:200 concentration of anti-Mortalin antibodies were incubated with the nanogenerator samples to successfully immobilise the antibodies. These samples were fully integrated into a nanoforce biosensor by implementing an electronic system to amplify and filter the voltage response due to the binding of the Mortalin protein onto the anti-Mortalin antibodies.

The fourth objective was to determine the ability of the biosensor to detect the concentration level of Mortalin in a biological sample. The biosensor tests show that the response from the tests with higher Mortalin concentrations are larger (and show less variance) than the response with a lower Mortalin concentration. However the

relationship between these responses is not proportional. Further testing is required to confirm these results.

8.1 Limitations and Future Recommendations

One of the main limitations in this study was the lack of access to instrumentation and equipment in a secure lab, for the development and manufacturing of the ZnO nanowire arrays. When working with ionic interactions, such as those that take place in the electrochemical deposition process of the ZnO nanowire arrays on Si100 substrates, it is recommended that all work is done in a clean room. A clean room is an environment in which there is minimal dust and proper ventilation. In this study, the silicon substrates and the final ZnO nanowire arrays were constantly transported around town because the various pieces of equipment used for the sample preparation, the furnace used for annealing, the electrochemical deposition setup and the analysis instrumentation were all in different facilities. This lead to an increase in the process time as well as an increase in the risk of contamination of samples.

Another limitation was the number of ZnO nanowire array samples that were deposited per batch. In order to increase the efficiency of sample production, it is recommended to adjust the electrochemical deposition setup to allow for 8 to 10 samples per batch, as opposed to 4 samples. A lack of samples at the end of the testing stage resulted in fewer tests being performed. It is recommended that more extensive testing is done on the biosensors to determine their ability to detect the concentration of Mortalin antigen in biological samples. More tests performed will confirm the repeatability of the results and allow for a relationship between the biosensor response (ΔV) and the Mortalin antigen concentration to be determined.

It is also recommended that the hot plate in the temperature control system, implemented as an aid in the electrochemical deposition process, be replaced by an induction heating system. The induction heating system would experience less energy losses, resulting in the desired temperature being reached in a shorter time. This would lead to a more efficient ZnO nanowire deposition process.

As discussed in Chapter 4, the implementation of incorrect electronic components resulted in a Sallen-key filter with a cutoff frequency 8 times higher than what was desired. Therefore, it is recommended for the biosensor system to be tested with the correct electronic implementation, along with an additional filter designed for a cutoff frequency as low as 1 to 10 Hz to eliminate the noise that can still be seen in the biosensor response.

Appendices

Appendix A

ZnO NW calculations

A.1 ZnO Seed Layer Calculations

Stoichiometric Calculations - ZnO NW Growth

The following calculations were performed during the ZnO NW electrochemical deposition process. These calculations show how the volumes, masses and concentrations of the different chemical constituents were calculated for the use in the nanowire synthesis process.

1) The ZnO seed layer development process:

The ZnO seed layer sol-gel solution consists of 2-methoxyethano(2M) as the solvent, zinc acetate dihydrate(ZAD) as the precursor and monoethanolamine (MEA) as the stabiliser.

Known ratios: a 0.1 M ZnO solution is required and the required molar ratio between the zinc acetate dihydrate precursor and the MEA stabiliser is 1:1.

The following calculations are for mixing 50 ml of the sol-gel solution:

$v_{2M} := 50\ \text{mL}$

$C_{ZAD} := 0.1\ \frac{\text{mol}}{\text{L}}$ $M_{ZAD} := 219.5\ \frac{\text{g}}{\text{mol}}$

$n_{ZAD} := C_{ZAD} \cdot v_{2M} = 0.005\ \text{mol}$

$m_{ZAD} := n_{ZAD} \cdot M_{ZAD} = 1.0975\ \text{g}$

Molar ratio of ZAD:MEA is 1:1 therefore:

$n_{MEA} := n_{ZAD} = 0.005\ \text{mol}$ $M_{MEA} := 61.08\ \frac{\text{g}}{\text{mol}}$

$m_{MEA} := n_{MEA} \cdot M_{MEA} = 0.3054\ \text{g}$ $\rho_{MEA} := 1.01\ \frac{\text{g}}{\text{cm}^3}$

$v_{MEA} := \frac{m_{MEA}}{\rho_{MEA}} = 0.3024\ \text{mL}$

A.2 ZnO Nanowire Electrochemical Deposition Calculations

2) The ZnO electrochemical deposition

The electrolyte solution was made up of DI water and zinc nitrate hexahydrate(ZNH) with a molar concentration of 1 mM.

The following calculations are for mixing 100 ml of the electrolyte solution:

$$v_{DI.H2O} := 100\ \text{mL}$$

$$M_{ZNH} := 297.5\ \frac{\text{g}}{\text{mol}}$$

$$C_{ZNH} := 0.001\ \frac{\text{mol}}{\text{L}} \qquad n_{ZNH} := C_{ZNH} \cdot v_{DI.H2O} = 0.0001\ \text{mol} \qquad m_{ZNH} := n_{ZNH} \cdot M_{ZNH} = 0.0298\ \text{g}$$

Appendix B

Temperature Control System Coding

```
#include <TSIC.h>       // include the library

// CONTROL VARIABLES
double SetPoint = 70;
double Threshold = 15;
double Threshold2 = 0;
bool counter = false;
bool count = false;

//TEMPERATURE SENSOR VARIABLES
uint16_t temperature = 0;
float Temp_C = 0;
const int thermocouple = 2; //pin nr of TC input
TSIC Sensor1(thermocouple);    // Signalpin, VCCpin, Sensor Type

//RELAY VARIABLES
const int relay = 4; //pin nr of relay output
const int fan = 7;

//TIMER VARIABLES
unsigned long delayStart = 0; // the time the delay started
unsigned long currentMillis = 0;
unsigned long prevMillis = 0;
bool delayRunning = false; // true if still waiting for delay to finish
unsigned long delayStart2 = 0; // the time the delay started
bool delayRunning2 = false; // true if still waiting for delay to finish
unsigned long i = 0;

unsigned long currMil = 0;
unsigned long prevMil = 0;
```

```
void setup() {
  // put your setup code here, to run once:

  Serial.begin(9600); // set up the serial port
  pinMode(relay, OUTPUT);
  pinMode(fan,OUTPUT);
//  delayStart = millis();
//  delayStart2 = millis();
//  delayRunning = true;
//  delayRunning2 = true;
}

void loop() {
  // put your main code here, to run repeatedly:

  THERMOCOUPLE();
  RELAY();

  currMil = millis();

  if ( currMil - prevMil >= 100){
  Serial.print(count);
  Serial.print(",");
  Serial.println(Temp_C);
    prevMil = millis();
  }
  //PWM();
}

void THERMOCOUPLE() {
  if (Sensor1.getTemperature(&temperature)) {
    Temp_C = Sensor1.calc_Celsius(&temperature);
  }
}
```

```
void RELAY() {
  if ((count == false) && (Temp_C <= (SetPoint - Threshold))) {
    if ((millis()- prevMillis) > 5000){
      //delayRunning = false;
      digitalWrite(relay, HIGH);
      prevMillis = millis();
      delay(2000);
      digitalWrite(relay, LOW);
      //counter = 0;
    }
    //digitalWrite(fan,HIGH);
  }
  if ((count == false) && (Temp_C > (SetPoint - Threshold))) {
    digitalWrite(relay, HIGH);
  }
  if (Temp_C >= SetPoint){
    count = 1;
  }
  if ((count == true) && (Temp_C < (SetPoint - Threshold2))){
    if ((millis()- prevMillis) > 5000){
      digitalWrite(relay, HIGH);
      prevMillis = millis();
      delay(3000);
      digitalWrite(relay, LOW);
    }
    digitalWrite(fan,LOW);
  }
  if ((count == true) && (Temp_C >= SetPoint)){
    digitalWrite(relay, HIGH);
    digitalWrite(fan, HIGH);
  }
}
```

```
//void TIMER(){
//  //check if delay has timed out after 1 second
//  if (delayRunning && ((millis() - delayStart) >= 1000)){
//    delayRunning = false;
//    digitalWrite(relay, HIGH);
//    Serial.println("Relay is off");
//  }
//
//}

//void PWM(){
//  if(millis() == (5000*i)){
//      digitalWrite(relay, LOW);
//      delay(3000);
//      digitalWrite(relay, HIGH);
//      i++;
//  }
//}
```

Appendix C

Sallen Key Biquad Filter

C.1 Calculations for Sallen-Key Filter Design

Design of a Sallen Key LPF

Assumptions and simplifications:

$\omega_0 := 1 \frac{rad}{s}$ $f_0 := \frac{\omega_0}{2 \cdot \pi} = 0.1592\ Hz$

and $C_1 := 1\ F$ $C_2 := 1\ F$

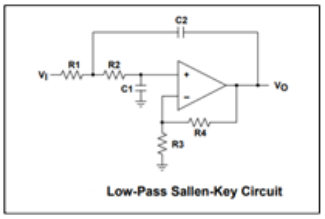

Low-Pass Sallen-Key Circuit

Ideal Sallen-Key LPF transfer function:

$$v_o := V_i \cdot \left(\frac{\frac{\mu}{R_1 \cdot R_2 \cdot C_1 \cdot C_2}}{s^2 + s \cdot \left(\frac{1}{R_1 \cdot C_1} + \frac{1}{R_2 \cdot C_1} + \frac{1-\mu}{R_2 \cdot C_2} \right) + \frac{1}{R_1 \cdot R_2 \cdot C_1 \cdot C_2}} \right) \qquad \mu := 1 + \left(\frac{R_a}{R_b} \right)$$

Butterworth worth design approach:

Why Butterworth?

1) no passband ripple

2) no stop-band ripple

3) no "bump" at the corner frequency as with many other transfer functions.

Note: Amplifier ends up with a >1 gain in the pass band

The polynomials are normalized by setting $\omega_c := 1 \frac{rad}{s}$. Therefore, it is necessary to scale component values according to scaled magnitude and frequency.

2nd order normalised butterworth polynomial:

$$s^2 + 1.41421 \cdot s + 1$$

Design:

From the design of a HPF, we choose $R_1 + R_2 = R_a || R_b$ for stability reasons. Although this is for a HPF, it will still work for my design as I have chosen $R_1 := R$, $R_2 := R$ and $C_1 := C_2$. The gain of the op-amp amplifier should be maintained less than 3, as Av greater than 3 makes the Sallen-Key filters unstable.

Design choices:

$C_1 = 1\ \text{F}$

$C_2 = 1\ \text{F}$ (easy to scale)

$\omega_c = 1\ \frac{\text{rad}}{\text{s}}$ (Butterworth condition)

From the normalised Butterworth polynomial:

$\frac{1}{R_1 \cdot R_2 \cdot C_1 \cdot C_2} = 1$ so $R := \sqrt{\frac{1\ \text{s}^2}{C_1 \cdot C_2}} = 1\ \Omega$ $R_1 = 1\ \Omega$ $R_2 = 1\ \Omega$

and

$\frac{1}{R_1 \cdot C_1} + \frac{1}{R_2 \cdot C_1} + \frac{1-\mu}{R_2 \cdot C_2} = 1.41421$ so $\mu_1 := 1 - \left(1.41421 \cdot \frac{1}{\Omega\ \text{F}} - \frac{1}{R_1 \cdot C_1} - \frac{1}{R_2 \cdot C_1}\right) \cdot R_2 \cdot C_2 = 1.5858$

By choosing $R_1 + R_2 = \frac{R_a \cdot R_b}{R_a + R_b}$ we have that $2 = \frac{R_a \cdot R_b}{R_a + R_b}$

Therefore $R_a := 5.4142\ \Omega$

$R_b := 3.1716\ \Omega$

Scaling:

$$R' = K_m R, \qquad L' = \frac{K_m}{K_f} L$$
$$C' = \frac{1}{K_m K_f} C, \qquad \omega' = K_f \omega$$

Frequency:

$\omega_c = 1\ \frac{\text{rad}}{\text{s}}$ $f_{c.real} := 1\ \text{kHz}$ $\omega_{c.real} := 2 \cdot \pi \cdot f_{c.real} = 6283.1853\ \frac{\text{rad}}{\text{s}}$

$K_f := \frac{\omega_{c.real}}{\omega_c} = 6283.1853$

Magnitude (scaling for C):

$C_1 = 1\ \text{F}$ $C_{1.real} := 330\ \text{nF}$ $C_{2.real} := C_{1.real} = 330\ \text{nF}$

$K_m := \frac{C_1}{C_{1.real} \cdot K_f} = 482.2877$

Note: Original design was for an fc of 1000Hz and used $C := 330\ \text{nF}$

Final scaled component values:

$R_{1.final} := K_m \cdot R_1 = 0.4823\ k\Omega$

$R_{a.final} := K_m \cdot R_a = 2.6112\ k\Omega$

$R_{2.final} := K_m \cdot R_2 = 0.4823\ k\Omega$

$R_{b.final} := K_m \cdot R_b = 1.5296\ k\Omega$

Standard values:

$R_{a.real} := 2.7\ k\Omega$

$R_{b.real} := 1.5\ k\Omega$

$\mu = 2.7071$

$R_{1.real} := 470\ \Omega$

$\mu_{real} := 1 + \frac{R_{a.real}}{R_{b.real}} = 2.8$

$R_{2.real} := 470\ \Omega$

C.2 Simulation Results

The following figure shows the results for a simulation completed by replacing the two 330 nF capacitors with 33 nF capacitors as discussed in Section 4.6 of Chapter 4.

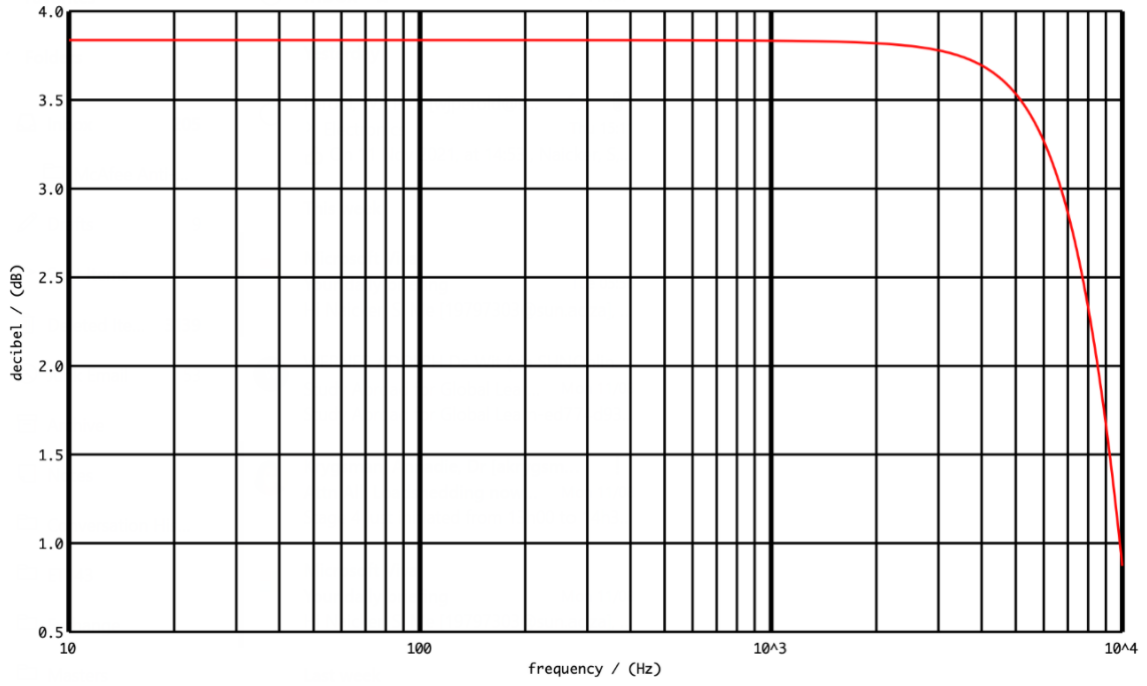

Figure C.1: Gain bode plot of Sallen-Key filter simulation with 33 nF capacitors

Appendix D

Antibody Immobilisation Calculations

Anti-Mortalin antibody immobilisation using Cysteamine and Glutaraldehyde

These calculations were performed to determine the amounts of the substances needed for thr immobilisation of anti-Mortalin antibodies onto ZnO nanowire-based nanogenerators using a Cysteamine SAM and a Glutaraldehyde cross-linker.

1. Cysteamine SAM - 0.01M in PBS

For 1 ml of the solution :

$C_{cys} := 0.01 \frac{mol}{L}$ $\quad v_{PBS} := 1\ mL$

$M_{cys} := 77.15 \frac{g}{mol}$

$n_{cys} := C_{cys} \cdot v_{PBS} = 1 \cdot 10^{-5}\ mol$

$m_{cys} := n_{cys} \cdot M_{cys} = 0.7715\ mg$

2. Glutaraldehyde - 1.5% in PBS

For 1ml of the solution :

$v_{PBS} = 1\ mL$

$v_{glut} := 0.015 \cdot v_{PBS} = 1.5 \cdot 10^{-5}\ L$ =15 µL

3. BSA - 5% in PBS

$C_{BSA} := \frac{5}{100} \frac{g}{mL} = 0.05 \frac{g}{mL}$

$v_{PBS2} := 5\ mL$

$m_{BSA} := C_{BSA} \cdot v_{PBS2} = 0.25\ g$

Appendix E

Additional Biosensor Results

Figure E.1 shows the Mortalin antigen test results for 3 µg/ml Mortalin antigen in PBS on biosensor Sample 7.

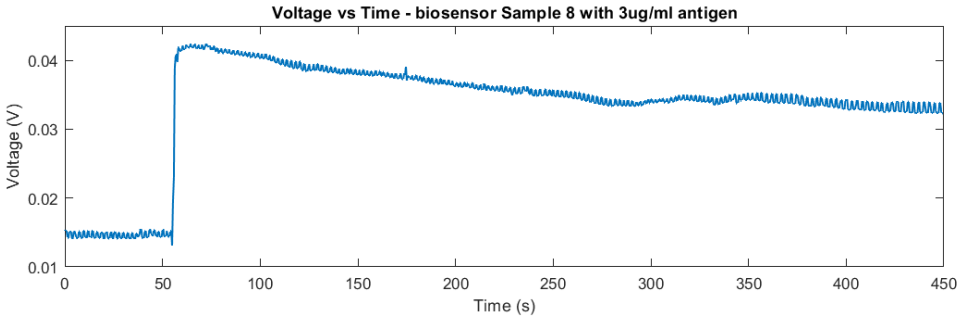

Figure E.1: Mortalin antigen test results for 3 µg/ml Mortalin antigen in PBS on biosensor

Figure E.2 shows the Mortalin antigen test results for 5 µg/ml Mortalin antigen in PBS on biosensor Sample 10.

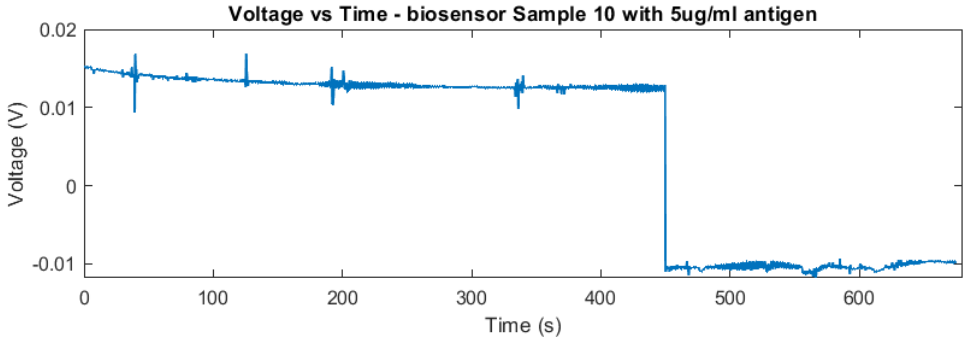

Figure E.2: Mortalin antigen test results for 5 µg/ml Mortalin antigen in PBS on biosensor

References

[1] Nussbaum, R.L. and Ellis, C.E.: Alzheimer's Disease and Parkinson's Disease. *The New England Journal of Medicine*, vol. 348, no. 14, 2003.

[2] Davie, C.A.: A review of Parkinson's disease. *British Medical Bulletin*, vol. 86, no. 1, pp. 109–127, 2008. ISSN 00071420.

[3] Mayo Clinic: Parkinson's disease. 2021.

[4] Downing, G.: NIH Definitions Working Group. Biomarkers and surrogate endpoints in clinical research: definitions and con- ceptual model. *Biomarkers and Surrogate Endpoints: Clinical Research and Applications*, pp. 1–9, 2000.

[5] Altintas, Z.: *Biosensors and Nanotechnology*. 2018. ISBN 9781119065012.

[6] Puntmann, V.O.: How-to guide on biomarkers: Biomarker definitions, validation and applications with examples from cardiovascular disease. *Postgraduate Medical Journal*, vol. 85, no. 1008, pp. 538–545, 2009. ISSN 00325473.

[7] Londono, C., Osorio, C., Gama, V. and Alzate, O.: Mortalin, apoptosis, and neurodegeneration. *Biomolecules*, vol. 2, no. 1, pp. 143–164, 2012. ISSN 2218273X.

[8] Garg, S., Wu, C., Ohmiya, Y., Kaul, S.C. and Wadhwa, R.: Express ELISA for detection of mortalin. *BioTechniques*, vol. 67, no. 4, pp. 166–171, 2019. ISSN 19409818.

[9] Wadhwa, R., Takano, S., Kaur, K., Deocaris, C.C., Pereira-Smith, O.M., Reddel, R.R. and Kaul, S.C.: Upregulation of mortalin/mthsp70/Grp75 contributes to human carcinogenesis. *International Journal of Cancer*, vol. 118, no. 12, pp. 2973–2980, 2006. ISSN 00207136.

[10] Singh, A.P., Bajaj, T., Gupta, D., Singh, S.B., Chakrawarty, A., Goyal, V., Dey, A.B. and Dey, S.: Serum Mortalin Correlated with α-Synuclein as Serum Markers in Parkinson's Disease: A Pilot Study. *NeuroMolecular Medicine*, vol. 20, no. 1, pp. 83–89, 2018. ISSN 15591174.
Available at: `https://doi.org/10.1007/s12017-017-8475-5`

[11] Rozenberg, P., Kocsis, J., Saar, M., Prohászka, Z., Füst, G. and Fishelson, Z.: Elevated levels of mitochondrial mortalin and cytosolic HSP70 in blood as risk factors in patients with colorectal cancer. *International Journal of Cancer*, vol. 133, no. 2, pp. 514–518, 2013. ISSN 00207136.

[12] Lewis, P.A. and Spillane, J.E.: Parkinson's disease. In: *The Molecular and Clinical Pathology of Neurodegenerative Disease*, pp. 83–121. 2019. ISBN 9780128110690.

[13] Lewis, P.A. and Spillane, J.E.: Alzheimer's disease and dementia. In: *The Molecular and Clinical Pathology of Neurodegenerative Disease*, pp. 25–82. 2019. ISBN 9780128110690.

[14] Zhang, W., Zhang, Q., Yang, Q., Liu, P., Sun, T., Xu, Y., Qian, X., Qiu, W. and Ma, C.: Contribution of Alzheimer's disease neuropathologic change to the cognitive dysfunction in human brains with Lewy body-related pathology. *Neurobiology of Aging*, pp. 1–10, 2020. ISSN 15581497.
Available at: `https://doi.org/10.1016/j.neurobiolaging.2020.02.022`

[15] Altintas, Z. and Davis, F.: General Introduction to Biosensors and Recognition Receptors. In: *Biosensors and Nanotechnology*, pp. 3–15. 2018. ISBN 9781119065012.

[16] Solanki, P.R., Kaushik, A., Agrawal, V.V. and Malhotra, B.D.: Nanostructured metal oxide-based biosensors. *NPG Asia Materials*, vol. 3, no. 1, pp. 17–24, 2011. ISSN 18844049.

[17] Bosch, M., Sanchez, A., Rojas, F. and Ojeda, C.: *Sensors*. 2007.

[18] Malhotra, B.D. and Pandey, C.M.: *Biosensors : Fundamentals and Applications*. 2017. ISBN 9781910242780.

[19] Rahman, M.S., Hasan, M.R., Rikta, K.A. and Anower, M.S.: A novel graphene coated surface plasmon resonance biosensor with tungsten disulfide (WS2) for sensing DNA hybridization. *Optical Materials*, vol. 75, pp. 567–573, 2018. ISSN 09253467.
Available at: `https://doi.org/10.1016/j.optmat.2017.11.013`

[20] Erickson, D., Mandal, S., Yang, A.H.J. and Cordovez, B.: Nanobiosensors: optofluidic, electrical and mechanical approaches to biomolecular detection at the nanoscale. *Microfluidics and Nanofluidics*, pp. 33–52, 2008. ISSN 1613-4990.

[21] Homola, J., Čtyroký, J., Skalský, M., Hradilová, J. and KoláÅová, P.: A surface plasmon resonance based integrated optical sensor. *Sensors and Actuators, B: Chemical*, vol. 39, no. 1-3, pp. 286–290, 1997. ISSN 09254005.

[22] Thévenot, D.R., Toth, K., Durst, R.A. and Wilson, G.S.: Electrochemical biosensors: Recommended definitions and classification. *Biosensors and Bioelectronics*, vol. 16, no. 1-2, pp. 121–131, 2001. ISSN 09565663.

[23] Davis, G.: Electrochemical techniques for the development of amperometric biosensors. *Biosensors*, vol. 1, no. 2, pp. 161–178, 1985. ISSN 0265928X.

[24] Su, L., Fong, C.C., Cheung, P.-Y. and Yang, M.: Development of Novel Piezoelectric Biosensor Using PZT Ceramic Resonator for Detection of Cancer Markers. In: *Biosensors and Biodetection*, vol. 2, 2nd edn, pp. 277–291. 2017. ISBN 9781493969104.

[25] Wang, Z.L.: Oxide Nanobelts and Nanowires - Growth, Properties and Applications. *Journal of Nanoscience and Nanotechnology*, vol. 8, pp. 27–55, 2007.

[26] Wang, Z.L., Wang, X., Song, J., Liu, J. and Gao, Y.: Piezoelectric Nanogenerators for Self-Powered Nanodevices. *Persuasive Computing - Implantable Electronics*, vol. 7, no. 1, 2008.

[27] Zhang, Y., Ram, M.K., Stefanakos, E.K. and Goswami, D.Y.: Synthesis, characterization, and applications of ZnO nanowires. *Journal of Nanomaterials*, vol. 2012, 2012. ISSN 16874110.

[28] The Free Dictionary: C axis. 2003.
Available at: `https://encyclopedia2.thefreedictionary.com/c+axis`

[29] Baruah, S. and Dutta, J.: Hydrothermal growth of ZnO nanostructures. *Science and Technology of Advanced Materials*, vol. 10, no. 1, 2009. ISSN 14686996.

[30] Dai, S. and Park, H.S.: Surface effects on the piezoelectricity of ZnO nanowires. *Journal of the Mechanics and Physics of Solids*, vol. 61, no. 2, pp. 385–397, 2013. ISSN 00225096. `1210.5435`.

[31] Wang, Z.L.: Nanostructures of zinc oxide. *International Journal of Nanotechnology*, vol. 6, no. 3-4, pp. 245–257, 2004. ISSN 14757435.

[32] Li, H., Wang, J., Liu, H., Yang, C., Xu, H., Li, X. and Cui, H.: Sol - Gel preparation of transparent zinc oxide films with highly preferential crystal orientation. *Vacuum*, vol. 77, no. 1, pp. 57–62, 2004. ISSN 0042207X.

[33] Wang, Z.L., Kong, X.Y., Ding, Y., Gao, P., Hughes, W.L., Yang, R. and Zhang, Y.: Semiconducting and piezoelectric oxide nanostructures induced by polar surfaces. *Advanced Functional Materials*, vol. 14, no. 10, pp. 943–956, 2004. ISSN 1616301X.

[34] Özgür, Ü., Alivov, Y.I., Liu, C., Teke, A., Reshchikov, M.A., DoÇ§an, S., Avrutin, V., Cho, S.J. and MorkoÌ§, H.: A comprehensive review of ZnO materials and devices. *Journal of Applied Physics*, vol. 98, no. 4, pp. 1–103, 2005. ISSN 00218979.

[35] Wang, Z.L.: Polar surface induced growth of semiconducting and piezoelectric oxide novel nanostructures. *Microscopy and Microanalysis*, vol. 12, no. SUPPL. 2, pp. 480–481, 2006. ISSN 14319276.

[36] Shetti, N.P., Bukkitgar, S.D., Reddy, K.R., Reddy, C.V. and Aminabhavi, T.M.: ZnO-based nanostructured electrodes for electrochemical sensors and biosensors in biomedical applications. *Biosensors and Bioelectronics*, vol. 141, no. June, p. 111417, 2019. ISSN 18734235.
Available at: `https://doi.org/10.1016/j.bios.2019.111417`

[37] Ong, C.B., Ng, L.Y. and Mohammad, A.W.: A review of ZnO nanoparticles as solar photocatalysts: Synthesis, mechanisms and applications. *Renewable and Sustainable Energy Reviews*, vol. 81, no. March 2017, pp. 536–551, 2018. ISSN 18790690.
Available at: `http://dx.doi.org/10.1016/j.rser.2017.08.020`

[38] Suh, D.I., Byeon, C.C. and Lee, C.L.: Synthesis and optical characterization of vertically grown ZnO nanowires in high crystallinity through vapor-liquid-solid growth mechanism. *Applied Surface Science*, vol. 257, no. 5, pp. 1454–1456, 2010. ISSN 01694332.
Available at: `http://dx.doi.org/10.1016/j.apsusc.2010.08.067`

[39] Bi, N., Zhang, L., Zheng, Q., Zhuge, F., Li, J., Gao, X.P. and Du, J.: Control of ZnO nanowire growth and optical properties in a vapor deposition process. *Journal of Materials Science and Technology*, vol. 33, no. 8, pp. 850–855, 2017. ISSN 10050302.
Available at: `http://dx.doi.org/10.1016/j.jmst.2017.03.024`

[40] Fan, Z. and Lu, J.G.: Zinc oxide nanostructures: Synthesis and properties. *Journal of Nanoscience and Nanotechnology*, vol. 5, no. 10, pp. 1561–1573, 2005. ISSN 15334880.

[41] Choi, H.-J.: Vapor-Liquid-Solid Growth of Semiconductor Nanowires. In: *Semiconductor Nanostructures for Optoelectronic Devices: Processing, Characterization and Applications, NanoScience and Technology*, vol. 58. 2012. ISBN 9783642224799.

[42] Neveling, D.P., Van Den Heever, T.S., Bucher, R., Perold, W.J. and Dicks, L.M.T.: Effect of Seed Layer Deposition , Au Film Layer Thickness and Crystal Orientation on the Synthesis of Hydrothermally Grown ZnO Nanowires. *Current Nanoscience*, vol. 10, pp. 827–836, 2014.

[43] Chen, M.-Z., Chen, W.-S., Jeng, S.-C., Yang, S.-H. and Chung, Y.-F.: Liquid crystal alignment on zinc oxide nanowire arrays for LCDs applications. *Optics Express*, vol. 21, no. 24, p. 29277, 2013. ISSN 1094-4087.

[44] Randall, M.: Electrolytic Cells. *American Journal of Physics*, vol. 7, no. 5, pp. 292–314, 1939.

[45] Sanchez, S., Lévy-Clément, C. and Ivanova, V.: Electrochemical Deposition of ZnO Thin Films and Nanowires for Photovoltaic Applications. *Journal of The Electrochemical Society*, vol. 159, no. 12, pp. D705–D712, 2012. ISSN 0013-4651.

[46] Science, M.L.: What are antibodies? .
Available at: `https://www.mblbio.com/bio/g/support/method/antibody.html`

[47] Science, M.L.: Types of antibodies. .
Available at: `https://ruo.mbl.co.jp/bio/e/support/method/antibody-isotype.html`

[48] Nimse, S.B., Song, K., Sonawane, M.D., Sayyed, D.R. and Kim, T.: Immobilization techniques for microarray: Challenges and applications. *Sensors (Switzerland)*, vol. 14, pp. 22208–22229, 2014.

[49] Rusmini, F., Zhong, Z. and Feijen, J.: Protein immobilization strategies for protein biochips. *Biomacromolecules*, vol. 8, no. 6, pp. 1775–1789, 2007.

[50] Chakraborty, S., Rusli, H., Nath, A., Sikder, J., Bhattacharjee, C., Curcio, S. and Drioli, E.: Immobilized biocatalytic process development and potential application in membrane separation: A review. *Critical Reviews in Biotechnology*, vol. 36, no. 1, pp. 43–48, 2016.

[51] Kausaite-Minkstimiene, A., Ramanaviciene, A., Kirlyte, J. and Ramanavicius, A.: Comparative study of random and oriented antibody immobilization techniques on the binding capacity of immunosensor. *Analytical Chemistry*, vol. 82, no. 15, pp. 6401–6408, 2010.

[52] Ouerghi, O., Diouani, M.F., Belkacem, A. and Elsanousi, A.: Adjunction of Avidin to a Cysteamine Self-Assembled Monolayer for Impedimetric Immunosensor. *Journal of Biomaterials and Nanobiotechnology*, vol. 7, no. January, pp. 1–12, 2016.

[53] Foo, K.L., Hashim, U., Muhammad, K. and Voon, C.H.: Solâgel synthesized zinc oxide nanorods and their structural and optical investigation for optoelectronic application. *Nanoscale Research Letters*, vol. 9, pp. 1–10, 2014.

[54] Tom, S.C.: The development of a hand-held, self-powering bio-sensing device for the early detection of Mycobacterium tuberculosis. 2019.

[55] du Toit, A.: Optimization of protein immobilization on gold surfaces. Tech. Rep., University of Stellenbosch, Stellenbosch, 2020.

[56] Wessendorf, M.: Autofluorescence: Causes and Cures. *Confocal list server archives*, pp. 1–8, 2004. ISSN 0022-1767.

[57] Lee, S., Choi, G.E., Yang, C., Wu, H.C. and Yu, J.: Autofluorescence generation and elimination: A lesson from glutaraldehyde. *Chemical Communications*, vol. 49, no. 29, pp. 3028–3030, 2013. ISSN 1364548X.